UNIVERSITÉ DU QUÉBEC À MONTRÉAL

CRCM PROJECTED CHANGES TO THE FREQUENCY AND MAGNITUDE OF EXTREME PRECIPITATION EVENTS OVER CANADA

THESIS PRESENTED

AS PARTIAL REQUIREMENT

FOR MASTER'S DEGREE IN ATMOSPHERIC SCIENCES

BY

BRATISLAV MLADJIC

NOVEMBER 2010

UNIVERSITÉ DU QUÉBEC À MONTRÉAL

CHANGEMENTS PROJETÉS DE LA FRÉQUENCE ET DE L'AMPLITUDE DES ÉVÉNEMENTS DE PRÉCIPITATION EXTRÊME DANS LA SIMULATION DU MRCC SUR LE CANADA

MÉMOIRE
PRÉSENTÉ
COMME EXIGENCE PARTIELLE
DE LA MAÎTRISE EN SCIENCES DE L'ATMOSPHÈRE

PAR

BRATISLAV MLADJIC

NOVEMBRE 2010

REMERCIEMENTS

Je tiens tout d'abord à remercier ma directrice de recherche, Mme Laxmi Sushama, pour m'avoir donné l'opportunité de réaliser ce projet. Je voudrais aussi remercier mon codirecteur de recherche, Naveed Khaliq. J'aimerais remercier le réseau de recherche du Modèle Régional Canadien du Climat (MRCC) pour le soutien financier qu'il m'a accordé pendant mes études de maîtrise, ainsi que tout le personnel du Département des sciences de l'atmosphère de l'Université du Québec à Montréal.

TABLE DES MATIÈRES

LISTE DES FIGURES

Figure Page

LISTE DES TABLEAUX

Tableau Page

LISTE DES ACRONYMES

AM	Annual Maximum
AMNO	Amérique du Nord
ARF	Areal Reduction Factor
CFCAS	Canadian Foundation for Climate and Atmospheric Sciences
CRCM	Canadian Regional Climate Model
CRCMD	Canadian Regional Climate Modelling and Diagnostics Network
ERA	European Centre for Medium-Range Weather Forecasts Re-Analysis
GBA	Grid-Box Analysis
GCM	Global Climate Model
GEV	Generalized Extreme Value
GLO	Generalized Logistic
GNO	Generalized Normal
GPA	Generalized Pareto
GREHYS	Groupe de recherche en hydrologie statistique
IPCC	Intergovernmental Panel on Climate Change
MITACS	Mathematics of Information Technology and Complex Systems

MRC	Modèle Régional du Climat
MRCC	Modèle Régional du Climat Canadien
PE3	Pearson Type 3
RS	Reference Simulation
RFA	Regional Frequency Analysis
RCM	Regional Climate Model
UQAM	Université du Québec à Montréal
VS	Validation Simulation

LISTE DES SYMBOLES

B	Number of bootstrap resamples
e_i	Bootstrap residuals
H	Heterogeneity measure
$SE(y^T)$	Standard error of y^T
l_i	i-th sample l-moments
t_2	Sample L-coefficient of variation
t_3	Sample L-skewness
t_4	Sample L-kurtosis
y^T	Estimate of the T-year regional growth factor
Z	Z goodness-of-fit test
α	Significance level
λ_1	L-mean
λ_2	L-standard deviation
ξ	Location

k	Shape parameter
$F(x)$	Cumulative distribution function
$\Phi(x)$	Standard normal cumulative distribution function
$G(x,\alpha)$	Incomplete gamma integral
$\Gamma(i)$	Gamma function

RÉSUMÉ

Les changements de l'intensité et de la fréquence des extrêmes hydro-climatiques peuvent avoir des impacts significatifs sur les secteurs liés aux ressources en eau. Il est donc nécessaire d'évaluer leur vulnérabilité face aux changements climatiques.

Cette étude porte sur l'estimation des changements de la fréquence et l'amplitude des événements de précipitations extrêmes au Canada en utilisant un ensemble de dix simulations de 30 ans effectuées avec le Modèle Régional Canadien du Climat (MRCC), pour une période de référence (1961–1990) et une période future (2040–2071). Les simulations futures utilisent le scénario A2 du SRES. Deux méthodes sont utilisées dans cette étude, avec l'hypothèse de stationnarité tranche de temps (en anglais «time-slice stationarity assumption»): Analyse Fréquentielle Régionale (RFA pour «Regional Frequency Analysis»), qui s'opère à l'échelle des unités statistiquement homogènes des régions climatiques prédéfinies, avec la possibilité de réduction au niveau du point de grille et l'analyse individuelle de point de grille (GBA pour «Grid-box analysis»). Des données d'observations réhabilitées et homogénéisées de 495 stations situées partout au Canada sont utilisées pour vérifier l'homogénéité statistique des régions climatiques canadiennes. Ces données sont également utilisées pour sélectionner la distribution régionale la plus appropriée parmi les cinq distributions candidates aux trois paramètres de la modélisation observée de 1, 2, 3, 5, 7 et 10 jours AM (AM pour «Annual Maxima») de la quantité de précipitations (i.e. les extrêmes d'un seul jour et de plusieurs jours), survenues entre les mois d'avril et de septembre, pour la période de 30 ans allant de 1961 à 1990. Les distributions candidates sont les suivantes: la distribution des valeurs extrêmes généralisées (GEV pour «General Extreme Value»), Pareto généralisée (GPA pour «Generalized Pareto»), Logistique généralisée (GLO pour «Generalized Logistic»), Pearson Type 3 (PE3 pour «Pearson Type 3») et Normal généralisée (GNO pour «Generalized Normal»). La validation du modèle de simulation pour les périodes de retour de 20, 50 et 100 ans des précipitations extrêmes d'une et de plusieurs journées en comparaison avec les observations durant la période 1961–1990 en utilisant les méthodes de RFA et GBA suggèrent une sous-estimation du MRCC pour une grande partie du Canada. Toutefois, le MRCC a tendance à surestimer légèrement sur la région de YUKON.

Les changements de l'amplitude et la fréquence des précipitations extrêmes d'un seul jour et de plusieurs jours au Canada sont estimés en utilisant les deux méthodes, celle de RFA et de GBA. Une estimation d'incertitude sous la forme d'intervalles de confiance des 20, 50 et 100 ans de périodes de retour à l'échelle régionale des cinq paires de simulations de la période de référence et celle du future est effectuée en utilisant la méthode de bootstrap vectoriel (en anglais «nonparametric vector bootstrap resampling method») et ensuite exprimé sous forme d'intervalle de confiance. Les résultats de l'étude ont des implications fortes pour des projets liés à la conception et la gestion des ressources en eau et pour estimer la durabilité des infrastructures existantes dans un climat changeant.

CHAPITRE I

INTRODUCTION

Les changements des événements extrêmes météorologiques et climatiques (par exemple les vagues de chaleur, les précipitations fortes, les sécheresses, les tempêtes hivernales, les ondes de tempête, etc.) ont des effets significatifs sur l'environnement, la société et l'économie. Le conséquences des événements extrêmes sur les changements des systèmes naturels et humains sont plus important que celles apportées pa le changements dans le moyennes climatiques (Parmesan, 2000). L'une des conclusions du quatrième rapport d'évaluation du Groupe d'Experts Intergouvernemental sur l'Évolution du Climat (IPCC, 2007) est que la confiance a augmenté quant à l'augumentation probable de la fréquence, de l'intensité et de l'étendue des événements extrêmes au cours du 21e siècle. Par conséquent, la capacité de la société à gérer les risques dans divers domaines, causés par les événements extrêmes, sera cruciale pour la résilience du développement et des conditions de vie.

De nombreuses catastrophes naturelles (inondations, glissements de terrain, etc.) à travers le monde provoqués par des phénomènes hydrométéorologiques intense amène la communuauté scientifique à comprendre leur lien possible avec l`augmentation de l'intensité des précipitations en raison d'activités anthropiques. Par conséquent, il est nécessaire d'étudier comment les caractéristiques des précipitations extrêmes seront affectées par le réchauffement planétaire dans les années à venir. Des recherches diverses (e.g. Fowler et Hennessy, 1995; Trenberth, 1999; Trenberth et al., 2003) ont suggéré que le réchauffement climatique entraînera une augmentation des précipitations intenses, dans la mesure où l'atmosphère plus chaude sera capable de contenir plus d'humidité et de produire un cycle hydrologique plus actif. Les simulations de modèles climatiques semblent en effet indiquer

que l'intensification du cycle hydrologique devrait se produire dans des conditions climatiques plus chaudes et cela pourrait entraîner une augmentation de l'intensité des précipitations, en particulier dans les événements extrêmes (McGuffie et al., 1999; Kharin et Zwiers, 2000; Palmer et Räisänen, 2002; Tebaldi et al., 2006). A l'échelle mondiale, les expériences avec le Modèle Climatique Global Canadien (CGCM; Kharin et Zwiers, 2000) montrent une augmentation de 8% des périodes de retour de 20 ans des précipitations extrêmes quotidiennes de 2040 à 2060 et une augmentation de 1% des précipitations annuelles moyennes. Par conséquent, il existe un besoin et un intérêt croissants à étudier les changements des caractéristiques des précipitations extrêmes. Les informations sur les changements de l'intensité et la fréquence des précipitations extrêmes sont importantes pour une meilleure gestion des ressources en eau, pour l'amélioration des normes de conception d'ingénierie et pour assurer la sécurité des infrastructures diverses dans des conditions climatiques changeantes. L'étude présentée dans ce mémoire se focalisera sur l'estimation des changements (projetés) des caractéristiques des précipitations extrêmes au Canada en utilisant les simulations du Modèle Régional Canadien du Climat (MRCC) pour une période de référence (1961–1990) et une période future (2041–2070).

En général, les valeurs extrêmes sont décrites en termes de périodes de retour ou quantiles. Ceux-ci sont des valeurs qui excèdent, en moyenne, une fois pour un nombre d'années spécifié, communément appelée période de retour. L'analyse fréquentielle est souvent utilisée pour modéliser des précipitations extrêmes afin de développer des relations fréquence-amplitude. Il s'agit d'ajuster une distribution de probabilité à une série d'extrêmes observés ou à ceux provenant des sorties des modèles climatiques afin de définir des probabilités d'occurrences de certains événements d'intérêt. Les méthodes d'analyse fréquentielle pour des échantillons individuels d'extrêmes sont bien établies. Dans divers cadres météorologiques/hydrologiques, de nombreux échantillons des extrêmes pourraient être reliés par les mécanismes physiques générant les précipitations. S'il y a des similarités statistiques entre les extrêmes observés au sein d'une région climatique ou hydrologique homogène identifiée, des analyses plus exhaustives concernant les relations de fréquence-magnitude sont possibles par l`analyse de l`enemble des échantillons au lieu de l'analyse individuels des échantillons. Cette approche est connue sous le nom d'analyse fréquentielle

régionale (RFA). La procédure de l'indice de crue (index-flood) de Darlymple (1960) en est un exemple. Au cours des années, l'approche RFA a été améliorée par un certain nombre de chercheurs, y compris l'évolution la plus notable par Hosking et Wallis (1997). Cette étude a pour but d'utiliser l'approche RFA et celle de l'analyse de point de grille/grid-box (GBA). Le GBA tient compte de chaque point de grille en tant qu'entité indépendante et admet une simulation par la méthode habituelle de modélaisation à site unique. L'approche régionale permet d'estimer l'amplitude des événements de précipitations d'une longue période de retour avec plus de fiabilité, tandis que le GBA montre la performance du MRC avec sa résolution à aire-limitée et il peut donner quelques détails spatiaux supplémentaires.

Du point de vue statistique, l'indépendance et la stationnarité sont les hypothèses essentielles qui doit avoir une analyse fréquentielle pour qu'èlle puisse se réaliser correctement. En outre, on émet souvent l'hypothèse que les données proviennent de la même distribution. L'hypothèse de l'indépendance ne peut pas être remplie dans les cas où la fréquence d'échantillonnage des données est assez élevée. En ingénierie, l'hypothèse de stationnarité est encore couramment utilisée pour de courts échantillons (ceux constitués de 20 ou 30 valeurs). Pour l'application des méthodes RFA et GBA, il est supposé que la distribution des extrêmes ne change pas au cours du temps durant les périodes 1961–1990 et 2041–2070, c.-à-d. qu'une stationnarité par tranche de temps (en anglais «timeslice stationarity») est supposée. De plus, la dépendance de série, si elle existe dans des échantillons de précipitations extrêmes d'un jour et de plusieurs jours, sera résolue en développement des intervalles de confiance, qui sont une partie essentielle de la procédure d'analyse fréquentielle. Cela peut être effectué en utilisant les approches appropriées telles que les méthodes de bootstrap rééchantillonnage par bloc (en anglais «block bootstrap resampling») (Khaliq et al., 2009). Par conséquent, l'influence de la corrélation sérielle n'est pas considérée explicitement lorsque des approches RFA et GBA sont appliquées aux précipitations extrêmes observées et modélisées.

Dans cette étude, les régions climatiques du Canada de Plummer et al. (2006) sont adoptées comme base pour élaborer l'approche RFA. L'analyse d'homogénéité statistique de

ces régions est effectuée en utilisant la méthodologie proposée par Hosking et Wallis (1997) et en utilisant la base de données observées des précipitations réhabilitée et homogénéisée d`Environement Canada (Mekis et Hogg, 1999; Vincent et Mekis, 2009). Il est important de noter que dans cette base de données de haute qualité le réseau de stations dans les régions centre-est et du nord est nettement moins dense que dans les autres régions du pays. Ainsi, le nombre limité des stations d'observation exclut des analyses d'homogénéité statistique fiables pour ces régions.

Les modèles climatiques constituent un des moyens pour étudier les changements de précipitations extrêmes. De nombreuses études ont examiné les changements dans les précipitations extrêmes dans des scenarios de croissance de gaz à effets de serre en utilisant les Modèles Climatiques Globaux (MCG) (e.g. Zwiers et Kharin, 1998; McGuffie et al., 1999; Tebaldi et al., 2006) ainsi que les Modèles Climatiques Régionaux (MRC) (par exemple, Fowler et al., 2005; Ekström et al., 2005; Beniston et al., 2007; Mailhot et al., 2007). Cependant, il est important de noter que la précipitation est un processus atmosphérique particulièrement complexe à modéliser. En effet, la modélisation doit reposer à reproduire exactement les processus physiques complexes tels que la micro-physique des nuages, la convection, la turbulence au seuil de la couche limite planétaire et les circulations à grande échelle. Les modèles climatiques simulent des précipitations à travers deux mécanismes principaux: les systèmes de précipitations synoptiques (ou stratiformes) et les systèmes de précipitations convectives. La précipitation à grande échelle se produit à la suite d`un soulèvement vertical de l'air lié au développement des systèmes de basse pression et des circulations orographiques ou de mousson, tandis que la precipitation convective est due à un soulèvement plus vigoureux de l'air, par exemple par le dégagement de chaleur latente. Les approches adoptées pour modéliser des systèmes de précipitations d`échelle synoptique peuvent être considérées comme plus simple que celles des systèmes convectifs. Ainsi, les différents types de paramétrage utilisés dans les modèles climatiques pour simuler ces processus physiques complexes peuvent influencer les mécanismes de précipitations extrêmes.

De nos jours, les MRC (pilotés par les MCG) constituent des outils pertinents pour l'étude des changements d'événements de précipitations extrêmes. La résolution grossiere de MCG est moins appropriée pour l'analyse des changements de précipitations extrêmes, puisque les systèmes responsables sont généralement plus petits dans l'étendue spatiale que la résolution du MCG. Par contre, les MRC fournissent une information spatiale et temporelle de haute résolution qui améliore l'estimation des changements spatiaux et temporels des précipitations extrêmes. L'information des changements climatiques des MRC est nécessaire pour les études d'impact dans des secteurs comme l'agriculture, l'énergie, les ressources en eau, la santé et l'assurance. Toutefois, il existe de nombreuses sources d'incertitudes associées aux modèles climatiques qui doivent être prises en compte: les incertitudes associées au développement de scénario de gaz à effet de serre, les erreurs de performance (en raison de la dynamique interne et du paramétrage du modèle), les erreurs de pilotage (en raison du pilotage de circulation à grande échelle des MCG), etc.

Les observations sont recueillies sur des sites spécifiques, tandis que les valeurs des précipitations de point de grille des modèles climatiques sont censées représenter des moyennes spatiales et donc la moyenne des précipitations pour une région sera toujours moindre que la précipitation estimée en un point (e.g. Osborn et Hulme, 1997). Pour aborder ce sujet, des coefficients d'abattement (ARF pour «Areal reduction factors») sont nécessaires pour relier les précipitations en un point de grille à la moyenne des précipitations spatiales. Toutefois, comme il n'existe pas une compréhension claire et un consensus sur la façon dont cette relation devrait être élaborée pour les précipitations à l'échelle des points de grille simulés par les MRC et les MCG, aucune considération explicite n'est donnée aux ARF dans les analyses présentées dans cette étude.

Après la validation des précipitations extrêmes simulées par le MRC et le calcul des périodes de retour, la dernière étape nécessaire consiste à estimer l'incertitude des périodes de retour. Une estimation d'incertitude dans les prévisions de période de retour donne une certaine confiance dans leur utilisation à des fins de conception. La mesure de l'incertitude est souvent exprimée sous forme d'un intervalle de confiance pour l'estimation de quantile.

Dans cette étude, les intervalles de confiance sont calculés en utilisant la méthode de bootstrap vectoriel (en anglais «nonparametric vector bootstrap resampling») (Efron et Tibshirani, 1993; GREHYS, 1996; Davison et Hinkley, 1997; Khaliq et al., 2009). L'avantage de cette approche par bootstrap est qu'il évite la nécessité de faire des hypothèses de distribution sur les échantillons des extrêmes pour calculer les intervalles de confiance.

Pour résumer, cette étude examine les changements à 1, 2, 3, 5, 7 et 10 jours des quantités de précipitations annuel maximales (AM) (i.e. extrêmes d'un seul jour et de plusieurs jours), pour la période Avril-Septembre, en appliquant l'approche RFA basée sur les L-moments et l'approche GBA à un ensemble d'intégrations du MRCC de quatrième génération pour la période de référence (1961–1990) et les climats futurs (2041–2070). Dans cette étude, un ensemble de dix simulations de 30 ans du MRCC est considéré, cinq correspondent à la période de référence (1961–1990) et les cinq autres à la période future (2041–2070). Le MRCC est piloté par le Modèle Climatique Global (MCCG3; McFarlane et al., 2005) suivant le scénario «observé du 20è siècle» du GIEC (IPCC, 2001) pour la période de référence et selon le scénario A2 du Rapport Spécial sur les Scénarios d'Emission (SRES pour Special Report on Emissions Scenario; IPCC, 2001) pour la période future. Toutes les simulations du MRCC sont effectuées avec une résolution horizontale de 45 km vrai à 60° N sur une grille couvrant l'Amerique du Nord (identifié par AMNO). Pour la simulation de validation et pour la période 1961–1990, le MRCC a été pilotée par les réanalyses ERA-40 (Uppala et al., 2005).

Objectifs principaux de l'étude sont de:

1) Analyser l'homogénéité statistique des régions climatiques du Canada prédéfinies et adoptées par Plummer et al. (2006), en utilisant la base de données observeés de précipitations réhabilitée et homogénéisée par Environnement Canada (Mekis et Hogg, 1999), ainsi que l'identification des distributions régionales les plus appropriées à partir d'un ensemble de cinq distributions à trois paramètres (i.e. la distribution des valeurs extrêmes généralisées (GEV), Pareto Généralisée (GPA), Logistique Généralisée (GLO), Pearson Type

3 (PE3) et Normal Généralisée (GNO)) pour la modélisation des précipitations extrêmes d'un seul jour et de plusieurs jours.

2) Étudier les caractéristiques statistiques des précipitations extrêmes provenant des bases de données d'observation pour la période 1961–1990 et celles issues des simulations du MRCC pour la période de référence (1961–1990) et la période future (2041–2070).

3) Valider le MRCC en utilisant les approches RFA et GBA en ce qui concerne la performance et les erreurs de pilotage (en anglais «boundary forcing errors»)

4) Estimer les changements prévisionnels à 20, 50 et 100 ans de périodes de retour des précipitations extrêmes des conditions climatiques du futur (2041–2070), considerant une période de référence (1961–1990), des conditions climatiques, en utilisant un ensemble de simulations du MRCC.

5) Fournir des estimations de l'incertitude des périodes de retour régionaux sélectionnées, sous forme d'intervalles de confiance, en utilisant la méthode de bootstrap vectoriel.

6) Discuter des implications des résultats obtenus pour le Canada à l'échelle régionale et nationale.

Organisation du mémoire:

L'introduction est présentée dans ce chapitre, suivie par le Chapitre II, qui est sous forme d'un article rédigé en anglais et qui représente le cœur du mémoire. Dans cet article, divers éléments du travail de recherche sont présentés et discutés, i.e. (1) le contexte et la problématique de l'étude, (2) la bibliographie utilisée, (3) la description des régions climatiques du Canada, du MRCC et les simulations et la méthodologie adoptée et (4) les résultats obtenus. Le dernier chapitre III contient la conclusion et la discussion des résultats. Les précipitations extrêmes de 1, 2, 3, 5, 7 et de 10 jours de durée sont analysées pour douze régions climatiques du Canada. Dans l'article, nous présentons les résultats détaillés de 1, 3 et 7 jours de précipitations extrêmes pour seulement six régions choisies. Quelques figures et tableaux de support qui ne sont pas inclus dans l'article, y compris des figures et tableaux se rapportant à 2, 5 et 10 jours de précipitations extrêmes pour les six autres régions, sont fournis dans les deux annexes (A et B). Pour faciliter la compréhension, un tableau est fourni

au début de chaque annexe, mettant en évidence les sections dans l'article où les figures/tableaux ont été utilisés directement ou indirectement.

CHAPITRE II

CANADIAN RCM PROJECTED CHANGES TO EXTREME PRECIPITATION CHARACTERISTICS OVER CANADA

B. Mladjic[1,*], L. Sushama[1], M.N. Khaliq[2], R. Laprise[1]

[1]Canadian Regional Climate Modeling and Diagnostics Network, University of Quebec at Montreal, 201 avenue Président-Kennedy, local PK-2315, Montreal, Quebec, Canada H2X 3Y7

[2]Atmospheric Science and Technology Directorate, Adaptation and Impacts Research Division, Environment Canada, Place Bonaventure, North-East Tower, 800 Gauchetiere Street West, Office 7810, Montreal, Quebec H5A 1L9, Canada

[*]Corresponding author address:
Bratislav Mladjic
Département des Sciences de la Terre et de l'Atmosphère, UQAM
P. O. Box 8888, Stn Downtown
Montréal, Québec, Canada H3C 3P8
Tel: +1 (514) 928-2029
Email: mladjic@sca.uqam.ca

To be submitted to: Journal of Climate

Abstract

Changes to the intensity and frequency of hydro-climatic extremes can have significant impacts on sectors associated with water resources and therefore it is important to assess their vulnerabilities in a changing climate. This study focuses on the assessment of projected changes to the frequency and magnitude of extreme precipitation events over Canada using an ensemble of ten 30-year integrations performed with the Canadian Regional Climate Model (CRCM), for reference (1961–1990) and future (2040–2071) periods; the future simulations correspond to A2 SRES scenario. Two methods, the regional frequency analysis (RFA), which operates at the scale of statistically homogenous units of pre-defined climatic regions, with the possibility of downscaling to grid-cell level, and the individual grid-box analysis (GBA) are used in this study, with the time-slice stationarity assumption. Validation of model simulated 20-, 50- and 100-year return levels of 1-, 2-, 3-, 5-, 7- and 10-day extreme precipitation events (i.e. single- and multi-day events) against those observed for the 1961–1990 period using both the RFA and GBA methods suggest underestimation by the CRCM over most of Canada. However, the CRCM tends to overestimate over the Yukon region. The CRCM projected changes to selected return levels for the future (2041–2070) period in comparison to the reference (1961–1990) period suggest an increase in event magnitudes, which appear to be significant, particularly for the western (West Coast, Western Cordillera), eastern (Northeast Forest) and Yukon Territory, Mackenzie Valley and Arctic regions as well as for the Northwest Forest Prairie region. In general, positive but relatively less significant changes are noticed for the Great Lakes, Maritimes and Prairie (Northern Plains) regions. The results of the study have strong implications for both design and management of water resources related projects and for assessing sustainability of existing infrastructures in a changing climate.

Keywords: Canadian climatic regions; climate change; precipitation extremes; regional climate modelling; regional frequency analysis.

2.1 Introduction

Extreme hydro-climatic events such as precipitation extremes, floods and droughts can impact society significantly, bringing enormous environmental, social and political repercussions. In the context of a changing climate, it is therefore important to investigate changes to characteristics of these events. Hence, this study focuses on changes to characteristics of precipitation extremes only. Information about changes to intensity and frequency of extreme precipitation events is crucial for better management of water resources, developing guidelines for revising engineering design standards and ensuring safety of various infrastructure facilities under changing climate conditions.

The Fourth Assessment Report of the Intergovernmental Panel on Climate Change (IPCC, 2007) discussed changes in mean precipitation observed over recent decades for many regions of the world and suggested that it is very likely that frequency and intensity of heavy precipitation events will increase over many regions in the future.

Assessment of changes to characteristics of precipitation extremes due to variations in greenhouse gas concentrations was investigated in previous studies using global climate model (GCM) simulations (e.g. Zwiers and Kharin, 1998) as well as using regional climate model (RCM) simulations, e.g. Fowler et al. (2005) and Ekström et al. (2005) for the United Kingdom, May (2008) and Beniston et al. (2007) for Europe and Mailhot et al. (2007) for southern Quebec. At the present point in time, RCMs offer the best information with respect to GCM, for studying changes to extreme precipitation events. Their advantage over the GCM is that they provide highly resolved spatial and temporal information that enhances assessment of spatial and temporal changes to extreme precipitation.

Extreme values are usually described in terms of return levels or quantiles. These are the values that are exceeded, on average, once every specified number of years. Return levels are generally computed by fitting a parametric distribution to a sample of annual maximum (AM) or peaks-over-threshold (POT) values. In the former method, which is very commonly

used because of its simple structure, only one value from each year/season is considered and in the latter, more than one value per year/season could be considered. Since extreme events are rare and historical records are often short, estimation of frequencies of extreme events is a challenging task. When data at a given location are insufficient for a reliable estimation of quantiles, regional frequency analysis (RFA) could be a useful alternative. The RFA has been an established method in hydrology for many years and it is also becoming popular in climatology because of its advantage mentioned above. It is often remarked that the RFA method substitutes space for time by using observations from different sites in a region to compensate short records at individual sites.

This study investigates changes to 1-, 2-, 3-, 5-, 7- and 10-day AM precipitation amounts, for the April–September period, applying the L-moments based RFA approach of Hosking and Wallis (1997) to an ensemble of the fourth generation Canadian RCM (CRCM) integrations for the reference (1961–1990) and future (2041–2070) climates. As a complementary approach to RFA, grid-box analysis (GBA), which operates on individual grid cells of the CRCM, is also performed. Rehabilitated and homogenized precipitation records of 495 stations from Environment Canada, located across Canada (Vincent and Mekis, 2009), is used for evaluating the CRCM performance for the period 1961–1990. For a successful implementation of the RFA approach, observational sites or grid boxes must be assigned to statistical homogeneous regions, since approximate homogeneity is required to ensure that RFA is more robust than an at-site analysis (Hosking and Wallis, 1997). Identification of homogeneous regions is usually the first and the most difficult task in RFA as it may involve many subjective decisions (GREHYS, 1996). For the purpose of this study, previously defined Canadian climatic regions from Plummer et al. (2006) are adopted as the basis for developing RFA approach. These climatic regions are tested for their statistical homogeneity and divided further into smaller sub-regions where necessary by maintaining the notion of contiguous homogeneous regions. Since 30 years long reference and future periods are located over sufficiently separated disjoint time intervals, time-slice stationarity for both the reference and future climate conditions is assumed for the analyses presented in this paper.

The paper is organized as follows. A brief description of the CRCM and its simulations used in the analysis are given in Section 2. Description of the Canadian climatic regions along with details of the observational records is provided in Section 3. Section 4 contains a description of the methodology used for estimating changes to extreme precipitation events. Detailed results of the CRCM validation and projected changes to precipitation extremes are presented in Section 5, followed by discussion and main conclusions of the study in Section 6.

2.2 Model and simulations

The model used in this study is the latest operational version of the CRCM (version 4.2.3), i.e. the fourth generation of the CRCM. A detailed description of the earlier versions of the CRCM can be found in Caya and Laprise (1999) and in Plummer et al. (2006). The CRCM's horizontal grid is uniform in polar stereographic projection and its vertical resolution is variable with a Gal-Chen scaled-height terrain following coordinate. In the most recent version, sub-grid scale physical parameterization largely follows the Canadian General Circulation Model Version III (CGCM3) physics (Scinocca and McFarlane, 2004; McFarlane et al., 2005), that is adapted to the regional model's grid and projection.

An ensemble of ten 30-year CRCM integrations are considered in this study, of which five correspond to the current climate (1961–1990) reference period and the other five are the matching simulations for the future (2041–2070) period. The CRCM performs dynamical downscaling of different members of an ensemble of CGCM3 simulations to produce climate projections at the regional scale following IPCC "observed 20th century" scenario (IPCC, 2001) for the reference and Special Report on Emissions Scenarios (SRES) A2 scenario (IPCC, 2001) for the future. In addition, a validation run spanning the 1961–1990 period, where the CRCM is driven by ERA40 (Uppala et al., 2005) is considered and will be referred to as "validation simulation" or simply VS hereafter. All CRCM simulations are performed at a horizontal resolution of 45 km true at 60°N over a North-American domain shown in Fig. 2.1. For the convenience of presentation, the five CGCM3 driven simulations for 1961–1990 are referred to as C1, C2, C3, C4 and C5, while corresponding simulations for 2041–2070 are

referred to as F1, F2, F3, F4 and F5 in this paper; together, these C1–C5 and F1–F5 simulations are respectively referred to as "reference simulations" and "future simulations".

2.3 Description of Canadian climatic regions and observational records

2.3.1 Climatic regions

A set of 10 predefined climatic regions is adopted from Plummer et al. (2006) for the purpose of this study. The northern regions include YUKON (Yukon Territory), MACK (Mackenzie Valley) and EARCT (East Arctic), the regions over the western Canada and Prairies are the WCOAST (West Coast), WCRDRA (Western Cordillera), NWFOR (Northwest Forest), and NPLNS (Northern plains), the eastern regions are the NEFOR (Northeast forest), GRTLKS (Great Lakes) and MRTMS (Canadian Maritimes). The WCOAST, WCRDRA, NPLNS and GRTLKS regions are spread over the Canadian and the US territory, however, only the Canadian portion of these regions is retained, as this study focuses on Canada. These climatic regions are shown in Fig. 2.1.

2.3.2 Observational records

Observational records consist of 495 stations included in the rehabilitated and homogenized precipitation database of Canada. This database was developed by applying adjustments for known reasons of non-homogeneity, e.g. changes in instrument type, station relocations, trace biases, etc. (Vincent and Mekis, 2009). Most of the records are available till 2007 and for some stations records go as far back as 1900. Data availability in much of the Canadian Arctic is restricted to 1948–2007. Spatial distribution of the CRCM grid cells containing at least one station out of 495 stations is shown in Fig. 2.1. It is clear from this figure that most of the stations are concentrated in southern parts of the country, along the border with the US. Central, east-central and northern regions have significantly less dense network of stations. This is an obvious limitation of the rehabilitated and homogenized database. This database is used for verifying statistical homogeneity of Canadian climatic regions, discussed in the previous section, and for selecting the most appropriate regional distribution for modelling observed 1-, 2-, 3-, 5-, 7- and 10-day AM precipitation, occurring

over the April to September months, for the 30-year period from 1961 to 1990 in an RFA setting, described in detail in the section to follow. The April to September period is chosen to avoid mixing of snow and rainfall extremes. To a greater extent, this time window helps to maintain homogeneity of the samples of precipitation extremes from a physical viewpoint as well as to preserve their seasonality. As the reliability of the analyses is highly dependent on the quality as well as on the completeness of records, a year with more than five missing daily values is considered a missing year and only those stations with at least 21 valid years are considered for the analyses. Though the records are available for time periods longer than 30 years, the 1961–1990 time window is chosen in order to match the CRCM reference period described earlier. The total number of available stations and those retained for analysis following the missing value and station inclusion criteria (given in brackets) are 21 (15) for YUKON, 16 (9) for MACK, 39 (33) for EARCT, 66 (58) for WCOAST, 65 (59) for WCRDRA, 58 (53) for NWFOR, 46 (43) for NPLNS, 86 (73) for NEFOR, 63 (59) for MRTMS and 35 (30) for GRTLKS regions. In total, the number of stations considered for analysis in this study is 432 out of 495.

2.4 Methodology

Two complementary methods are used to assess the CRCM performance and projected changes to frequency and magnitude of extreme precipitation events over Canada: the RFA and GBA. For the application of these two methods it is assumed that the distribution of extremes does not change over time during the periods 1961–1990 and 2041–2070. In other words, time, time-slice stationarity is assumed. Analyses are performed using 1-, 2-, 3-, 5-, 7- and 10-day observed and modeled AM precipitation amounts. The RFA approach allows estimation of desired return levels, particularly those corresponding to higher return periods, with more reliability compared to a single site based estimation (Hosking and Wallis, 1997); analogously this remark can be extended to a single grid-cell based estimation as well. Advantages of the RFA are especially evident when only short records are available. This assertion appears to be applicable for the present analyses because at the most 30 values per station or grid-cell are included in the analysis in order to be consistent with the time-slice CRCM experiments. Compared to the RFA approach, the GBA shows performance of the

CRCM at grid-cell scale and hence it could provide more detailed spatial information. The usefulness of the RFA and the GBA approaches have been investigated in a few recent studies on modeling regional climate model simulated precipitation extremes, e.g. Fowler et al. (2005), Ekström et al. (2005) and Mailhot et al. (2007).

The CRCM performance and boundary forcing errors (Sushama et al., 2006) are assessed: performance errors are due to the internal dynamics and physics of the regional model and boundary forcing errors are due to the errors present in the driving data. Comparison of selected observed return levels with those from the validation simulations for the period 1961–1990 is used to assess performance errors. Comparison of selected return levels from the validation and reference simulations provide assessment of boundary forcing errors. This validation is performed using both the RFA and GBA approaches. Assessment of the performance of the CRCM is followed by an analysis of the CRCM reference and future period integrations, in order to study changes to characteristics of extreme precipitation events over Canada.

2.4.1 The L-moments based RFA approach

In general, there are two main steps involved in an RFA approach: (1) identification of suitable statistical homogeneous regions and (2) selection of an appropriate regional distribution to generate regional growth curves or factors. A regional growth curve represents a dimensionless relationship between frequency and magnitude of extreme values. In this study, a standard RFA approach based on L-moments of Hosking and Wallis (1997) is used to generate regional growth curves for the observed data and validation (VS), reference (C1–C5) and future (F1–F5) integrations. In theory, L-moments characterize a wider range of distributions and they are believed to be more robust to the presence of outliers (Hosking and Wallis, 1997). Because of this reason, the estimators based on L-moments tend to be less biased compared to product moment based estimators. Also, L-moments based estimators are sometimes more accurate for small samples than those obtained using the maximum likelihood procedures (Hosking, 1986). A brief description of the sample L-moments required for the analysis of observed and simulated extremes and that of the theoretical L-

moments, along with the selected candidate distributions, is provided in Appendix A. Candidate distributions include the Generalized Extreme Value (GEV), Generalized Pareto (GPA), Generalized Logistic (GLO), Pearson-Type 3 (PE3) and Generalized Normal (GNO). For a single site or a single grid-cell, parameter estimation for any candidate distribution is performed by equating sample L-moments (more preferably their ratios) to their theoretical counterparts and solving the resulting equations directly or through iterative numerical algorithms. For the RFA approach, sample size-weighted averaged values of L-moment ratios are used for parameter estimation of the candidate distributions.

For verifying statistical homogeneity of Canadian climatic regions and their subdivision into smaller homogeneous regions, regional homogeneity tests based on L-moment ratios are used. According to Hosking and Wallis (1997), heterogeneity measures for a region are based on values of H_1, H_2 and H_3, where H_1, H_2 and H_3 are weighted standard deviations of (i) L-coefficient of variation, (ii) L-skewness and (iii) L-kurtosis, respectively. These measures are derived using Monte Carlo simulations. A region may be regarded as "acceptably" homogenous for H values below 1, "possibly" heterogeneous for H values between 1 and 2 and "definitely" heterogeneous for H values equal and above 2. For regions with H values greater than 2, a further subdivision into smaller regions is undertaken with the objective of improving on quantile estimates. This subdivision is undertaken using the cluster analysis algorithm (Hosking and Wallis, 1997) if this analysis resulted in meaningful contiguous subdivisions.

In order to select an appropriate regional distribution from the GEV, GPA, GLO, PE3 and GNO distributions for developing regional growth curves, the Z-statistic developed by Hosking and Wallis (1997) is used here. This statistic is described in Appendix B. A candidate distribution passes the Z goodness-of-fit test, for instance, at 10% significance level, if the $|Z^{DIST}| < 1.64$. It is possible that more than one distribution would appear adequate following this testing procedure. In that situation and in situations where none of the candidate distributions passed the Z test, a best candidate distribution is chosen as the one with the smallest value of the Z^{DIST}. After selection of an appropriate regional distribution

for each statistically homogeneous climatic region, comparisons of the selected return levels obtained from observations and VS of the model for the period 1961–1990 is carried out to validate the CRCM. This validation is followed by the CRCM reference and future integrations analysis in order to study changes to extreme precipitation events in an RFA setting. Whichever is the type of the best fitting regional distribution for observed extremes, the same distribution is assumed for the analysis of extremes derived from the validation (VS) and reference (C1–C5) and future (F1–F5) integrations. This approach is followed in order to maintain distributional consistencies under the assumption that a three-parameter best fit distribution is sufficiently flexible to describe changes in distributional shapes that would occur with reference and future period integrations.

2.4.2 The GBA approach

For this approach, frequency analysis is performed by considering each CRCM grid-cell as an independent entity. However, the influence of spatial correlations on future levels is taken into account when deriving confidence intervals. Distribution fitting analysis and selection of the best fitting distribution for each grid-cell can be performed in a similar manner as for the RFA approach described above. However, this analysis can only be performed for those grid cells, where an observation station is found. For the remaining grid cells, one has to subjectively assume a distribution. Alternatively, based on a goodness-of-fit test, one could use different distribution types that could vary from one grid-cell to the next and also from reference to future period integrations. The latter possibility does not seem to be logical because of the inconsistencies arising from different distributional types for the same grid-cell. Therefore, to avoid such problems, the overall best fitting distribution, found after implementing the RFA approach, is used for the GBA for the entire study area. Thus, for all grid cells, the type of the distribution stays the same for both reference and future period integrations. Validation of the CRCM using the GBA approach is performed for only those grid cells where an observation station is found.

2.5 Results

Since statistical homogeneity of Canadian climatic regions is a pre-requisite for the RFA approach, results for this analysis are presented first followed by those of the CRCM validation, in terms of performance and boundary forcing errors. The CRCM validation would furnish an overview of how the model reproduces various statistical characteristics of single- and multi-day extreme precipitation events. After discussing validation of the CRCM, results for projected changes to characteristics of extreme precipitation events are presented and discussed. Though complete analyses are performed for 1-, 2-, 3-, 5-, 7- and 10-day precipitation extremes, detailed results are presented only for 1-, 3- and 7-day events. Where appropriate, results for the remaining (i.e. 2-, 5- and 10-day) extremes are also discussed.

2.5.1 Statistical homogeneity analysis of Canadian climatic regions

Statistical homogeneity of each of the predefined climatic regions, adopted from the work of Plumer et al. (2006), is examined, with the available number of stations which satisfy the station inclusion criteria, described earlier in the section on methodology. For this purpose, 1-, 2-, 3-, 5-, 7- and 10-day observed precipitation extremes are considered. If the calculated values of the H statistics are higher than 2 for at least three out of six cases (e.g. if H statistics are simultaneously higher than 2 for 1-, 3- and 7-day precipitation extremes) then further subdivision of the region is undertaken, conditional to a successful implementation of the cluster analysis algorithm. Seven predefined regions, i.e. the YUKON, MACK, WCOAST, NWFOR, NPLNS, GRTLKS and MRTMS pass these criteria, while the remaining WCRDRA, EARCT and NEFOR regions do not, and hence their subdivision into smaller regions is undertaken.

The WCRDRA, EARCT and NEFOR regions are found to have higher than permissible value of the H_1 statistic and therefore cluster analysis is performed to subdivide these three regions into smaller homogeneous sub-regions. Satisfactory cluster analysis is feasible for EARCT and NEFOR regions only. Hence, EARCT region is subdivided into EARCT1 and EARCT2 (shown in Fig. 2.1) and NEFOR into NEFOR1 and NEFOR2 (also

shown in Fig. 2.1). It is not possible to subdivide the WCRDRA region into smaller contiguous homogeneous regions and hence this region was considered as is, despite its suspected homogeneity. Perhaps it may be possible to subdivide this region into smaller non-contiguous homogeneous regions but such a subdivision is not considered since the focus of this study was to find contiguous smaller homogeneous regions within the predefined larger climatic regions of Plummer et al. (2006). Based on the analyses presented and discussed above, a set of 12 climatic regions (shown in Fig. 2.1) is considered for RFA of AM values of daily and multi-day precipitation events.

2.5.2 Validation of the CRCM simulations

Validation of the CRCM simulated precipitation extremes is performed using the VS for the period 1961–1990, after implementing the following three steps: (1) For all 12 regions, observed regional growth curves are developed based on precipitation extremes of those stations that fall within each region. The observed regional growth curves are used to develop, dimensionless growth factors for selected return periods (i.e. y^T values, where T is the return period) and these factors in turn are used to estimate at-site return levels using the at-site l_1 values for each aggregation level considered (i.e. 1-, 2-, 3-, 5-, 7- and 10-day); (2) Regional growth curves are developed for each region based on the simulated precipitation extremes (i.e. the ones derived from the VS) for all grid cells that fall within each region. From the regional growth curves, dimensionless growth factors for selected return periods are obtained and these growth factors in turn are used to estimate return levels for each grid-cell using the corresponding l_1 value for each aggregation level considered; (3) For each of the 12 regions, scatter plots of 20-, 50- and 100-year return levels are developed for only those CRCM grid cells where at least one station is found. Such plots are useful to examine the extent of under- or over-estimation of various quantiles and therefore help assess CRCM 'performance errors' due to the internal dynamics and physics of the regional model.

Observed regional growth curves are compared to those developed from model simulated extremes in Fig. 2.2 for six selected regions, i.e. YUKON, WCOAST, MRTMS,

GRTLKS, NWFOR and EARCT2. These regions were chosen such that they represent western, eastern, southern, interior and northern parts of Canada. The shapes of growth curves for these six regions also represent the variety of shapes noted for the remaining six regions. The growth curves for each of the region were developed using the best fitting regional distribution found on the basis of Z-statistic, described in Appendix B. Many of the observed growth curves tend to follow a straight line, suggesting a light upper tail. However, the curves for MACK (figures not shown), MRTMS, NEFOR2 (figures not shown) and GRTLKS regions exhibit slight upward curvature, suggesting that distributions could be slightly heavy tailed. This behaviour is particularly evident for 1-day precipitation extremes for GRTLKS. The slight heavy tailed behaviour could be due to extremes occurring because of strong convective activity, which is usually responsible for heavy rainfall during the summer (June to August) months over short time periods. Compared to observed growth curves, VS growth curves generally exhibit light tail behavior, suggesting that extreme upper tail is underrepresented by the model. This type of behavior of climate models has been noted by other investigators as well (e.g. Fowler et al., 2005).

After comparing shapes of the regional growth curves, a direct comparison of 20-, 50- and 100-year return levels is carried out and selected results for the same six regions, as mentioned above, are shown in Fig. 2.3. Since the maximum length of individual samples included in the analysis is just 30 years, we assume that it is reasonable to study events associated with one in 100 years frequency. Beyond this level, it will be difficult to place any reasonable confidence on the events associated with very low frequency (i.e. return levels associated with return periods of longer than 100 years). In general, model underestimates selected return levels for most of the regions except a tendency toward mixed behaviour for YUKON, WCOAST and WCRDRA regions. It is important to mention here that grid-cell based precipitation of GCMs and RCMs have the spatial characteristics of areal averages and hence average precipitation for an area will always be less than the precipitation estimated at a point (e.g. Osborn and Hulme, 1997). To address this point, areal reduction factors (ARFs) are used to relate the point precipitation with the areal average precipitation. However, there is no clear understanding and consensus on how this relationship should be developed for grid-cell based precipitation simulated by regional and global climate models. Because of this

uncertainty, we do not attempt to apply any empirically derived ARF to convert point precipitation into areal average. Plots of sample size-weighted average of all l_1 values for stations that fall within each grid-cell and the average ensemble growth factors obtained from regional growth curves (not shown), corresponding to 20- 50- and 100-year return periods, for all the 12 regions, also show similar behaviour as in Fig. 2.3. In summary, the above presented results suggest that the CRCM tends to underestimate extreme precipitation quantiles in most of the regions except for the YUKON region, where it overestimates, particularly for multi-day events.

In order to assess the influence of boundary forcing data (i.e. the influence of the driving CGCM3 simulations) on simulated precipitation extremes, a comparison between regional growth curves for the validation and reference simulations would be beneficial and therefore the regional growth curves for C1–C5 simulations are developed for all the 12 regions following the same procedure as explained above and results for the selected six regions are shown in Fig. 2.2, which is also referred to in the above discussion. These growth curves exhibit similar behaviour as presented above for the VS except some noticeable differences in the extreme upper tails for some regions, e.g. YUKON and MRTMS. Thus, the effect of boundary forcing data on the shapes of the growth curves appears to be important for some regions particularly for larger return levels. The spread amongst the members (C1–C5) is particularly large for higher return periods. Nevertheless, in general, the members demonstrate similar behaviour in underestimation/overestimation dependent on the region. Twenty-, 50- and 100-year return levels for C1–C5 simulations are derived in a manner as explained above and scatter plots for selected six regions are shown in Fig. 2.4, where these return levels are plotted against the ones obtained from the VS. For some regions (e.g. MRTMS and NPLNS), an average value of return levels for C1–C5 simulations would lie close to the line of perfect match, while for others (e.g. GRTLKS and YUKON), the average value would fall below (and in some cases, much below) the line of perfect match suggesting negative boundary forcing error. For 20-, 50- and 100-year return levels of 1-day (7-day) precipitation extremes, average boundary forcing errors are -19% (-22%) for YUKON, -16% (-10%) for MACK, -13% (-16%) for EARCT1, -10% (-10%) for EARCT2, -5% (2%) for WCOAST, -0% (-4%) for WCRDRA, -3% (-5%) for NWFOR, 2% (-6%) for NPLNS, -10%

(-13%) for NEFOR1, -6% (-8%) for NEFOR2, -2% (-2%) for MRTMS and -11% (-3%) for GRTLKS regions.

Similar assessment of CRCM performance is also carried out for the GBA approach. In this approach the GEV distribution is fitted by the method of L-moments to samples of single- and multi-day observed precipitation extremes, derived from daily precipitation time series obtained by averaging the daily precipitation values recorded at stations that fall within each grid-cell. This strategy offers a mean to address the effects of ARFs because spatial averaging is a simpler form of the ARFs. Similar to the observed extremes, the GEV distribution is fitted to simulated extremes, derived from the VS. It is important to mention here that the GEV distribution is found to be the overall best fitting distribution in the RFA for majority of the single- and multi-day precipitation extremes. Because of this reason, the GEV distribution is selected for the GBA. To evaluate the CRCM performance at the grid-cell scale, scatter plots of observed vs. validation simulation quantiles for grid cells with at least two precipitation recording stations are shown in Fig. 2.5(a) for eastern and western part of the country, described in the figure caption. This strategy serves simultaneously two purposes: the CRCM performance evaluation and the effect of ARFs. The severe underestimation by the model for the eastern parts reduced considerably, particularly for multi-day precipitation extremes (Fig. 2.5a). However, the results for the western regions appear to be the same as presented earlier for the RFA approach. The effect of boundary forcing error is evaluated in Fig. 2.5b following the same strategy as used in Fig. 2.5a. This evaluation suggests that an ensemble average of various quantiles for the C1–C5 simulations would compare reasonably well with those derived from the validation simulation, suggesting reduced boundary forcing errors.

2.5.3 Projected changes to extreme precipitation events

2.5.3.1 The RFA approach

Projected changes to extreme precipitation events are studied at the regional and grid-cell scales. In order to derive these changes, it is necessary to develop regional growth curves

for F1–F5 simulations. For this purpose, the same best-fit regional distribution that is found in the validation experiment is used and the regional growth curves are developed in the same manner as for the C1–C5 simulations. For brevity, the plots of future regional growth curves are not shown.

From the regional growth curves for each of the reference and future simulations, growth factors are derived for 20- 50- and 100-year return periods. After that, averaged l_1 values (denoted l_{1R}) for each region for the reference and future periods are obtained. For each pair of the reference and future period simulations (i.e. C1~F1, C2~F2, C3~F3, C4~F4 and C5~F5), regional return levels are derived from respective regional growth factors and l_{1R} values. These five pairs, for each of the 20-, 50- and 100-year return levels, can serve as the basis to derive range of changes (i.e. maximum and minimum values) in regional-scale return levels. Ensemble averaged 20-, 50- and 100-year regional return levels, shown in Fig. 2.6, are derived from the averaged regional growth factors and averaged l_{1R} values for the C1–C5 reference simulations.

Regional level projections

The lowest regional level increase (3–8 mm) in the 20-year return levels of 1-day to 7-day precipitation events is found for northern (YUKON, MACK, EARCT1 and EARCT2), NWFOR, NPLNS and MRTMS regions, while the largest increase (5–13 mm) is found for WCOAST and NEFOR1 regions. In terms of percentage increase, for the 20-year return levels of 1-day to 7-day precipitation events, the lowest increase (5–11%) is found for NPLNS, MRTMS and GRTLKS, while the largest increase (12–18%) is found for northern (YUKON, MACK, EARCT1 and EARCT2), and NEFOR1 regions.

The 50- and 100-year regional return levels of 3- and 7-day events are projected to increase by 13–17% for NEFOR1 and those for northern (YUKON, MACK, EARCT1 and EARCT2) regions are projected to 12–19% increase (Fig. 2.7). The lowest percentage increase of 3–4% and 10% is noted respectively for MRTMS and NPLNS for 1-day events,

and that for 7-day events is 6% and 9%, respectively. For the remaining regions, percentage increase lies in the 10–13% range for 50- and 100-year return levels of 1-day to 7-day precipitation extremes.

Grid-cell level projections

To downscale regional return levels to grid cells for more detailed spatial information, ensemble averaged regional growth factors are multiplied by the corresponding ensemble averaged grid-cell level l_1 values. These detailed spatial diagrams for 20-, 50- and 100-year return levels for the reference period are shown in Fig. 2.8. An interesting feature of these diagrams is that they still maintain the statistical homogeneity of various regions and additionally provide more spatial details of changes.

For 20-year return level, the dominant increase varies between 4–10 mm for 1-day events and between 9–18 mm for 7-day events. Maximum increases of the order of 16–24 mm for 3-day events and of the order of 18–33 mm for 7-day events are found over WCOAST, WCRDRA and NEFOR1 (figure not shown). Relatively smaller changes as well as areas with negative changes appear in some parts of northern (YUKON, MACK, EARCT1 and EARCT2), NWFOR, NPLNS and MRTMS regions. For 50- and 100-year return levels of 1-day events, overall dominant increase in magnitude is between 3 and 10 mm, while for 7-day events it is between 8 and 18 mm. Maximum increases (10–18mm) appear over WCOAST, NEFOR1 and GRTLKS regions for 1-day events and they reach up to 18 and 35 mm for 7-day events.

In terms of percentage increase, for 20-year return levels of 1- to 7-day events, there are significant areas with largest relative increase of more than 28% in northern (EARCT1, EARCT2 and MACK) regions (Fig. 2.9). Some areas in the WCRDRA, NWFOR and NPLNS show negative changes (-1 to -4%) for 20-year return levels. Compared to areas with relative increases, the areas with relative negative changes are much less widespread with the minimum values of -2 to -5%. For higher return levels for single- and multi-day events, an

increase of 10–22% in magnitude over all regions is noted. The pattern of spatial distributions of maximum relative increases and decreases remain almost the same as for the 1- to 7-day extreme precipitation events.

2.5.3.2 The GBA approach

For the GBA approach, analysis is performed for each grid-cell individually and hence it is expected that this approach may provide some additional details about changes in precipitation extremes. The GBA is implemented by fitting the GEV distribution to grid-cell based extreme precipitation amounts derived from reference (C1–C5) and future (F1–F5) simulations. Grid-cell based ensemble averaged 20-, 50- and 100-year return levels are derived as explained in the section of methodology and their resulting spatial distributions for the reference period are shown in Fig. 2.10, for 1-, 3- and 7-day precipitation extremes.

For 20-year return level of 1-day events, dominant changes in magnitude from 3–10 mm are found in majority of the Canadian regions (figure not shown). Areas with most prominent change, up to 15 mm, are found in WCOAST, eastern part of NEFOR2, NEFOR1, MRTMS and GRTLKS. The WCRDRA, NWFOR, NPLNS and southern MRTMS show the lowest decrease and even negative change in some areas. A similar pattern is found for longer duration events but with dominant changes of 5–15 mm and 10–20 mm for 3- and 7-day events, respectively.

For higher return levels, the spatial distribution of increases and decreases in 1-day events is similar to that of 20-year return level but with slightly higher values for changes, e.g. 5–20 mm for 100-year return level. The largest increases (up to 30 mm) are found in MACK, WCRDRA, NWFOR, NEFOR1, MRTMS and GRTLKS. For 7-day events, central and western regions exhibit increases up to 32 mm and 73 mm for 50- and 100-year return levels, respectively. Decreases of -1 to -20 mm are widespread for 7-day events and tend to be larger in grid boxes located in WCRDRA, NWFOR, NPLNS, NEFOR1 and MRTMS.

In terms of percentage changes, 5–30% increase in 20-year return level of 1-day events is dominant in all regions (Fig. 2.11). Decreases of -5 to -15% are mainly distributed in WCRDRA, NWFOR, NPLNS, NEFOR2 and MRTMS but are present also in northern regions with lower values of change. For 7-day events, significant areas with 21–45% increase are noticed in northern regions, north-eastern part of NPLNS and northern part of NEFOR1, while areas with decreases of -3 to -11% are concentrated in WCRDRA, NWFOR, NPLNS and MRTMS. For 50- and 100-year return levels of 1-day events, dominant increases are of the order of 10–50% and 10–60%, respectively. For higher return periods, distribution of decreases remains the same as for the 20-year return level, noticed in isolated grid-cells within regions and dominant range of change from 0 to -5 %. For the 50- and 100-year return levels of 7-day events, 2–20% and 5–25% increases, respectively, are dominant. Maximum increases of 25–50% for 50-year return level and 30–62% for 100-year return level are distributed over northern regions. Decreases for 50-year return level and for 100-year return level are present in NWFOR, NPLNS, NEFOR1 and MRTMS regions.

2.5.3.3 Estimating uncertainty

Usually, uncertainty is expressed in the form of a confidence interval for a given return level. For the RFA approach, this relates to the range in which the regional growth curves can be expected to lie. Therefore, an estimate of uncertainty in the regional growth curves for each of the five pairs of reference and future period simulations is carried out using the nonparametric vector bootstrap resampling method (Efron and Tibshirani, 1993; GREHYS, 1996; Davison and Hinkley, 1997; Khaliq et al., 2009). Firstly, this method is followed not only to address the issues of randomness but also the influence of first-order spatial correlations on estimates of uncertainty and secondly, to examine how the uncertainty intervals vary across various CRCM ensemble members. For each of the 12 regions and for each of the ensemble members, $B = 999$ resamples are used to develop $(1-\alpha)\%$, where α is the significance level, confidence intervals using the test-inversion approach (Carpenter, 1999; Faulkner and Jones, 1999; Burn, 2003). For implementing this approach, bootstrap residuals, $e_i = y_i^T - y^T$, where y^T is an estimate of the T-year regional growth factor for each of the C1–C5 and F1–F5 simulations, are ranked in an ascending order to obtain

$m = \frac{\alpha}{2}(B+1)$ and $p = (1-\frac{\alpha}{2})(B+1)$ percentile values. For a $(1-\alpha)\%$ confidence interval, this means choosing the *m*th and *p*th e_i values and obtaining the confidence interval as $(y^T - e_p,\ y^T - e_m)$. These intervals and the y^T values are multiplied by the regionally averaged l_1 (i.e. l_{1R}) to obtain an estimate of uncertainty as well as the regional return level. The results of this analysis, with $\alpha = 5\%$, are shown in Fig. 2.12 for six selected regions. Altogether for all the 12 regions and for 1-, 3- and 10-day precipitation extremes, one could perform 180 comparisons of $(1-\alpha)\%$ confidence intervals for each of the 20-, 50- and 100-year return levels for the reference and future simulations. If for any comparison the confidence intervals do not overlap, then it would be a clear indication that the change for a given return level, from reference to future climate conditions, is statistically significant. For 20-, 50- and 100-year regional return levels, the percentage number of comparisons, where the confidence intervals do not overlap, is given in Table 2.1. The results suggest significant increases in the regional-scale 20-year return levels for most of the regions except MRTMS and NPLNS, where the percentage number of significant changes is not as high as for other regions. Although 50- and 100-year return levels are projected to increase over all regions, the increases are not as strongly significant as for the 20-year return level.

An alternate approach for developing confidence intervals is to obtain an estimate of the bootstrap standard deviation from y_i^T values which is commonly referred to as standard error of y^T, i.e. $SE(y^T)$, and then estimate confidence intervals using the Gaussian assumption. According to this approach, 95% confidence interval is given by $[y^T \pm 1.96 \times SE(y^T)]$. This would result in symmetric confidence intervals unlike the test-inversion approach which leads to asymmetric confidence intervals. The results of this latter approach, provided in Table 2.1, for 20-, 50- and 100-year return levels for all regions, and in Fig. 2.13, for six selected regions, also suggest the same conclusions as presented above for the test-inversion approach. Thus, the above conclusions drawn using the test-inversion approach remain almost valid with the *SE*-based approach. Similar uncertainty analysis for

the GBA-based results is also possible but it was not attempted. It is important to mention that much narrow and almost symmetric confidence intervals than the ones shown in Fig. 2.12 and 2.13 resulted when the effects of spatial correlations were ignored indicating that ignoring spatial dependence of CRCM grid-cell-based precipitation extremes can result in incorrect estimates of uncertainty.

2.6 Discussion and conclusions

In this study, the CRCM transient climate change simulations are used to study projected changes to precipitation extremes over Canada. An ensemble of ten 30-year simulations is considered: five simulations are for the reference (1961–1990) climate and the other five are the corresponding simulations for the future (2041–2070) climate, which were driven by different members of an ensemble of CGCM3 following the IPCC SRES A2 scenario (Nakićenović et al., 2000). A validation simulation of the CRCM, for the 1961–1990 period, when driven by reanalysis ERA40 (i.e. so called, near perfect boundary conditions) in conjunction with the rehabilitated and homogenized precipitation records of 495 stations, located across Canada, are used to evaluate performance of the CRCM. Two complementary modelling approaches (i.e. the RFA and GBA) are used to study performance of the CRCM and projected changes to characteristics of precipitation extremes. The RFA approach relies heavily on the notion of statistical homogeneity of Canadian climatic regions and hence provides information about projected changes on a regional scale (i.e. a large-scale view of changes). Compared to this, the GBA approach provides information about projected changes on the CRCM grid-cell-scale. The results presented should be assessed with caution due to the lack of high quality observational records, particularly for the northern Canadian regions for performing validation, and limitations of the CRCM. It is important to mention here that Emori et al. (2005) showed that the simulation of extreme daily precipitation may be significantly dependent on model parameterization. Therefore, formulation of RCMs contributes significantly to uncertainties involved in extreme precipitation assessments. In that respect, future improvements of model parameterization and changes in scenario development may produce different, perhaps better, estimates than the ones presented in this

study. However, it is less likely that the sign of change will vary significantly for many parts of Canada.

For most of the Canadian climatic regions, the CRCM integrations for the reference climate, in general, produce results that are statistically consistent with observed distributions of precipitation extremes, given the widespread understanding that the grid-cell-based precipitation, simulated by climate models, exhibit characteristics of spatially averaged precipitation compared to point estimates, which are known to be much higher than the areal average precipitation. With this assertion, the transient climate change integrations of the CRCM can be used with some confidence to estimate future distributions of precipitation extremes.

From the analysis presented in this study, the following conclusions can be drawn:

1. Seven of ten original Canadian climatic regions (YUKON, MACK, WCOAST, NWFOR, NPLNS, GRTLKS and MRTMS) satisfy homogeneity criteria required for performing RFA of single- and multi-day precipitation extremes. In order to perform meaningful RFA, two of three remaining regions (EARCT and NEFOR) are divided into two sub-regions using the cluster analysis algorithm. However, the same algorithm did not result in useful contiguous subdivisions of the WCRDRA region and hence the results of RFA for this region could be questioned.
2. For YUKON, MACK, NWFOR, NEFOR1, GRTLKS, MRTMS regions, GEV is found to be the most suitable regional distribution for modeling precipitation extremes, while GNO is the most suitable regional distribution for WCOAST, WCRDRA, NPLAINS and NEFOR2 regions. PE3 is most suitable for EARCT2 region and GLO for EARCT1. Overall, GEV is found to be the most suitable distribution for modeling the majority of single- and multi-day precipitation extremes. However, to perform RFA, the identified most suitable regional distribution is used for each of the twelve regions.
3. On regional basis, northern Canadian climatic regions (MACK, EARCT1 and EARCT2) exhibit the lowest absolute but highest percentage change in 20-, 50- and

100-year return levels of precipitation extremes. The range of absolute changes in 20-year return levels of 1- to 7-day extremes is the minimum, between 3-8 mm, for northern regions, NWFOR, NPLNS and MRTMS and maximum, between 5-13 mm, for WCOAST and NEFOR1. The projected changes in regional return levels for 20-year return period are more likely to be statistically significant than those of the 50- and 100-year return periods, suggesting that return levels of small return periods are more sensitive to climate change. It is also possible that 30 years of data are not sufficient to estimate 50- and 100-year future return levels.

4. Dominant range of projected changes for the 20-year return levels, realized using the RFA approach, at the CRCM grid-cell level is between 4-10 mm for 1-day precipitation extremes and it increases to 9-18 mm for 7-day extremes. For 50- and 100-year return levels, this range of projected change does not vary much. Negative changes are found mostly in southern parts of the study domain for scattered grid cells, but with no coherent patterns at the regional level.
5. For the GBA approach, dominant projected changes in 20-year return levels of 1-day precipitation extremes is between 3-10 mm and it increases to 5-15 mm and 10-20 mm for 3- and 7-day precipitation extremes, respectively. Negative changes at grid-cell scale are present nearly in all climatic regions. Though negative changes of larger magnitude are noticed, majority of these changes lie in the range from zero to -5%.
6. The results of the projected changes, realized with the RFA and GBA approaches, at the CRCM grid-cell level are more similar for the 20-year return period than for the 50- and 100-year return periods, suggesting that GBA approach suffers from small sample uncertainties for higher return periods.
7. Concerning practical implications, it is expected that increase in magnitude for short (i.e. 1-day) and longer (i.e. 7-day) duration precipitation extremes will have severe implications for various water resource related development and management activities such as combined sewer systems, flood control and water storage systems, etc.
8. Since uncertainties related to the choice of a regional distribution for frequency analysis of single- and multi-day precipitation extremes and spatial correlations for

deriving confidence intervals are taken into account when assessing significance of changes, future directions and challenges involve apportionment of sources of uncertainty coming from scenario development and model parameterization as well as other unidentifiable factors.

Acknowledgements

This research is funded by the Canadian Foundation for Climate and Atmospheric Sciences (CFCAS), MITACS, Ouranos Consortium and Pacific Climate Impacts Consortium. Thanks are due to Éva Mekis, from Atmospheric Science and Technology Directorate of Environment Canada, for help with the homogenized precipitation database. The Climate Simulations Team of Ouranos Consortium, for providing CRCM simulations used in this study is gratefully acknowledged.

Appendix A

Sample L-moments

L-moments are defined as certain linear combinations of probability weighted moments (PWMs). For a sample $x_1, x_2, \ldots, x_n$ of size n, sorted in an increasing order of magnitude, PWMs are defined as:

$$b_0 = \frac{1}{n}\sum_{j=1}^{n} x_j \quad \text{and} \tag{A.1}$$

$$b_r = \frac{1}{n}\sum_{j=r+1}^{n} \frac{(j-1)(j-2)\ldots(j-r)}{(n-1)(n-2)\ldots(n-r)} x_j \tag{A.2}$$

The first four L-moments which have interpretations as measures of location, dispersion and shape of the data sample are given by:

$$l_1 = b_0 \tag{A.3}$$

$$l_2 = 2b_1 - b_0 \tag{A.4}$$

$$l_3 = 6b_2 - 6b_1 + b_0 \tag{A.5}$$

$$l_4 = 20b_3 - 30b_2 + 12b_1 - b_0 \tag{A.6}$$

where the coefficients are calculated as shifted Legendre polynomials. L-moment ratios, i.e. the coefficient of L-variation (t_2), coefficient of L-skewness (t_3) and coefficient of L-kurtosis (t_4) are respectively defined by:

$$t_2 = l_2/l_1, \quad t_3 = l_3/l_2, \quad \text{and} \quad t_4 = l_4/l_2 \tag{A.7}$$

Theoretical L-moments and selected candidate distributions

For each of the five selected distributions, the form of the cumulative distribution function [$F(x)$] and expressions for the L-moments (λ_1 : L-mean; λ_2 : L-standard deviation; τ_3 : L-skewness; τ_4 : L-kurtosis) in terms of distribution parameters [commonly referred to as location (ξ), scale (α) and shape parameters (k)] are given here:

Generalized Pareto distribution (GPA):

$$F(x) = 1 - \{1 - k(x-\xi)/\alpha\}^{\frac{1}{k}}, \ \xi \le x \le \xi + \frac{\alpha}{k} \text{ if } k > 0 \qquad \xi \le x < \infty \text{ if } k \le 0 \tag{A.8}$$

$$\lambda_1 = \xi + \frac{\alpha}{1+k}; \ \lambda_2 = \frac{\alpha}{(1+k)(2+k)}; \ \tau_3 = \frac{(1-k)}{(3+k)}; \ \tau_4 = \frac{(1-k)(2-k)}{(3+k)(4+k)} \tag{A.9}$$

Generalized Extreme Value distribution (GEV):

$$F(x) = \exp[-\{1 - k(x-\xi)/\alpha\}^{\frac{1}{k}}], \ -\infty \le x \le \xi + \frac{\alpha}{k} \text{ if } k > 0 \qquad \xi + \frac{\alpha}{k} \le x < \infty \text{ if } k < 0 \tag{A.10}$$

$$\lambda_1 = \xi + \frac{\alpha}{k}[1 - \Gamma(1+k)]; \ \lambda_2 = \frac{\alpha}{k}(1 - 2^{-k})\Gamma(1+k); \ \tau_3 = 2\frac{(1-3^{-k})}{(1-2^{-k})} - 3; \tag{A.11}$$

$$\tau_4 = \frac{\{5(1-4^{-k}) - 10(1-3^{-k}) + 6(1-2^{-k})\}}{(1-2^{-k})}$$

Generalized Logistic distribution (GLO):

$$F(x) = [1 + \{1 - k(x-\xi)/\alpha\}^{\frac{1}{k}}]^{-1}, \ -\infty < x \le \xi + \frac{\alpha}{k} \text{ if } k > 0 \qquad -\infty < x < \infty \text{ if } k = 0 \qquad \xi + \frac{\alpha}{k} \le x < \infty \text{ if } k < 0 \tag{A.12}$$

$$\lambda_1 = \xi + \alpha\left(\frac{1}{k} - \frac{\pi}{\sin k\pi}\right);\ \lambda_2 = \frac{\alpha k\pi}{\sin k\pi};\ \tau_3 = -k;\ \tau_4 = \frac{\left(1+5k^2\right)}{6} \tag{A.13}$$

Pearson Type III distribution (PT3):

$$F(x) = \left\{ \begin{array}{l} G\left(\dfrac{(x-\mu+2\frac{\sigma}{\gamma})}{\left|\frac{1}{2}\sigma\gamma\right|}, \dfrac{4}{\gamma^2}\right),\ \gamma > 0, \xi \le x < \infty \\ 1 - G\left(\dfrac{-(x-\mu+2\frac{\sigma}{\gamma})}{\left|\frac{1}{2}\sigma\gamma\right|}, \dfrac{4}{\gamma^2}\right),\ \gamma < 0, -\infty < x \le \xi \end{array} \right\} \tag{A.14}$$

$$\lambda_1 = \xi + \alpha\beta;\ \lambda_2 = \frac{\pi^{-\frac{1}{2}}\beta\Gamma(\alpha+\frac{1}{2})}{\Gamma(\alpha)};\ \tau_3 = 6I_{\frac{1}{3}}(\alpha,2\alpha) - 3 \tag{A.15}$$

This parameterization is in terms of the first three conventional moments of the distribution: the mean (μ), the standard deviation (σ) and the skewness (γ). $G(x,\alpha) = \{\Gamma(\alpha)\}^{-1}\int_0^x t^{\alpha-1}e^{-t}dt$ is the incomplete gamma integral, while $I_x(p,q) = \dfrac{\Gamma(p+q)}{\Gamma(p)\Gamma(q)}\int_0^x t^{p-1}(1-t)^{q-1}dt$ is the incomplete beta function ratio. There is no simple expression for τ_4. However, rational-function approximation can be found in Hosking and Wallis (1997).

Generalized Normal distribution (GNO):

$$F(x)=\Phi\left[-k^{-1}\log\left(\left\{1-\frac{k}{\alpha}(x-\xi)\right\}\right)\right],-\infty<x<\xi+\frac{\alpha}{k}\ \text{if}\ k>0 \qquad (A.16)$$

$$-\infty<x<\infty\ \text{if}\ k=0$$

$$\xi+\frac{\alpha}{k}<x<\infty\ \text{if}\ k<0$$

$$\lambda_1=\xi+\frac{\alpha}{k}\left(1-e^{\frac{k^2}{2}}\right);\lambda_2=\frac{\alpha}{k}e^{\frac{k^2}{2}}\{1-2\Phi(\frac{-k}{\sqrt{2}})\} \qquad (A.17)$$

Where $\Phi(x)=(2\pi)^{-\frac{1}{2}}\int_{-\infty}^{x}\exp(\frac{-t^2}{2})dt$ is the standard Normal cumulative distribution function. There are no simple expressions for the L-moment ratios τ_3 and τ_4, but rational-function approximations can be found in Hosking and Wallis (1997).

Appendix B

The Z goodness-of-fit test

In order to select a more appropriate regional distribution from the GEV, GPA, GLO, PE3 and GNO distributions for developing regional growth curves, the *Z*-statistic developed by Hosking and Wallis (1997) is used. This statistic is given by:

$$Z^{DIST}=\frac{1}{\sigma_4}(\tau_4^{DIST}-\tau_4^R+B_4) \qquad (B.1)$$

where τ_4^{DIST} is the theoretical L-kurtosis, τ_4^R is the weighted regional L-kurtosis and σ_4 and B_4 are given by

$$\sigma_4=\left\{\frac{1}{N_{SIM}}\left[\sum_{m=1}^{N_{SIM}}\left[\tau_4^{(m)}-\tau_4^R\right]^2-N_{SIM}B_4^2\right]\right\}^{\frac{1}{2}} \qquad (B.2)$$

$$B_4 = \frac{1}{N_{SIM}} \sum_{m=1}^{N_{SIM}} \left[\tau_4^{(m)} - \tau_4^R \right] \tag{B.3}$$

where N_{SIM} is the number of simulations and $\tau_4^{(m)}$ is the regional average L-kurtosis for the mth simulated region. Five hundred simulations ($N_{SIM} = 500$) are used to evaluate Z-statistic. A candidate distribution passes the Z goodness-of-fit test, for instance, at 5% significance level, if the $| Z^{DIST} | < 1.96$.

FIGURES

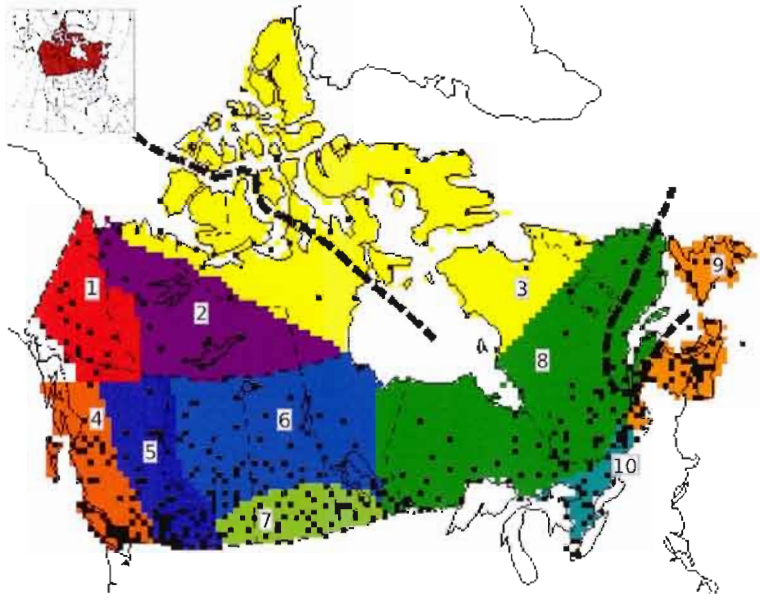

Figure 2.1 Canadian climatic regions: 1–YUKON, 2–MACK, 3–EARCT, 4–WCOAST, 5–WCRDRA, 6–NWFOR, 7–NPLNS, 8–NEFOR, 9–MRTMS and 10–GRTLKS. Each of the EARCT and NEFOR regions are divided into two sub-regions, i.e. (EARCT1 and EARCT2) and (NEFOR1 and NEFOR2), respectively. These divisions are shown by dotted lines; the region above (below) the dotted line is EARCT1 (EARCT2) and the same description is applicable for NEFOR region. Black squares correspond to spatial distribution of CRCM grid cells, where at least one observation station is found. Experimental domain of the CRCM is shown in the inset.

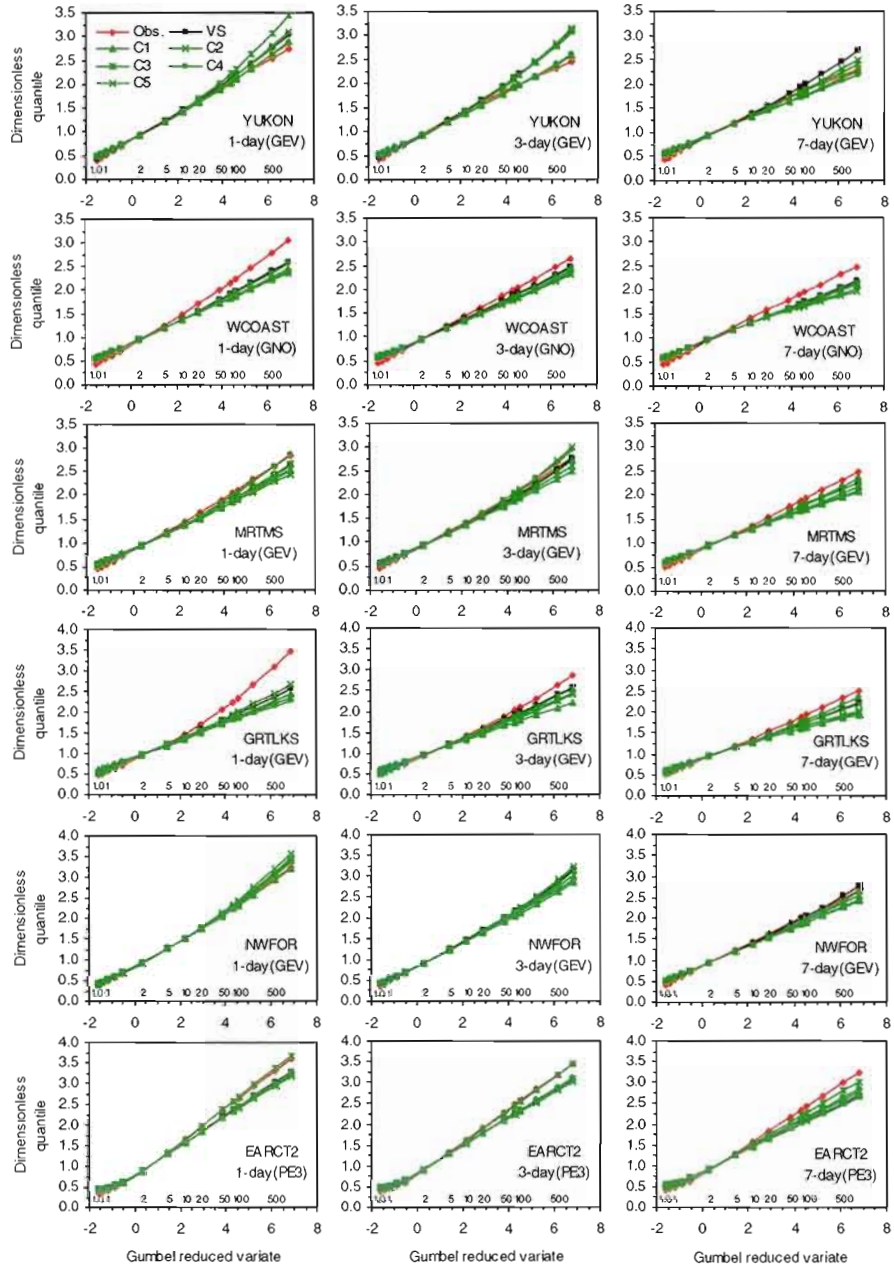

Figure 2.2 Comparison of regional growth curves for 1-, 3- and 7-day annual (April–September) maximum precipitation amounts, derived from the observed data, validation simulation (VS) and reference simulations (C1–C5), for six selected regions. The plots are developed on Gumbel probability paper, wherein the inner scale along the x-axis shows return periods. The best fitting regional distribution is indicated in each panel.

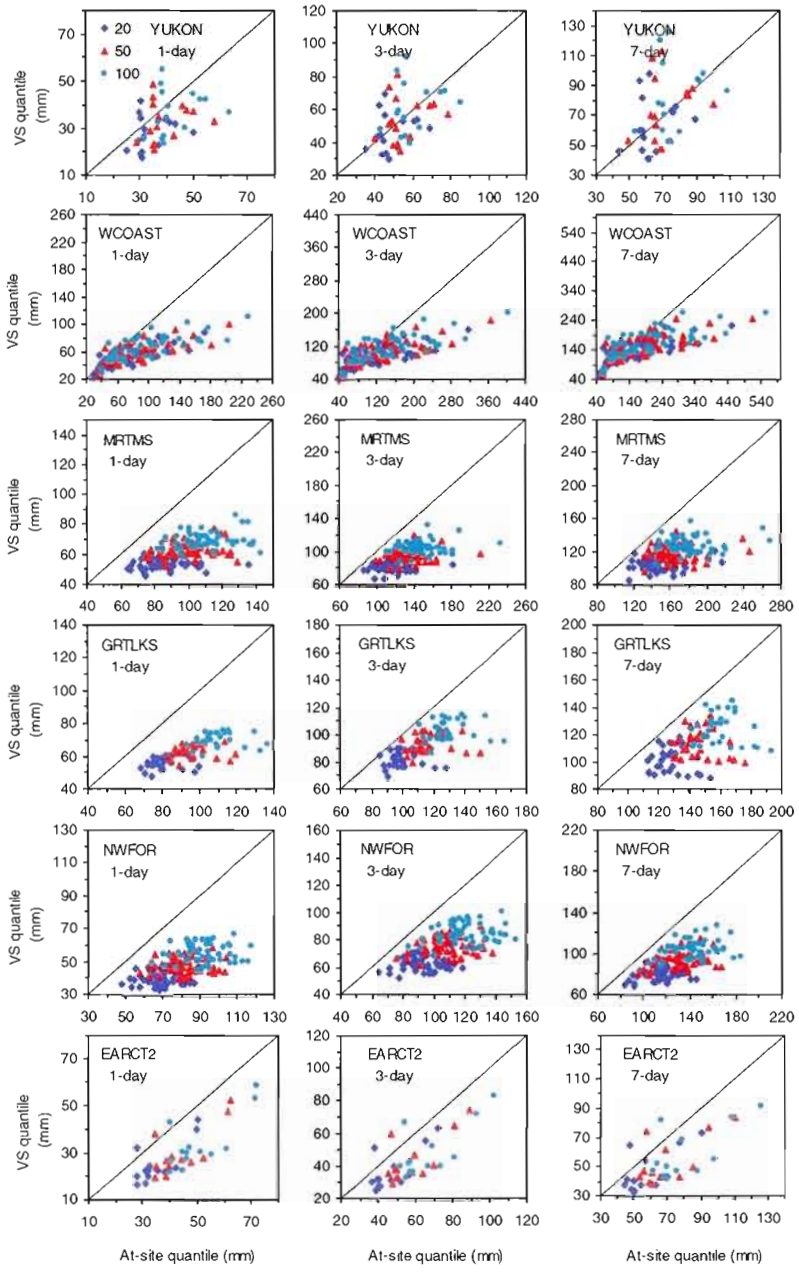

Figure 2.3 Scatter plots of 20-, 50- and 100-year return levels/quantiles of 1-, 3- and 7-day precipitation extremes derived from observations (shown along the x-axis) and validation simulation (VS) (shown along the y-axis) for the period 1961–1990. Results for six selected regions are shown only.

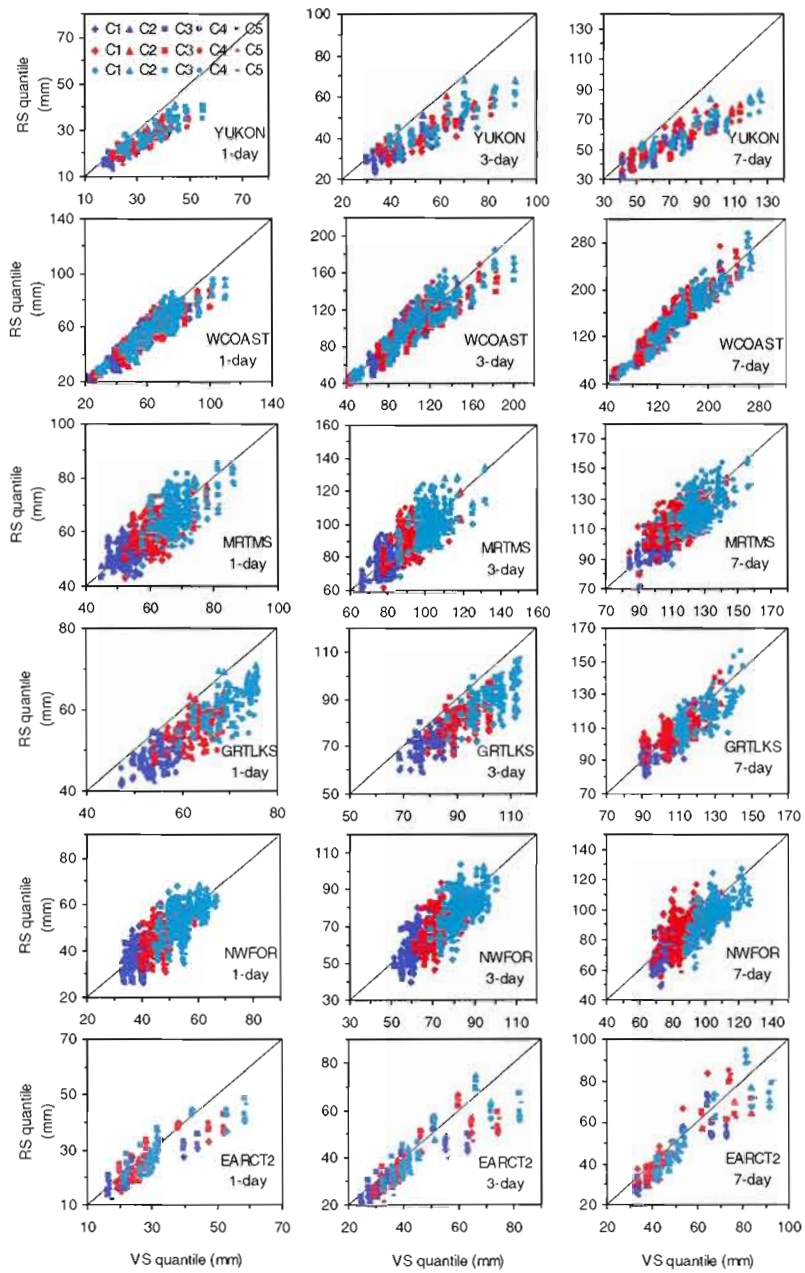

Figure 2.4 Scatter plots of 20- (dark blue), 50- (red) and 100-year (light blue) return levels/quantiles of 1-, 3- and 7-day precipitation extremes derived from the validation (shown along the x-axis) and reference (C1–C5) simulations (shown along the y-axis) for the period 1961–1990 for six selected regions.

a)

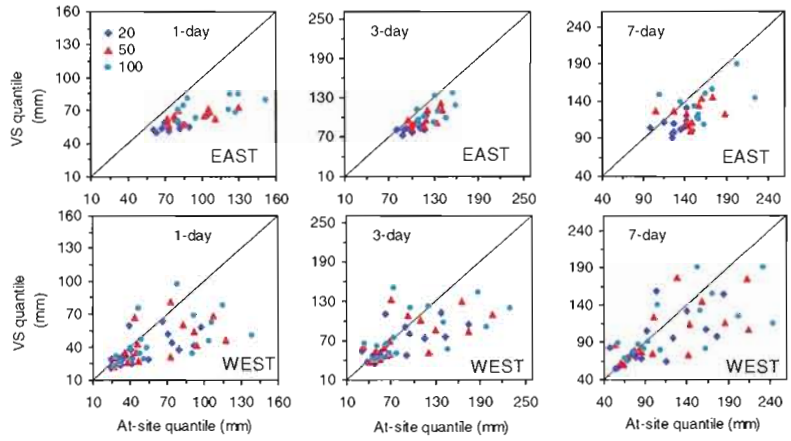

b)

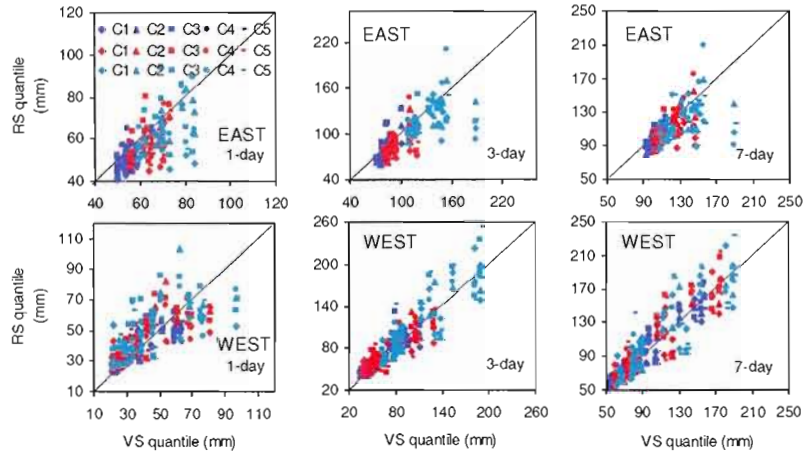

Figure 2.5 (a) Scatter plots of 20-, 50- and 100-year return levels/quantiles of 1-, 3- and 7-day precipitation extremes derived from observations (shown along the x-axis) and validation simulation (VS) (shown along the y-axis) using the GBA approach for the period 1961–1990, considering only those grid cells where at least two precipitation recording stations are found; (b) scatter plots of 20- (dark blue), 50- (red) and 100-year (light blue) return levels derived from the VS and reference simulations (C1–C5) for the period 1961–1990. EAST refers to GRTLKS, MRTMS, NEFOR1 and NEFOR2 regions, while WEST refers to WCOAST and WCRDRA regions.

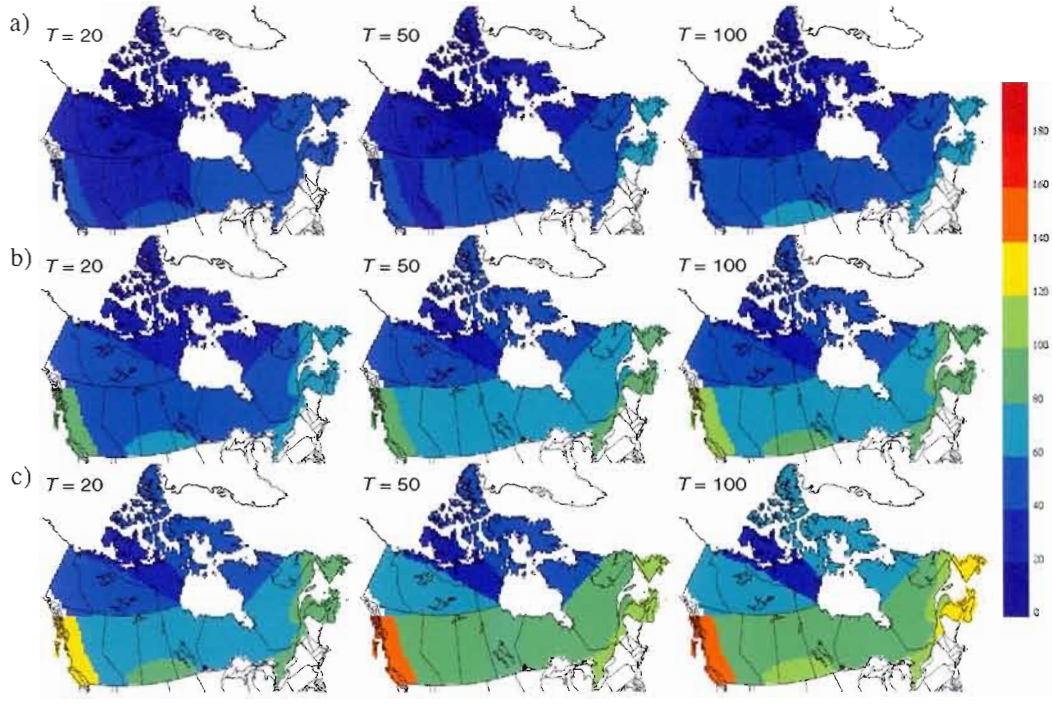

Figure 2.6 Spatial distributions of regional level 20-year (left column), 50-year (middle column) and 100-year (right column) return levels of (a) 1-day, (b) 3-day and (c) 7-day precipitation extremes for the reference (1961–1990) period. A common legend (in mm) is used for all these plots.

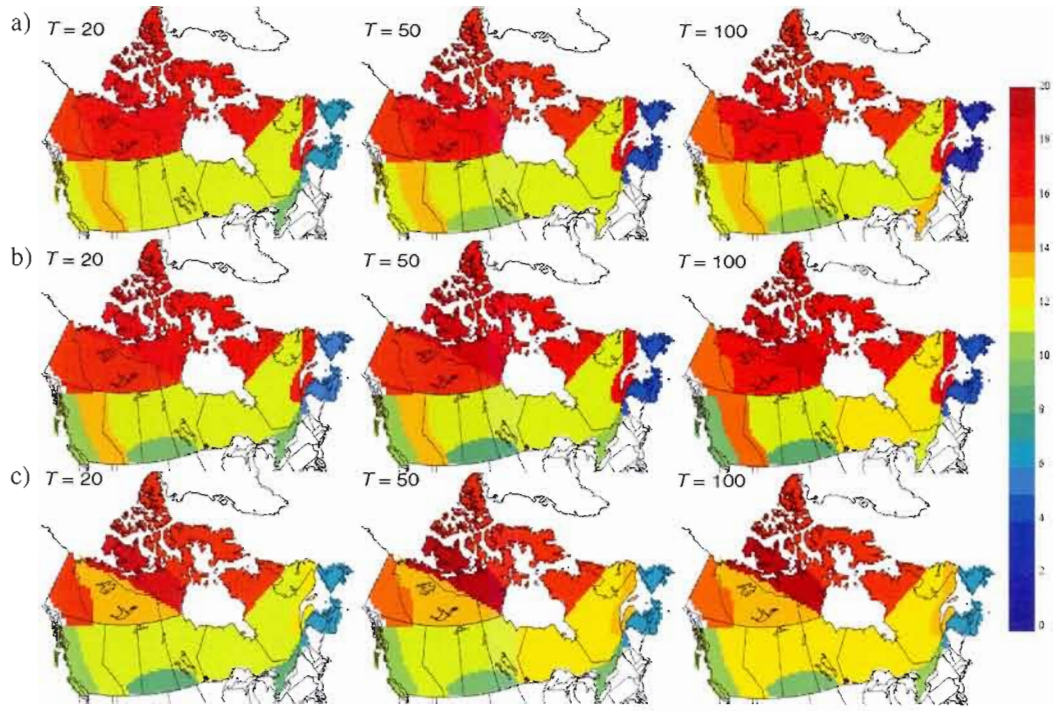

Figure 2.7 Spatial distribution of percentage change (increase/decrease) in 20-year (left column), 50-year (middle column) and 100-year (right column) regional return levels for (a) 1-day, (b) 3-day and (c) 7-day precipitation extremes.

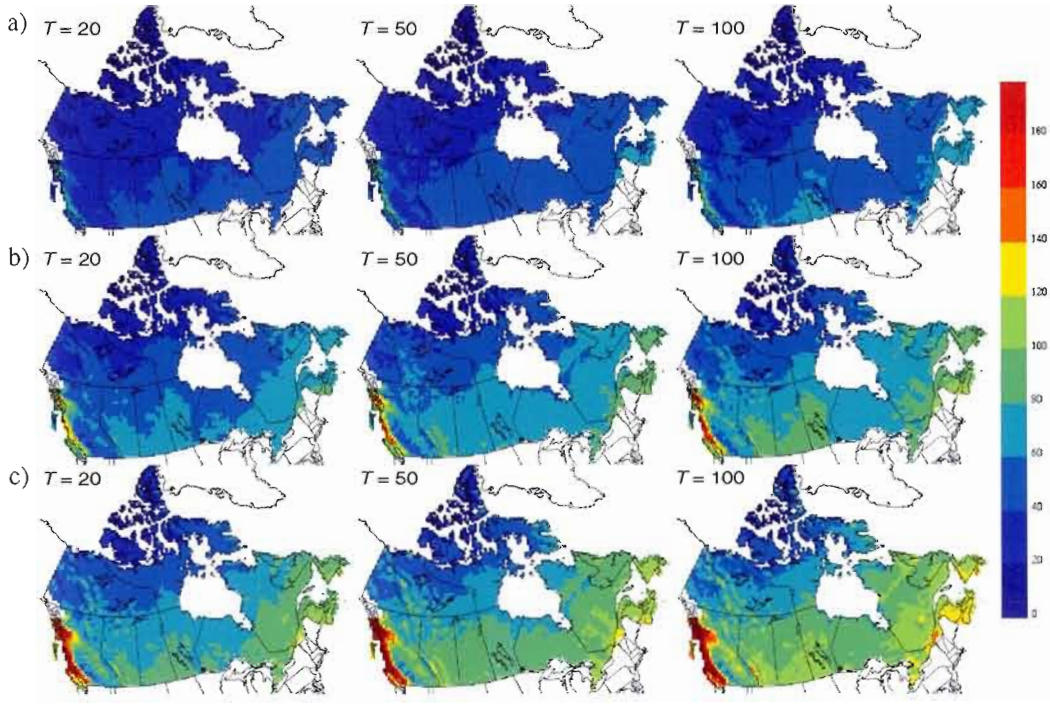

Figure 2.8 Spatial distributions of 20-, 50- and 100-year return levels of 1-, 3- and 7-day precipitation extremes at the CRCM grid-cell level, for the reference (1961–1990) period obtained using the RFA approach. Remaining notation is the same as in Figure 2.6.

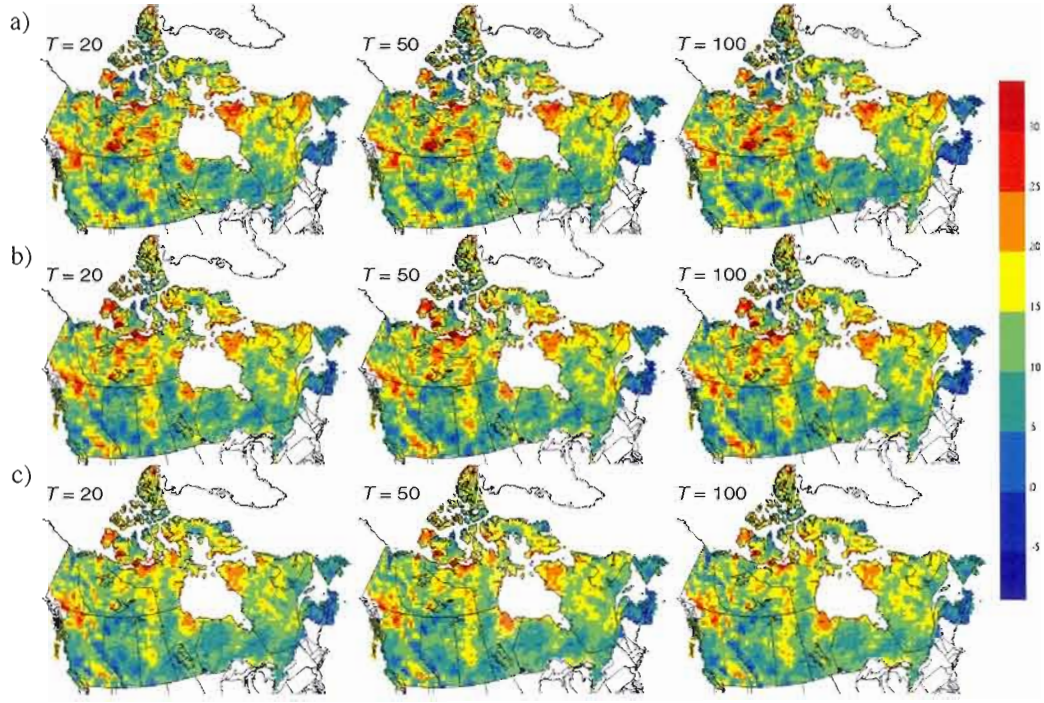

Figure 2.9 Spatial distribution of percentage change (increase/decrease) in 20-year (left column), 50-year (middle column) and 100-year (right column) return levels of (a) 1-day, (b) 3-day and (c) 7-day precipitation extremes at the CRCM grid cell level obtained using the RFA approach.

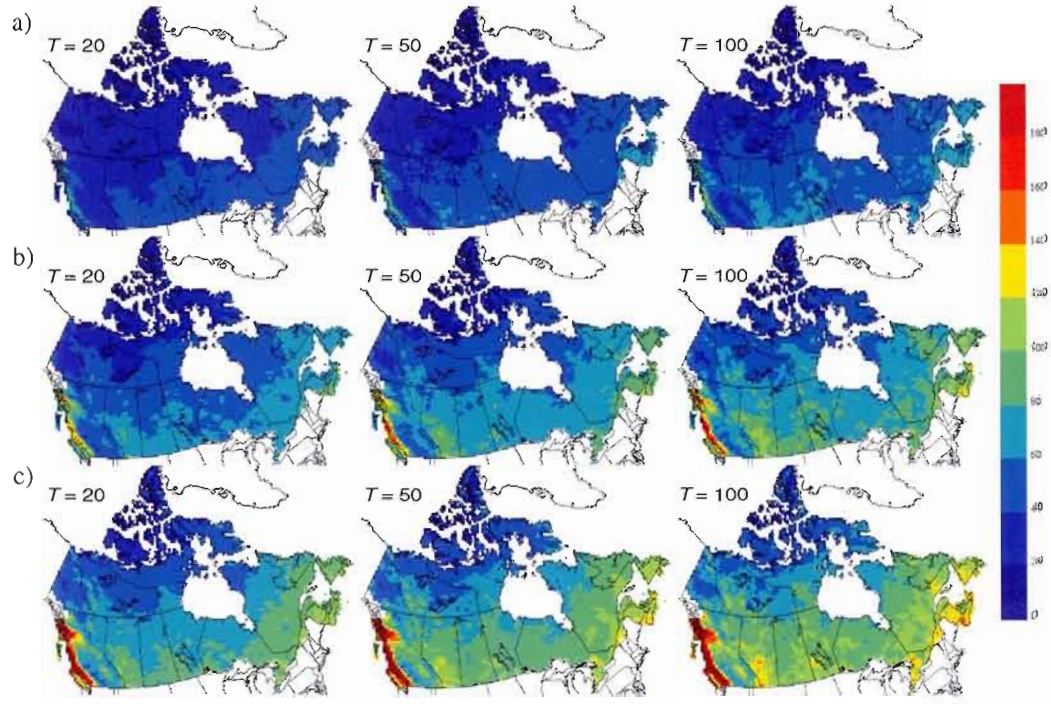

Figure 2.10 Spatial distributions of ensemble averaged 20-, 50- and 100-year return levels of 1-, 3- and 7-day precipitation extremes at the CRCM grid-cell-scale for the reference (1961–1990) period, obtained using the GBA approach. Remaining notation is the same as in Figure 2.6.

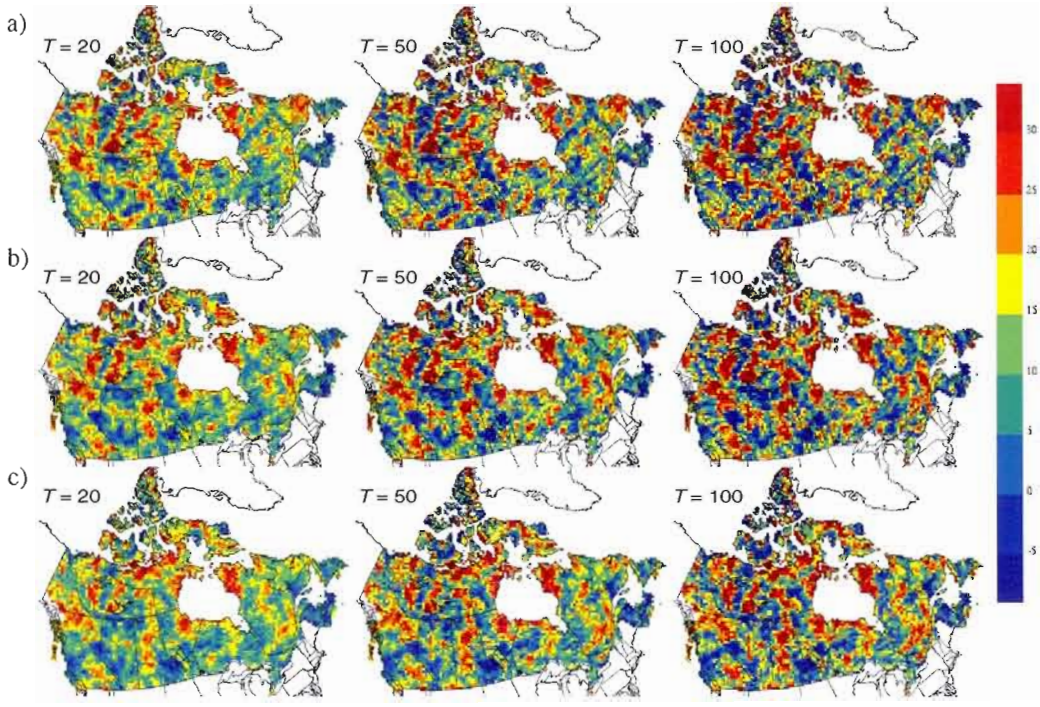

Figure 2.11 Spatial distribution of percentage change (increase/decrease) in 20-year (left column), 50-year (middle column) and 100-year (right column) return levels of (a) 1-day, (b) 3-day and (c) 7-day precipitation extremes at the CRCM grid cell level obtained using the GBA approach.

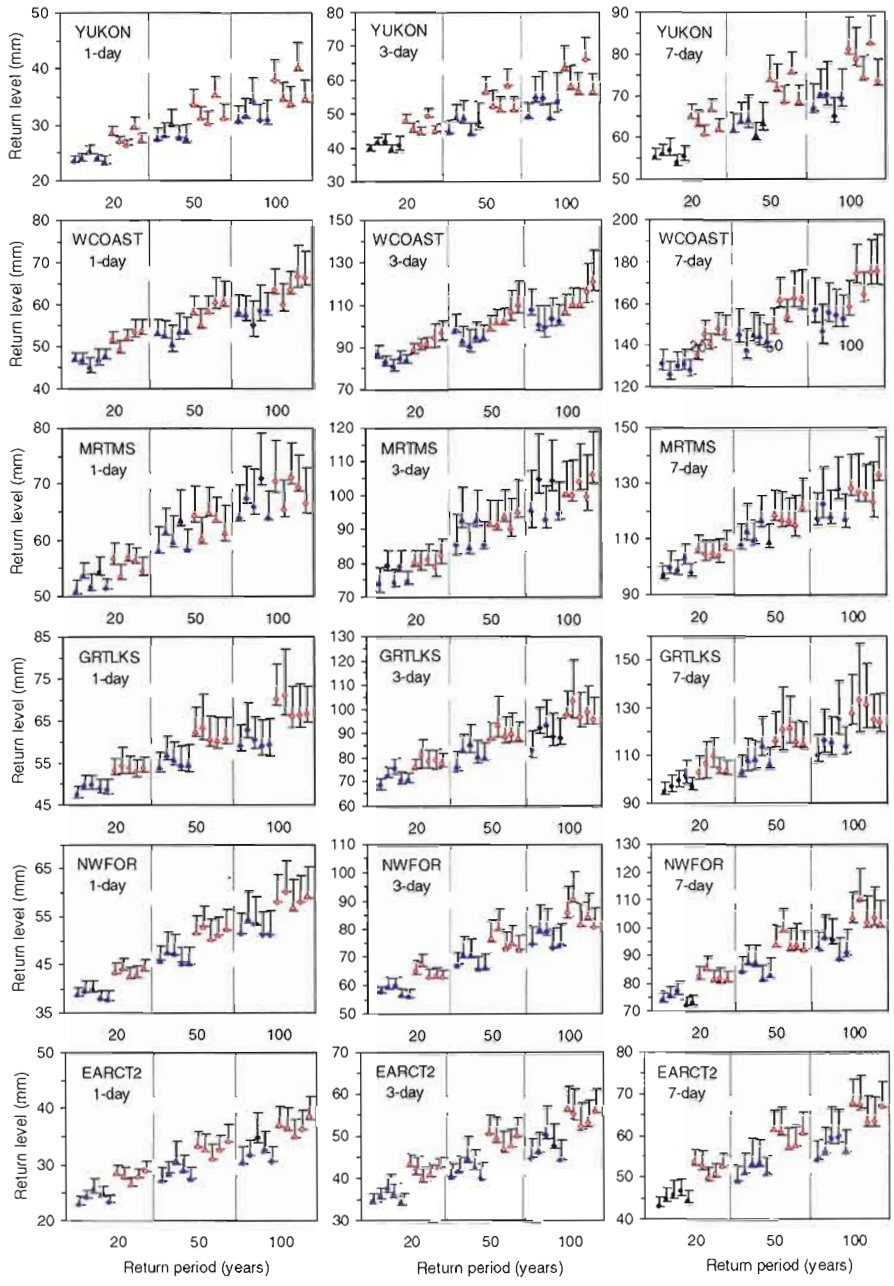

Figure 2.12 Regional scale 20-, 50- and 100-year return levels of 1-, 3- and 7-day precipitation extremes for the C1–C5 (filled blue symbols) and F1–F5 (unfilled red symbols) simulations. Vertical bars are the 95% confidence intervals obtained using the vector block bootstrap resampling approach and the test-inversion method. In each pentad, plots from left to right respectively correspond to C1–C5 simulations and the same description is applicable for F1–F5 simulations.

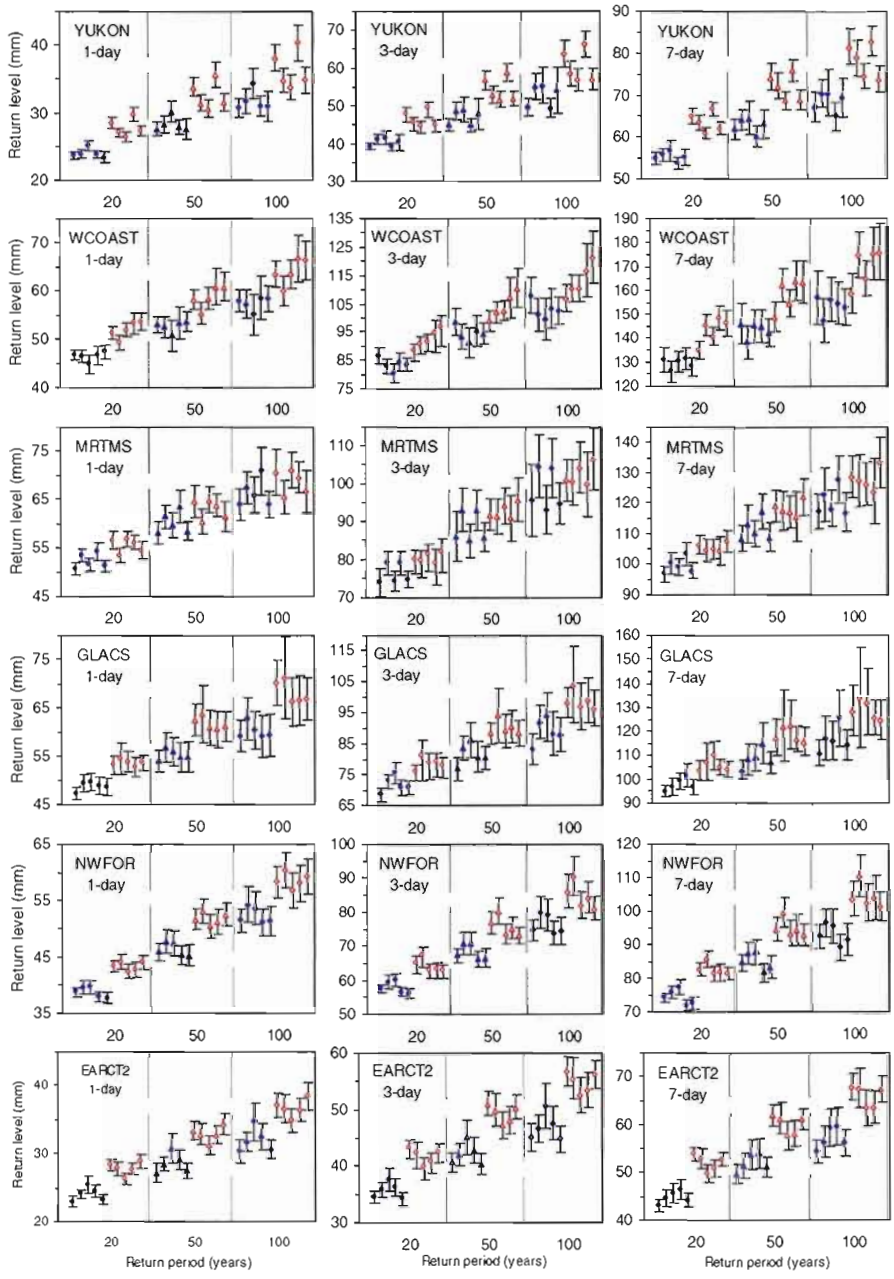

Figure 2.13 Regional scale 20-, 50- and 100-year return levels of 1-, 3- and 7-day precipitation extremes for the C1–C5 (filled blue symbols) and F1–F5 (unfilled red symbols) simulations. Vertical bars are the 95% confidence intervals obtained using the vector block bootstrap resampling approach and standard error-based method. In each pentad, plots from left to right respectively correspond to C1–C5 simulations and the same description is applicable for F1–F5 simulations.

TABLEAUX

Table 2.1 Percentage of 95% confidence interval comparisons wherein changes in 20-, 50- and 100-year regional-scale return levels of 1-, 3- and 7-day precipitation extremes are found statistically significant.

Region	Test-inversion method			Standard error based method		
	20-year	50-year	100-year	20-year	50-year	100-year
YUKON	93	93	66	93	93	67
WCOAST	87	80	60	87	80	60
MRTMS	60	53	20	53	47	20
GRTLKS	80	60	40	80	60	40
NWFOR	93	87	73	87	80	73
EARCT2	87	87	66	87	87	76
EARCT1	87	87	66	100	100	100
MACK	100	100	80	100	100	60
NEFOR1	93	93	73	93	93	67
NEFOR2	100	100	100	100	100	100
NPLNS	53	47	33	53	47	27
WCRDRA	100	93	93	100	93	80

CHAPITRE III

CONCLUSION

L'objectif principal de cette étude était d'estimer les changements projetés dans la fréquence et l'amplitude des événements de précipitations extrêmes, en utilisant des simulations du MRCC et des méthodes statistiques appropriées. Des données d'observation réhabilitées et homogénéisées de précipitation de 495 stations situées partout au Canada, avec un ensemble de simulations du MRCC pilotées par un ensemble de simulations du MCCG3 (Tableau A.1) utilisant le scénario A2 du SRES (IPCC, 2001) été utilisés pour l'analyse dans cette étude.

Les changements de 1, 2, 3, 5, 7 et 10 jours de quantités de précipitations annuelles maximales pour la période d'Avril à Septembre ont été étudiés, à l'aide des deux méthodes suivantes: RFA basée sur les L-moments et GBA. Celles-ci ont été appliquées à un ensemble d'intégrations du MRCC pour la période de référence (1961–1990) et pour le climat futur (2041–2070). La période Avril-Septembre a été choisie afin d'éviter le confusion entre les extrêmes de neige et ceux de pluie, de maintenir l'homogénéité des échantillons de précipitations extrêmes d'un point de vue physique et finalement, afin de préserver leur caractère saisonnier. Les simulations du MRCC pilotées par les MCCG3 et les réanalyses ERA40 sur la période de référence (1961–1990) ont été comparées avec les données d`observation afin d`analyser la performance du modèle et les erreurs dues au pilotage.

L'approche RFA qui repose sur l'homogénéité statistique des régions, produit des estimations plus fiables, en ce qui concerne les intensités des périodes de retour de 50 et 100 ans. Par rapport au RFA, l'approche GBA fournit quelques informations supplémentaires sur

la distribution spatiale des extrêmes. Les deux méthodes ont été utilisées avec succès dans des études antérieures (e.g. Fowler et Kilsby, 2003). Pour notre étude, on a supposé que l'hypothèse de stationnarité est respectée pour les échantillons de maximum annuel de 30 ans.

Pour l'approche RFA, l'adoption des régions climatiques homogéns définis par Plummer et al. (2006) était un bon point de départ. Sept des dix régions climatiques canadiennes (YUKON, MACK, WCOAST, NWFOR, NPLNS, GRTLKS et MRTMS) ont satisfait les critères d'homogénéité statistique, contrairement aux régions WCRDRA, EARCT et NEFOR. Pour les régions EARCT et NEFOR, une subdivision en deux sous-régions a été effectuée, alors qu'aucune subdivision utile n'a été possible pour la région WCRDRA. Selon Hosking et Wallis (1997), le nombre optimal de stations est de 20 par région. La particularité de cette région est que, même si elle contient un nombre suffisant de stations d'observation, une différence significative due notamment à la variabilité de l'altitude rend l'analyse de l'homogénéité difficile.

Parmi les cinq distributions théoriques potentielles, la GEV sèst avérée comme la distribution regionale la plus appropriée pour la modélisation des précipitations extrêmes pour les six régions climatiques canadiennes: le YUKON, MACK, NWFOR, NEFOR1, GRTLKS et MRTMS. La distribution GNO a été utilisée pour les régions WCOAST, WCRDRA, NPLAINS et NEFOR2. La distribution PE3 a été la plus appropriée pour la région EARCT2 et la distribution GLO pour EARCT1.

Pour la plupart des régions climatiques canadiennes, les simulations du MRCC pour le climat de référence produisent, en général, des résultats qui sont statistiquement consistent avec les distributions observées des précipitations extrêmes bien que le plus souvent sous-estimées pour les valeurs les plus élevées. A noter qu'il est généralement considéré que la precipitation simulée par les modèles climatiques, présente des caractéristiques moyennes spatiales beaucoup moins élevés que les précipitations moyennes locales. Aussi, les simulations du climat fait par le MRCC peuvent être utilisées avec une certaine confiance

pour estimer les distributions futures des précipitations extrêmes. Cependant, les résultats du MRCC ont indiqué une sous-estimation quasi-systématique pour les 20, 50 et 100 ans des périodes de retour pour la plupart des régions, avec une légère tendance à la surestimation de la région dans la région du YUKON. En général, le forçage aux frontières a admis des erreurs relatives négatives. Pour 20, 50 et 100 ans de niveaux de retour de 1 jour (7 jours) de précipitations extrêmes, les erreurs moyennes dues au pilotage étaient plus éleveés [-19% (-22%)] pour la région du YUKON et plus faibles [-2% (-2%)] pour MRTMS (Tableau B.4 et B.5).

Les changements prévus dans l'intensité des événements extrêmes (en mm) pour les périodes de retour étudiées sont présentés dans les figures A.16-21, et ceux en pourcentage sont présentés dans les figures 2.9-2.11 et figures A.13-15.

Au niveau régional, les changements prévus se sont révélés positifs pour toutes les régions selon l'approche RFA. Le changement futur dans les périodes de retour régionaux est plus marqué pour les régions WCOAST et NEFOR1, pour les événements de courte et de plus longue durée, tandis que dans les régions du Nord du Canada le changement absolu suggéré est plus faible avec toutefois un changement relatif plus élevé qu'ailleurs tout comme la région NEFOR1. Les régions avec un changement relatif plus faible ont été MRTMS, NPLNS et GRTLKS. La gamme de changements sur une base régionale pour la période de retour de 20 ans pour les événements de précipitations de 1 jour à 7 jours est minimale, entre 3-8 mm, pour les régions nordiques, NWFOR, NPLNS et MRTMS, alors qu'elle est maximale, entre 5 - 13 mm, pour WCOAST et NEFOR1.

Pour l'approche RFA, la gamme dominante des changements au niveau de point de grille était de l'ordre de 4-10 mm pour des événements de 1 jour, et d'une augmentation de 9-18 mm pour les événements de 7 jours. Pour les niveaux de retour de 50 et 100 ans de 1 à 7 jours la gamme des augmentations importantes n'a pas beaucoup varié d'ùne région à l'autre. Des changements négatifs ont été constatés aux différents points de la grille sans toutefois se ressentir à l'échelle régionale.

L'approche GBA a montré une grande variabilité spatiale, qui a été particulièrement évidente dans WCOAST, MRTMS et GRTLKS, ainsi que dans les régions centrales, i.e. NWFOR, NPLNS et WCRDRA. Dans toutes les régions, le GBA a prévu des diminutions. Toutefois, des changements dominants dans l'amplitude ont été constatés entre 3-10 mm pour les périodes de retour de 20 ans des événements de 1 jour, alors qu'ils étaient entre 5-15 mm et 10-20 mm pour les événements de 3 à 7 jours, respectivement.

Des incertitudes liées au choix d'une distribution régionale et des corrélations spatiales ont été prises en compte quand on estimait l'importance des changements des périodes de retour régionaux des précipitations extrêmes. La méthode de bootstrap vectoriel nonparametrique a été utilisée en conjonction avec l'approche du test d'inversion (en anglais «test-inversion approach») et l'approche basée sur l'erreur standard (en anglais «standard error based approach») pour l'estimation des intervalles de confiance. Ces approches ont indiqué une augmentation significative dans les péeriods de retour à l'échelle régionale pour la plupart des régions, à l'exception de MRTMS et NPLNS, où les changements tendent à être moins importants. Pour les niveaux de retour de 50 et de 100 ans, les augmentations n'ont pas été aussi significatives que pour celle de 20 ans. Les orientations et les défis futures impliquent une diminution de l'importance des sources d'incertitude provenant de l'élaboration de scénarios et du paramétrage du modèle en autre.

Enfin, il est important de mentionner que le traitement les nombreuses sources de limitations et d'incertitudes reliées à ce projet suggèrent donc de'importance de continuer la recherche dans le futur sur ce sujet. Par exemple, l'amélioration de la qualité de la base des données d'observation, en particulier pour les régions nordiques du Canada, améliorerait les résultats RFA de ces régions. D'autre part, comme la plupart des incertitudes du climat futur dépend du choix du modèle climatique et du scénario d'émission (Déqué et al., 2007), une meilleure compréhension et évaluation du changement éventuel futur peut être obtenue en utilisant des simulations à partir d'une gamme de différents modèles climatiques globaux et régionaux.

ANNEXE A

RELEVANT SECTIONS/SUBSECTIONS OF THE PAPER WHERE THE RESULTS, PRESENTED IN THE INDICATED FIGURES, ARE DIRECTLY OR INDIRECTLY USED

A.1	Subsection 2.5.2 Validation of the CRCM simulations
A.2	Subsection 2.5.2 Validation of the CRCM simulations
A.3	Subsection 2.5.2 Validation of the CRCM simulations
A.4	Subsection 2.5.2 Validation of the CRCM simulations
A.5	Subsection 2.5.2 Validation of the CRCM simulations
A.6	Subsection 2.5.2 Validation of the CRCM simulations
A.7	Subsection 2.5.2 Validation of the CRCM simulations
A.8	Subsection 2.5.2 Validation of the CRCM simulations
A.9	Subsection 2.5.2 Validation of the CRCM simulations

A.10	Subsection 2.5.3.1 The RFA approach
A.11	Subsection 2.5.3.1 The RFA approach
A.12	Subsection 2.5.3.2 The GBA approach
A.13	Subsection 2.5.3.1 The RFA approach
A.14	Subsection 2.5.3.1 The RFA approach
A.15	Subsection 2.5.3.2 The GBA approach
A.16	Subsection 2.5.3.1 The RFA approach
A.17	Subsection 2.5.3.1 The RFA approach
A.18	Subsection 2.5.3.1 The RFA approach
A.19	Subsection 2.5.3.1 The RFA approach
A.20	Subsection 2.5.3.2 The GBA approach
A.21	Subsection 2.5.3.2 The GBA approach
A.22	Section 2.6 Discussion and conclusions
A.23	Section 2.6 Discussion and conclusions
A.24	2.5.3.3 Estimating uncertainty
A.25	2.5.3.3 Estimating uncertainty

Note: Figures corresponding to precipitation extremes of 1-, 3- and 7-day duration are included in the article, while those for 2-, 5-, and 10-day durations are presented in this appendix

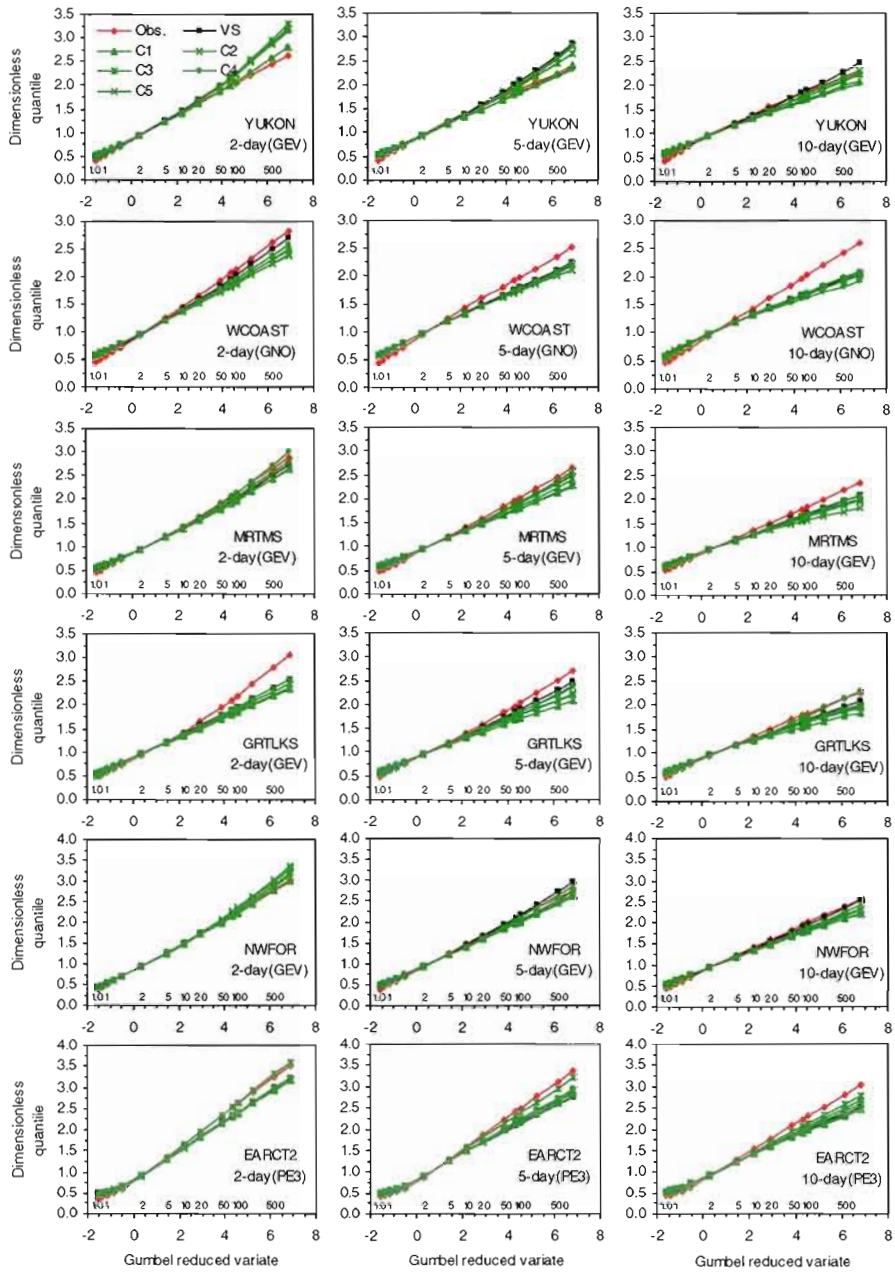

Figure A. 1 Comparison of regional growth curves for 2-, 5- and 10-day annual (April–September) maximum precipitation amounts, derived from the observed data, validation simulation (VS) and reference simulations (C1–C5), for six selected regions. The plots are developed on Gumbel probability paper, wherein the inner scale along the x-axis shows return periods. The best fitting regional distribution is indicated in each panel.

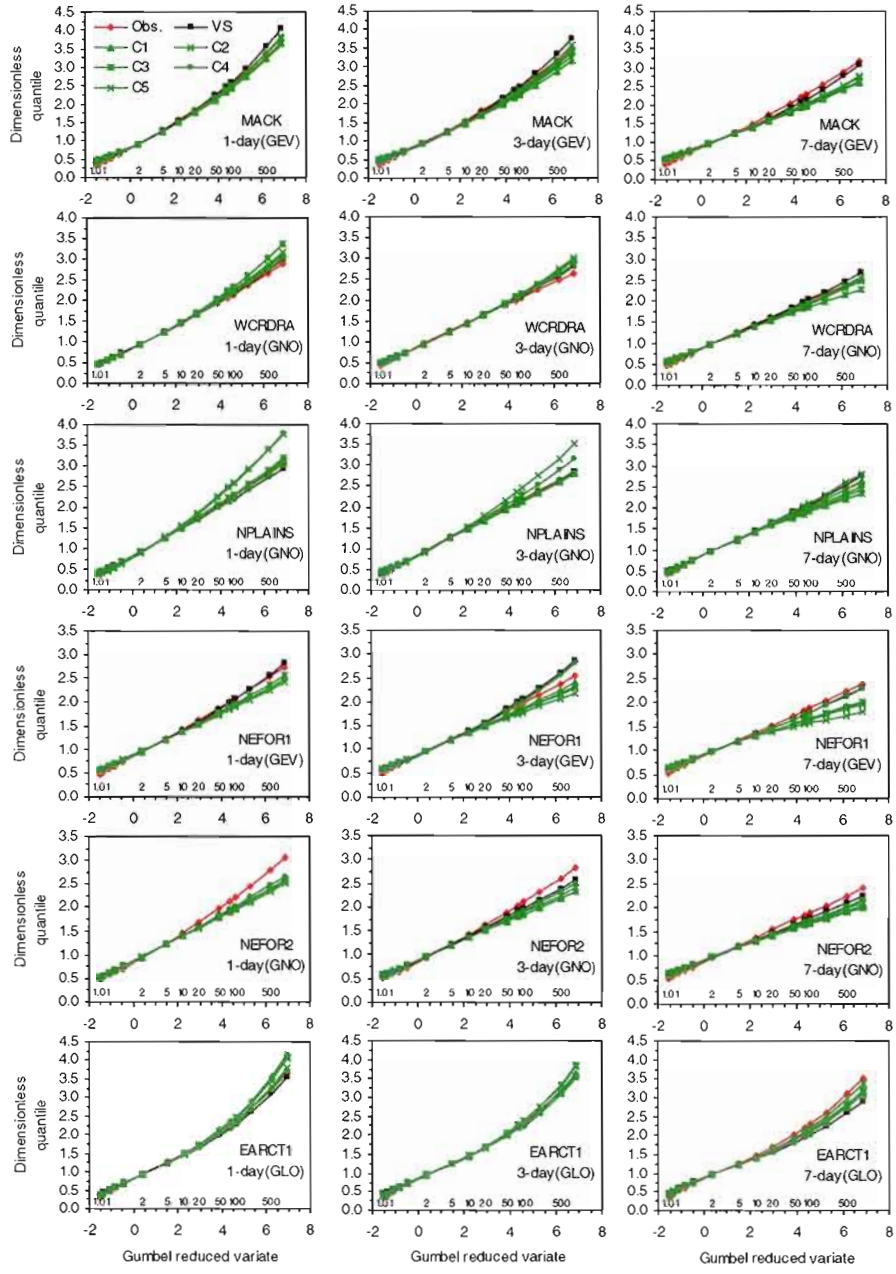

Figure A. 2 Comparison of regional growth curves for 1-, 3- and 7-day annual (April–September) maximum precipitation amounts, derived from the observed data, validation simulation (VS) and reference simulations (C1–C5), for six regions not shown in the article.

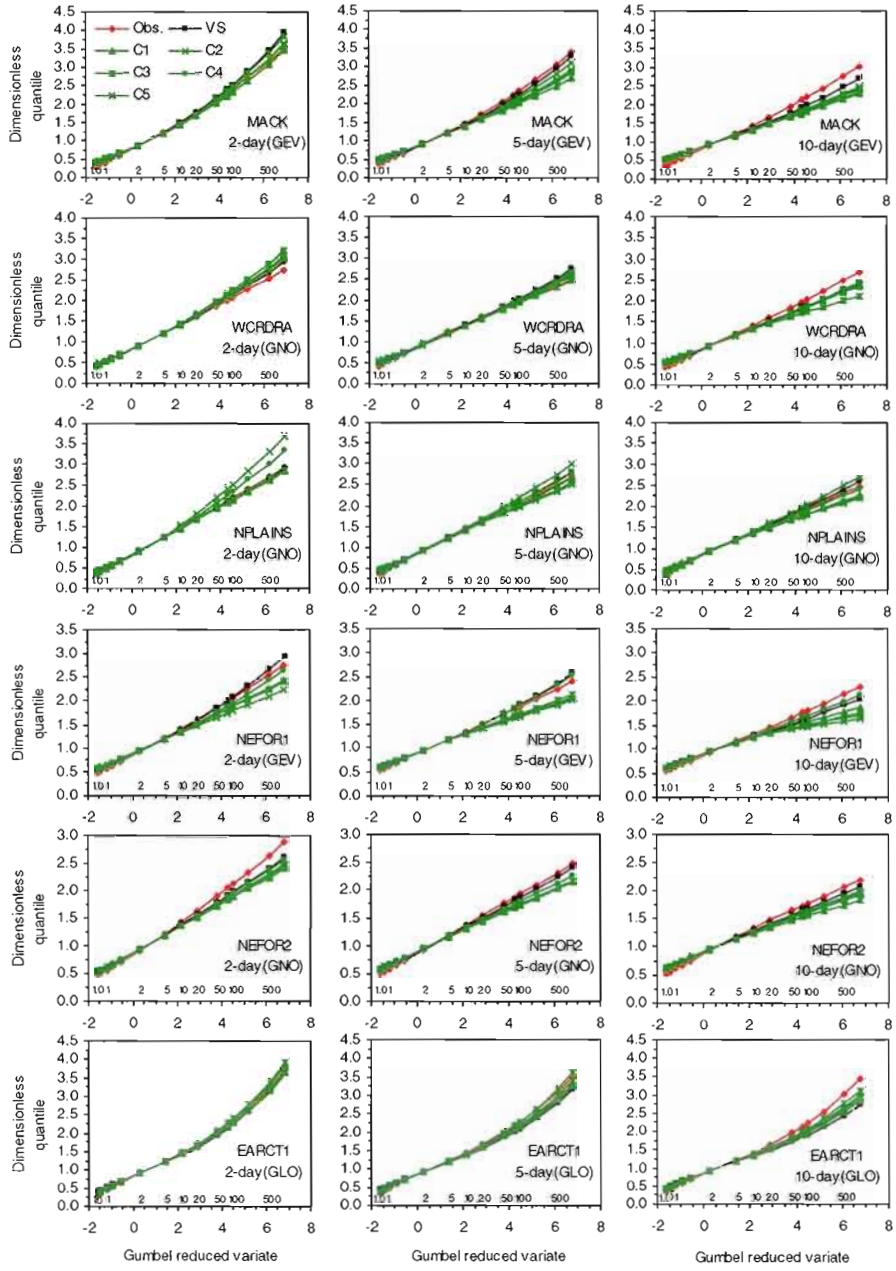

Figure A. 3 Comparison of regional growth curves for 2-, 5- and 10-day annual (April–September) maximum precipitation amounts, derived from the observed data, validation simulation (VS) and reference simulations (C1–C5), for six regions not shown in the article.

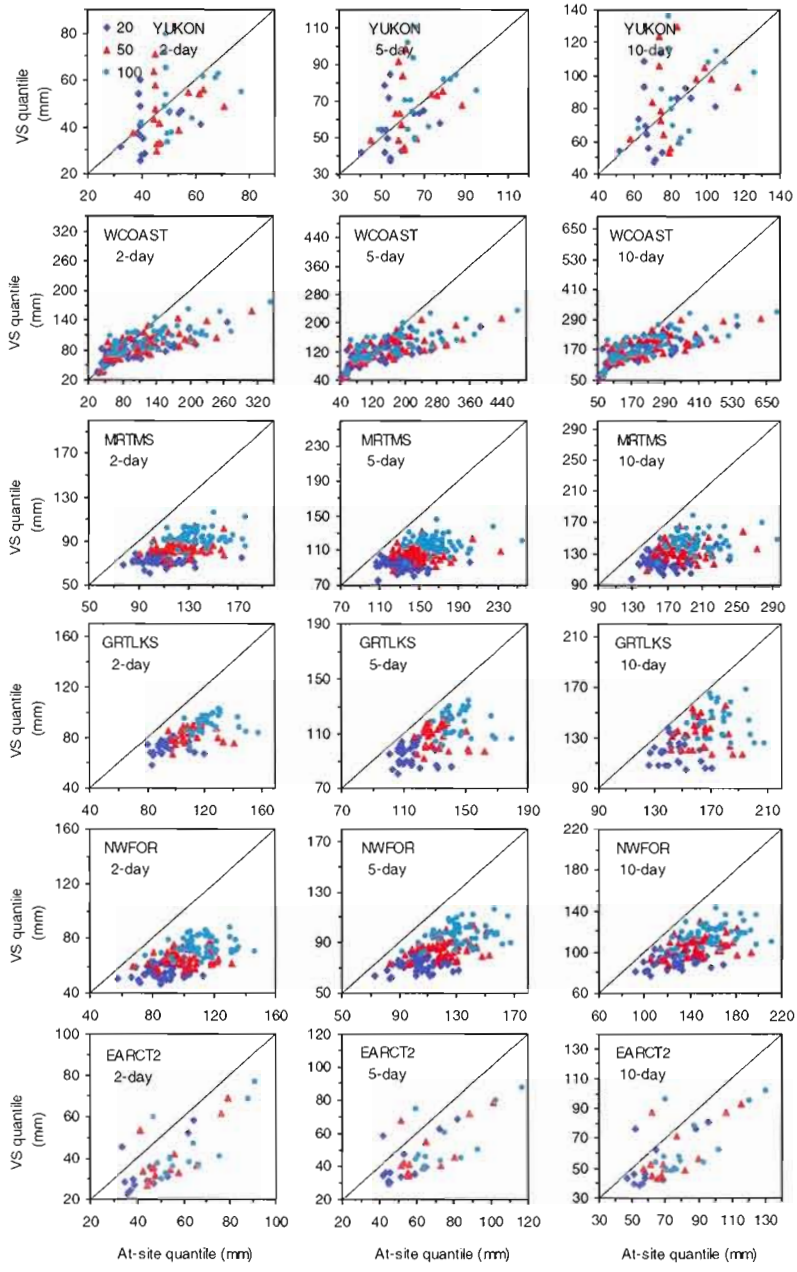

Figure A. 4 Scatter plots of 20-, 50- and 100-year return levels of 2-, 5- and 10-day precipitation extremes derived from observations (shown along the x-axis) and validation simulation (VS) (shown along the y-axis) for the period 1961–1990. Results for the six regions selected for the article.

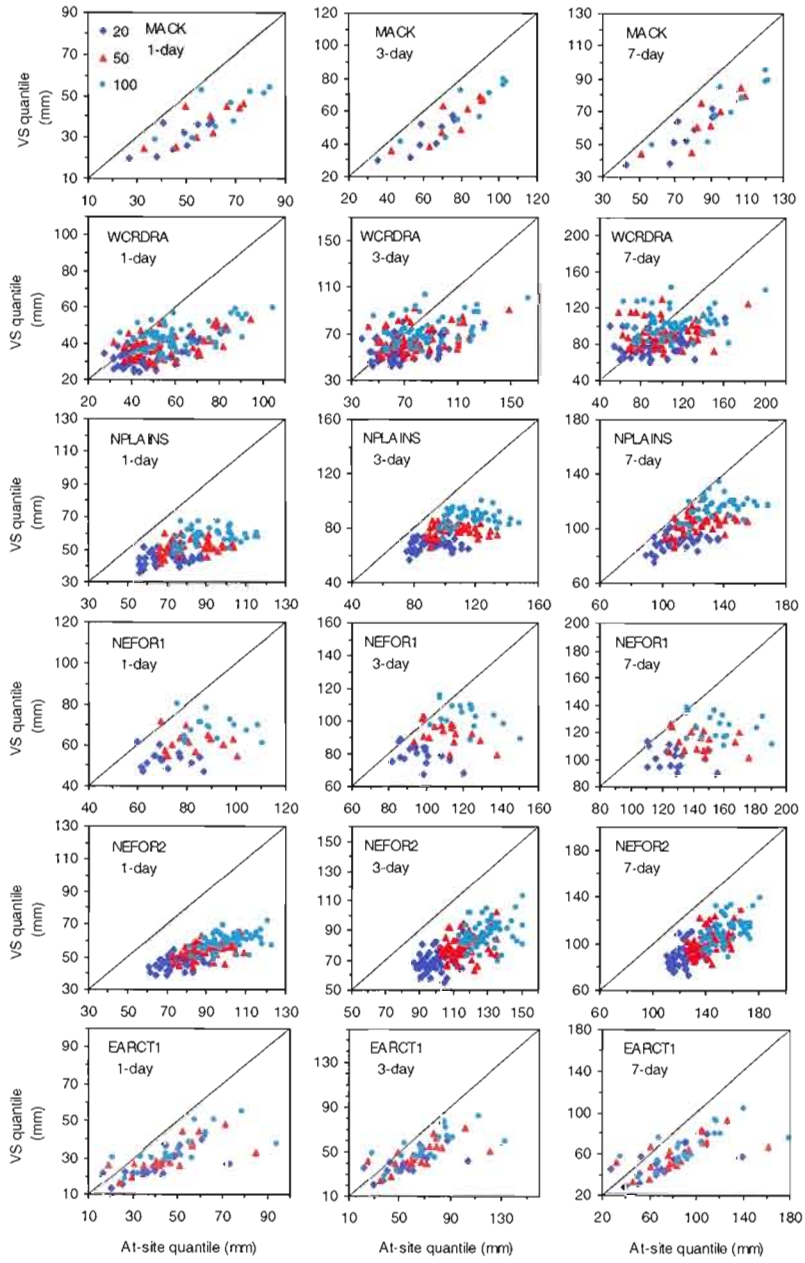

Figure A. 5 Scatter plots of 20-, 50- and 100-year return levels of 1-, 3- and 7-day precipitation extremes derived from observations (shown along the x-axis) and validation simulation (VS) (shown along the y-axis) for the period 1961–1990. Results for the six selected regions not shown in the article figures.

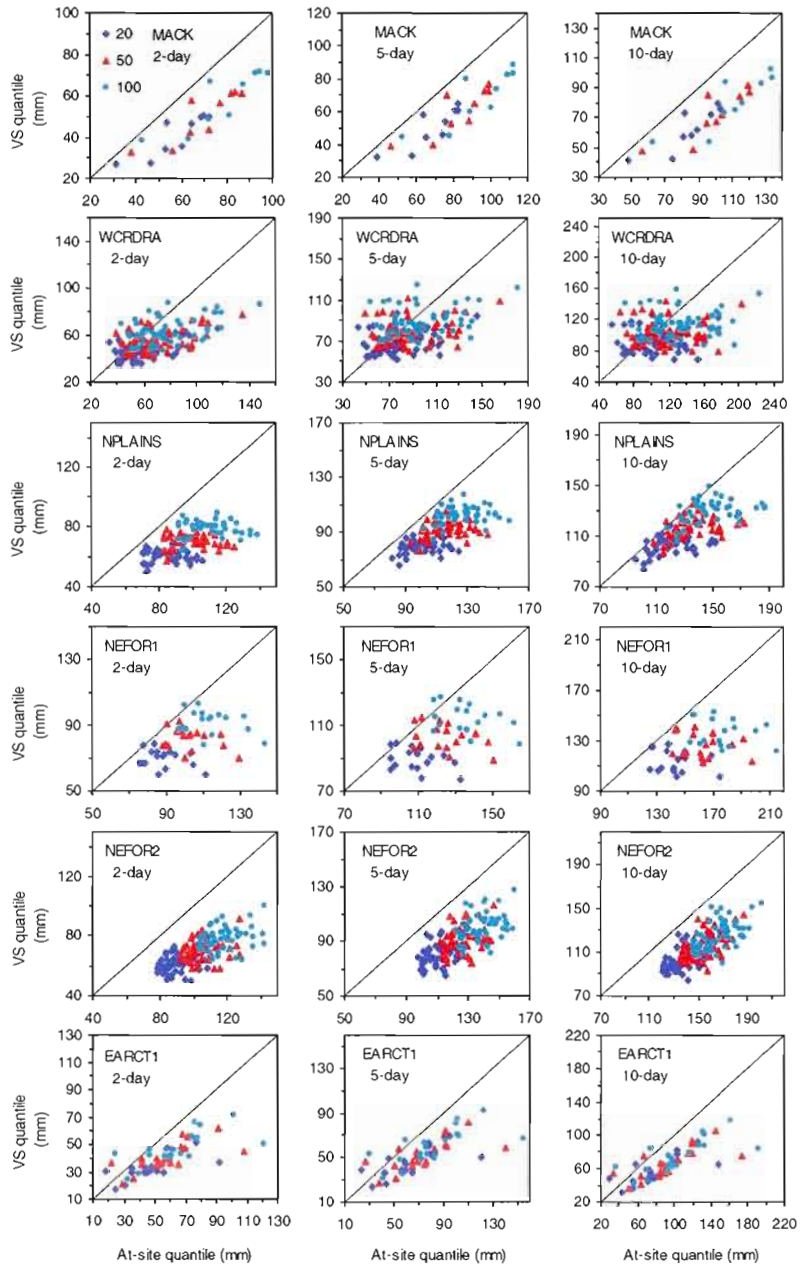

Figure A. 6 Scatter plots of 20-, 50- and 100-year return levels of 2-, 5- and 10-day precipitation extremes derived from observations (shown along the x-axis) and validation simulation (VS) (shown along the y-axis) for the period 1961–1990. Results for six regions not shown in the article figures.

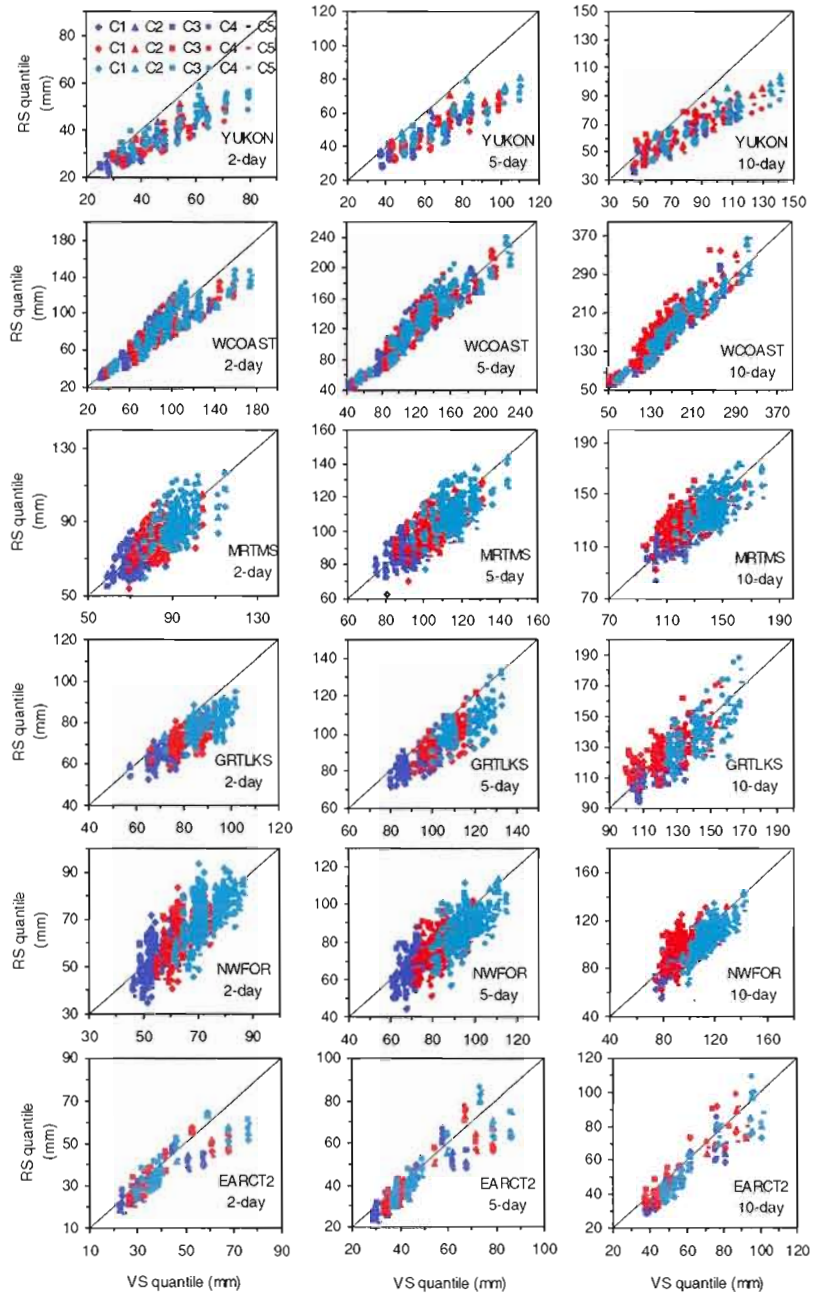

Figure A. 7 Scatter plots of 20- (dark blue), 50- (red) and 100-year (light blue) return levels of 2-, 5- and 10-day precipitation extremes derived from the validation (shown along the x-axis) and reference (C1–C5) simulations (shown along the y-axis) for the period 1961–1990. Results for the six regions selected for the article.

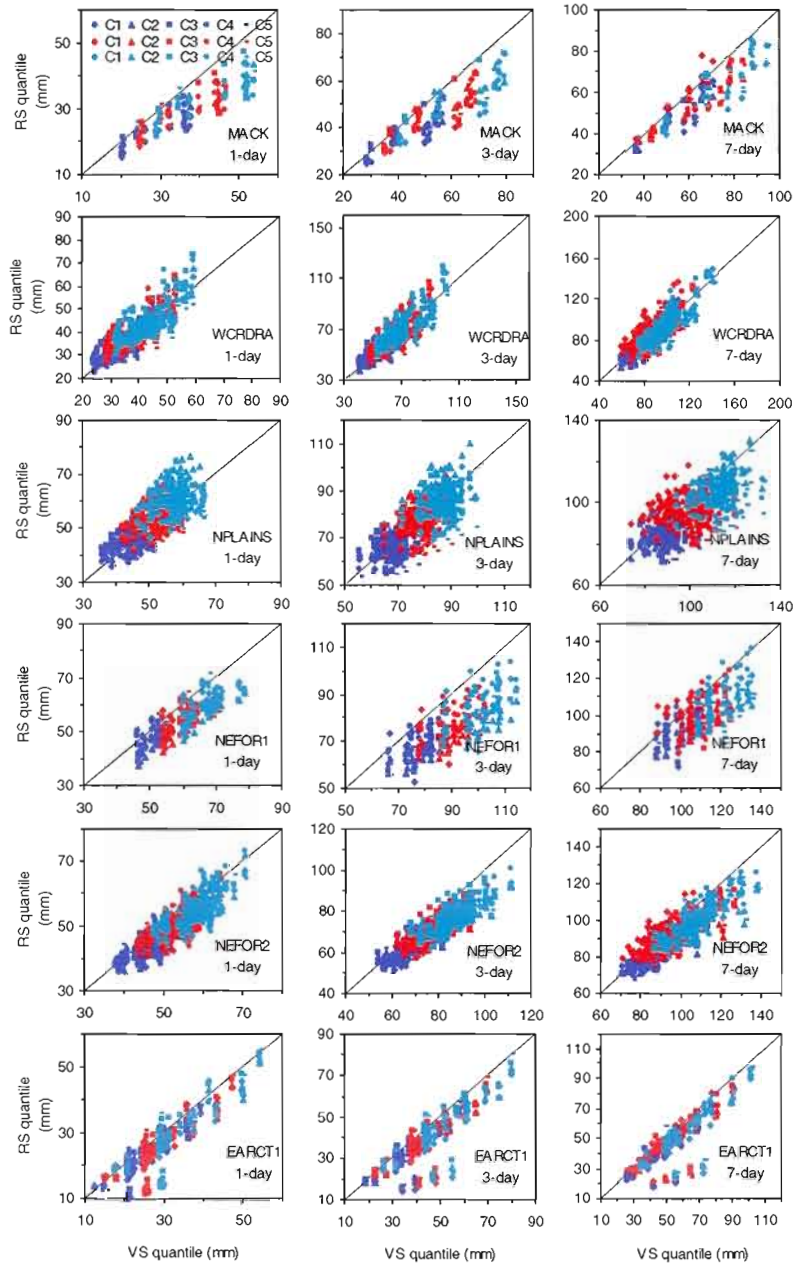

Figure A. 8 Scatter plots of 20- (dark blue), 50- (red) and 100-year (light blue) return levels of 1-,3- and 7-day precipitation extremes derived from the validation (shown along the x-axis) and reference (C1–C5) simulations (shown along the y-axis) for the period 1961–1990. These regions are not shown in the article figures.

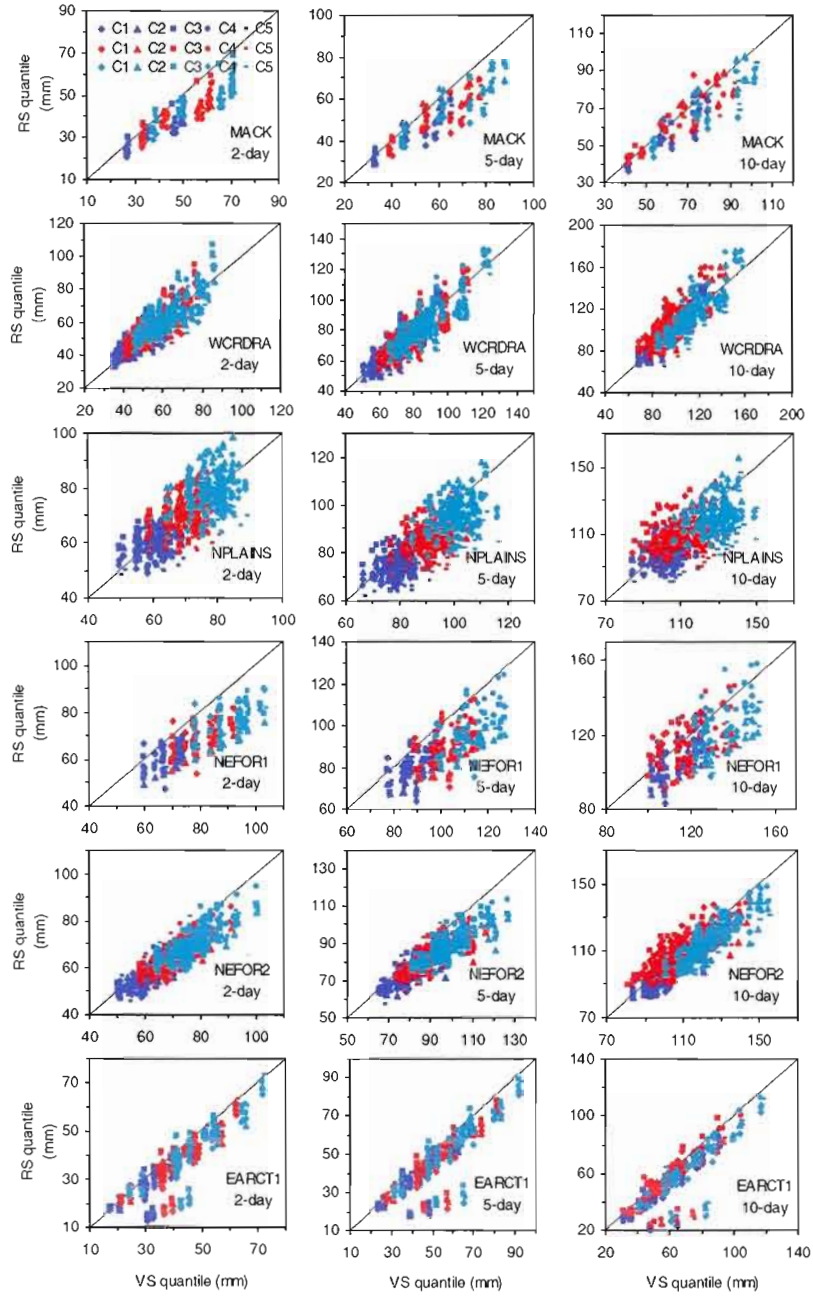

Figure A. 9 Scatter plots of 20- (dark blue), 50- (red) and 100-year (light blue) return levels of 2-,5- and 10-day precipitation extremes derived from the validation (shown along the x-axis) and reference (C1–C5) simulations (shown along the y-axis) for the period 1961–1990. These regions are not shown in the article figures.

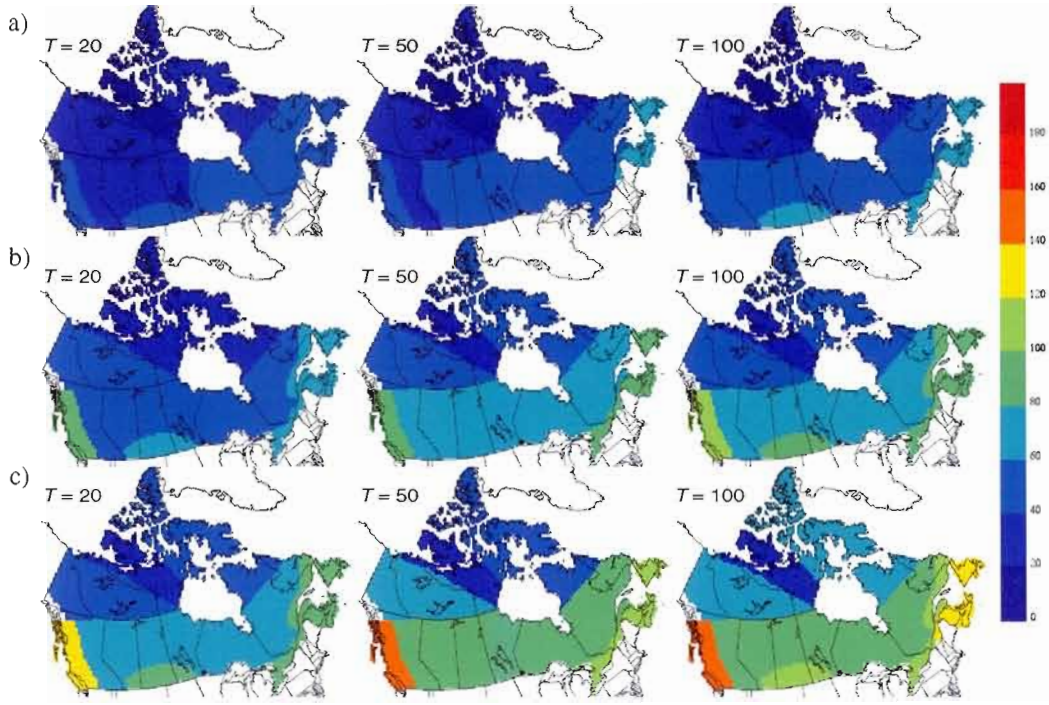

Figure A. 10 Spatial distributions of regional level 20-year (left column), 50-year (middle column) and 100-year (right column) return levels of (a) 2-day, (b) 5-day and (c) 10-day precipitation extremes for the reference (1961–1990) period. A common legend (in mm) is used.

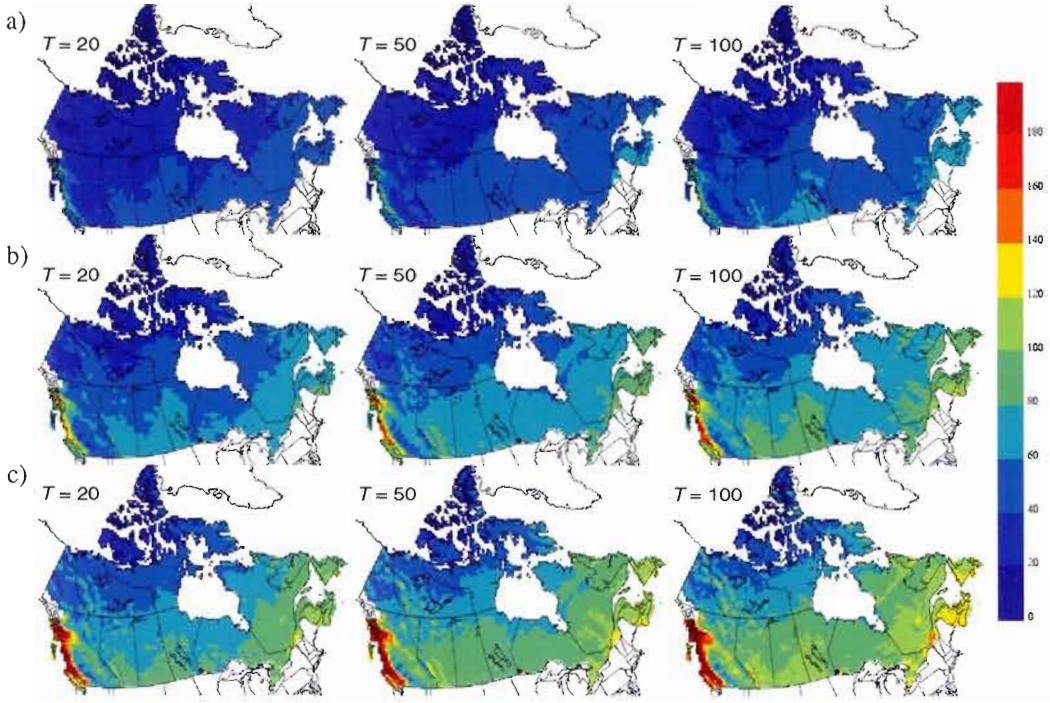

Figure A. 11 Spatial distributions of 20-, 50- and 100-year return levels of 2-, 5- and 10-day precipitation extremes at the CRCM grid-cell level for the reference (1961–1990) period obtained using RFA approach. A common legend (in mm) is used.

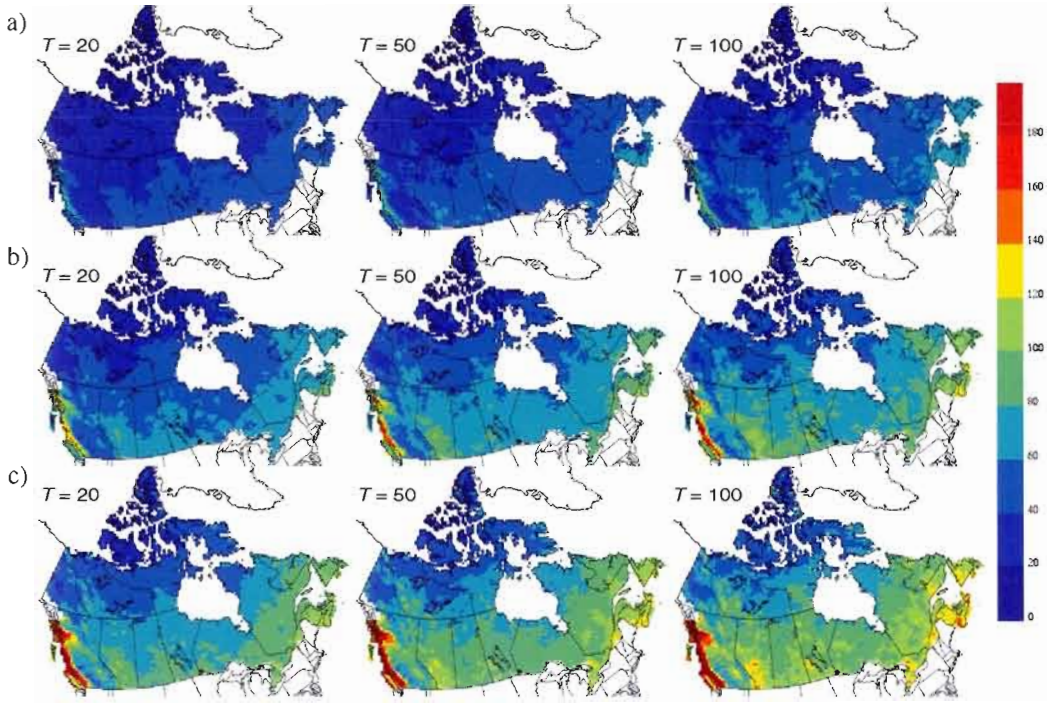

Figure A. 12 Spatial distributions of ensemble averaged 20-, 50- and 100-year return levels of 2-, 5- and 10-day precipitation extremes at the CRCM grid-cell-scale for the reference (1961–1990) period obtained using the GBA approach. A common legend (in mm) is used.

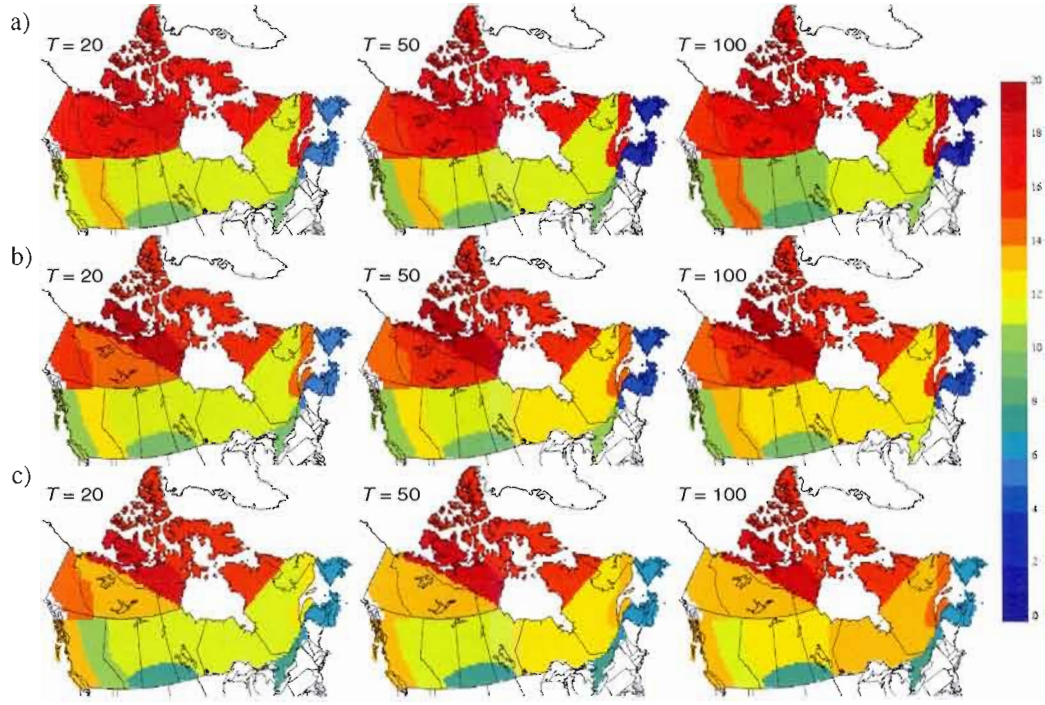

Figure A. 13 Spatial distribution of percentage change (increase/decrease) in 20-year (left column), 50-year (middle column) and 100-year (right column) regional return levels for (a) 2-day, (b) 5-day and (c) 10-day precipitation extremes.

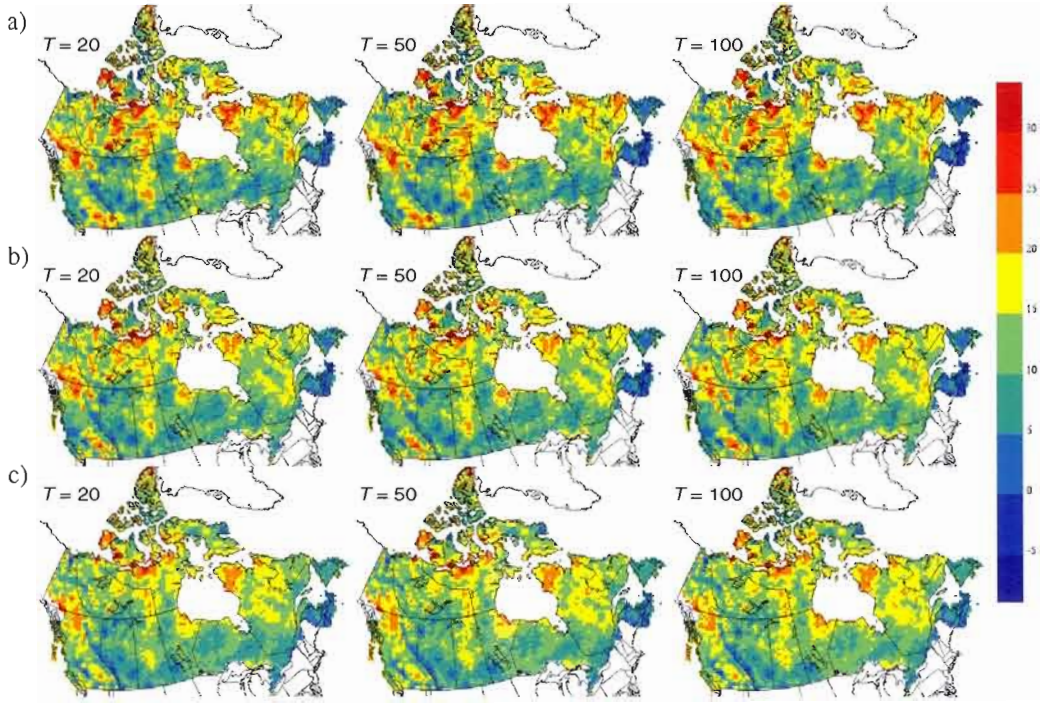

Figure A. 14 Spatial distribution of percentage change (increase/decrease) in 20-year (left column), 50-year (middle column) and 100-year (right column) return levels of the (a) 2-day, (b) 5-day and (c) 10-day precipitation extremes at the CRCM grid cell level obtained using RFA approach.

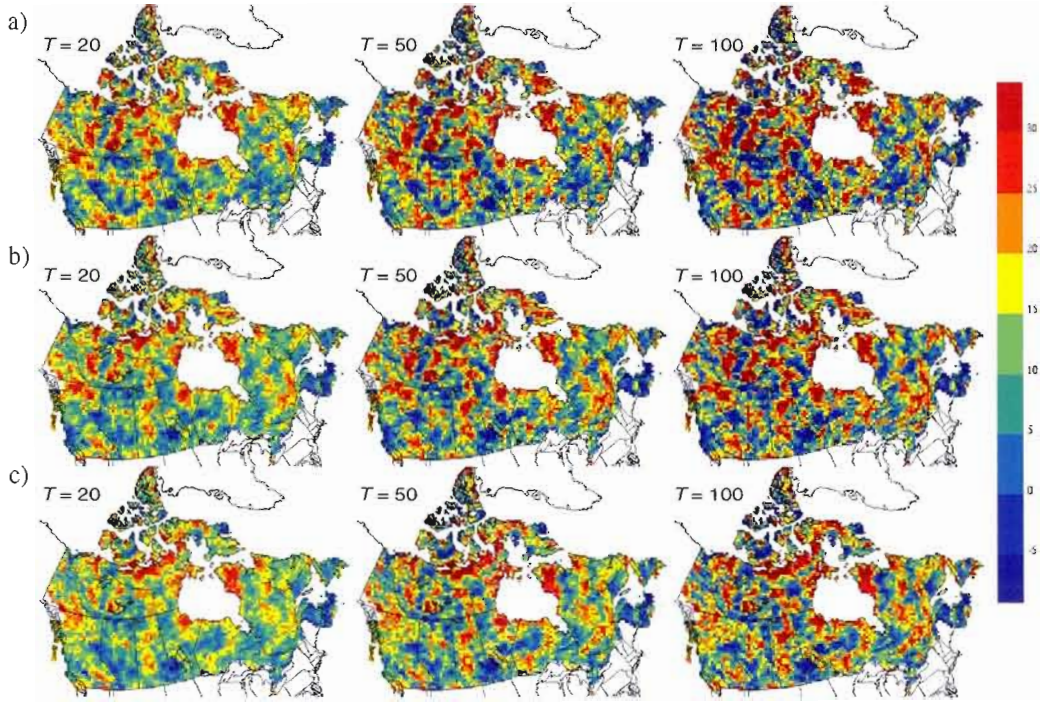

Figure A. 15 Spatial distribution of percentage change (increase/decrease) in 20-year (left column), 50-year (middle column) and 100-year (right column) return levels of (a) 1-day, (b) 3-day and (c) 7-day precipitation extremes at the CRCM grid cell level obtained using the GBA approach.

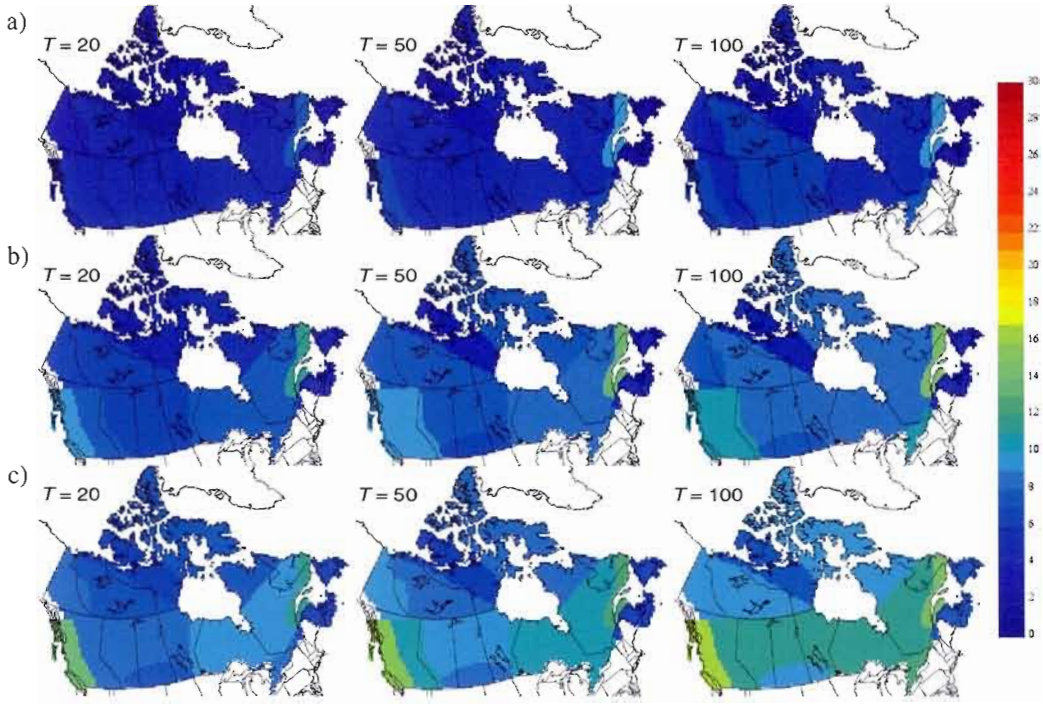

Figure A. 16 Difference (in mm) between future and reference period of (a) 1-day, (b) 3-day and (c) 7-day precipitation extremes. 20-year (left column), 50-year (middle column) and 100-year (right column) regional return levels.

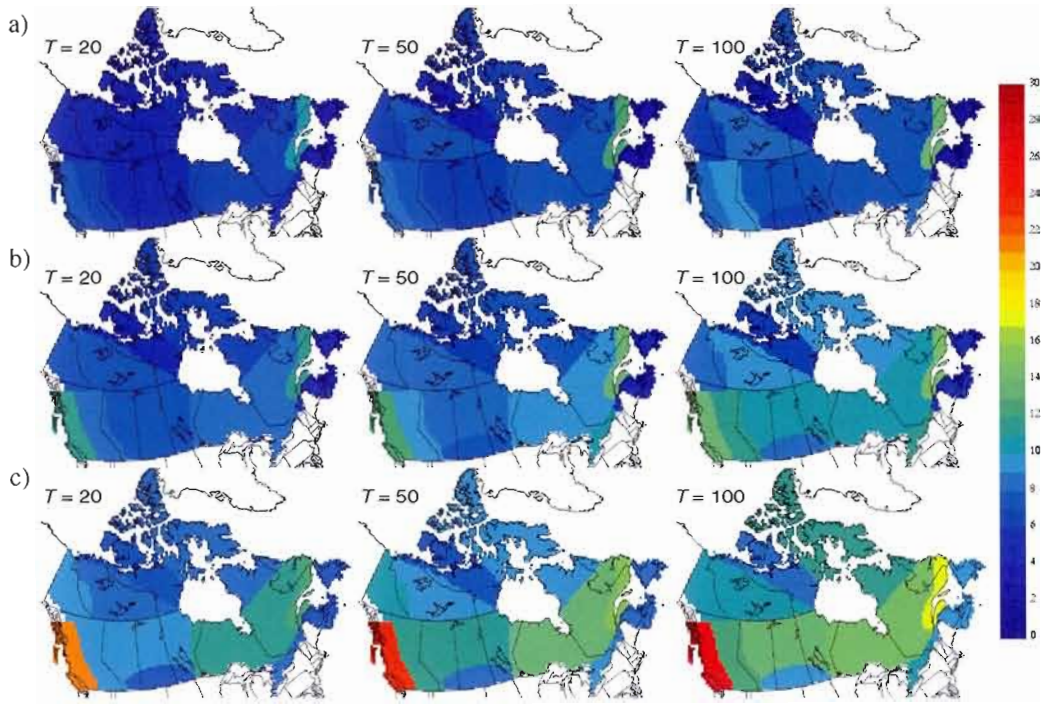

Figure A. 17 Difference (in mm) between future and reference period of (a) 2-day, (b) 5-day and (c) 10-day precipitation extremes. 20-year (left column), 50-year (middle column) and 100-year (right column) regional return levels.

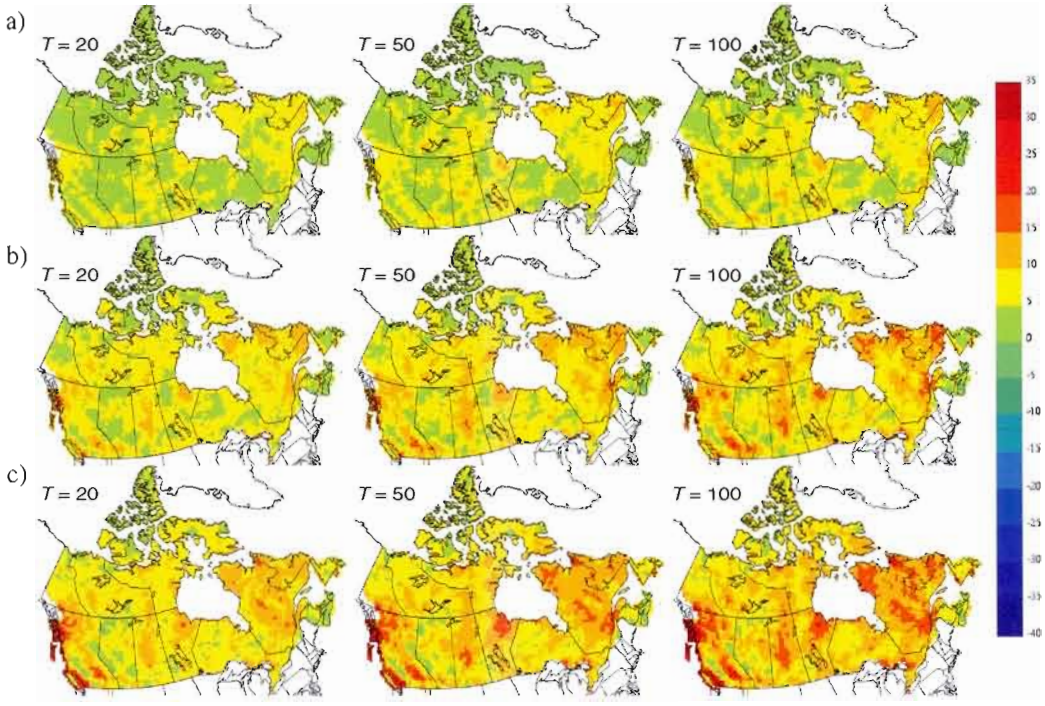

Figure A. 18 Difference (in mm) between future and reference period 20-year (left column), 50-year (middle column) and 100-year (right column) return levels (obtained using the RFA approach) of (a) 1-day, (b) 3-day and (c) 7-day precipitation extremes at the CRCM grid-cell level.

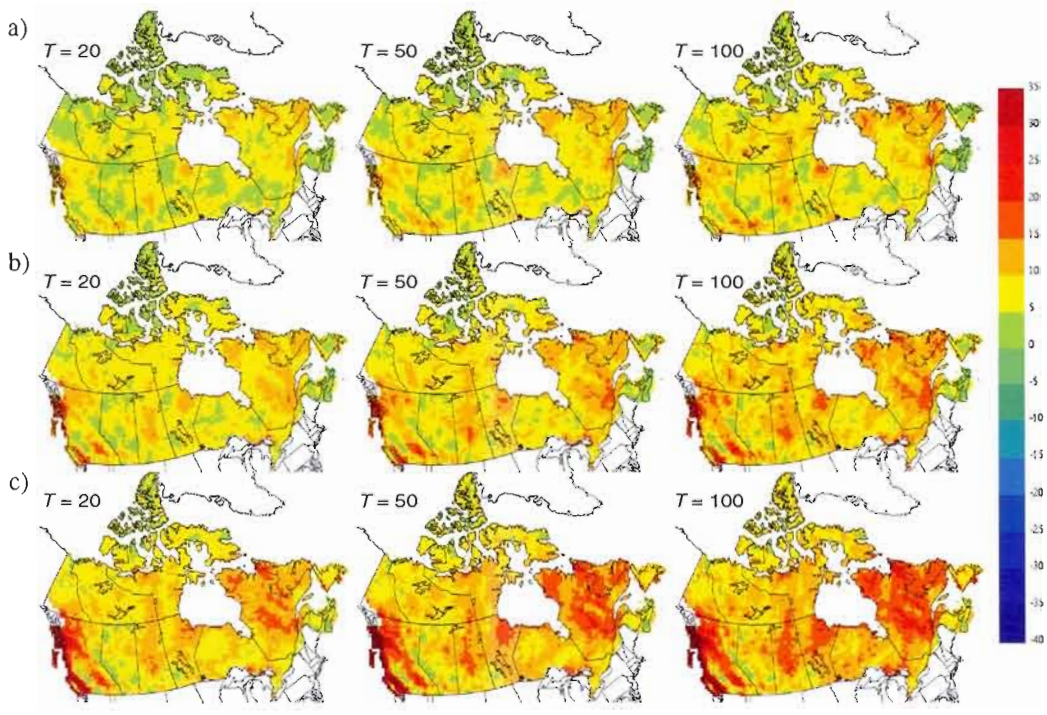

Figure A. 19 Difference (in mm) between future and reference period 20-year (left column), 50-year (middle column) and 100-year (right column) return levels (obtained using the RFA approach) of (a) 2-day, (b) 5-day and (c) 10-day precipitation extremes at the CRCM grid-cell level.

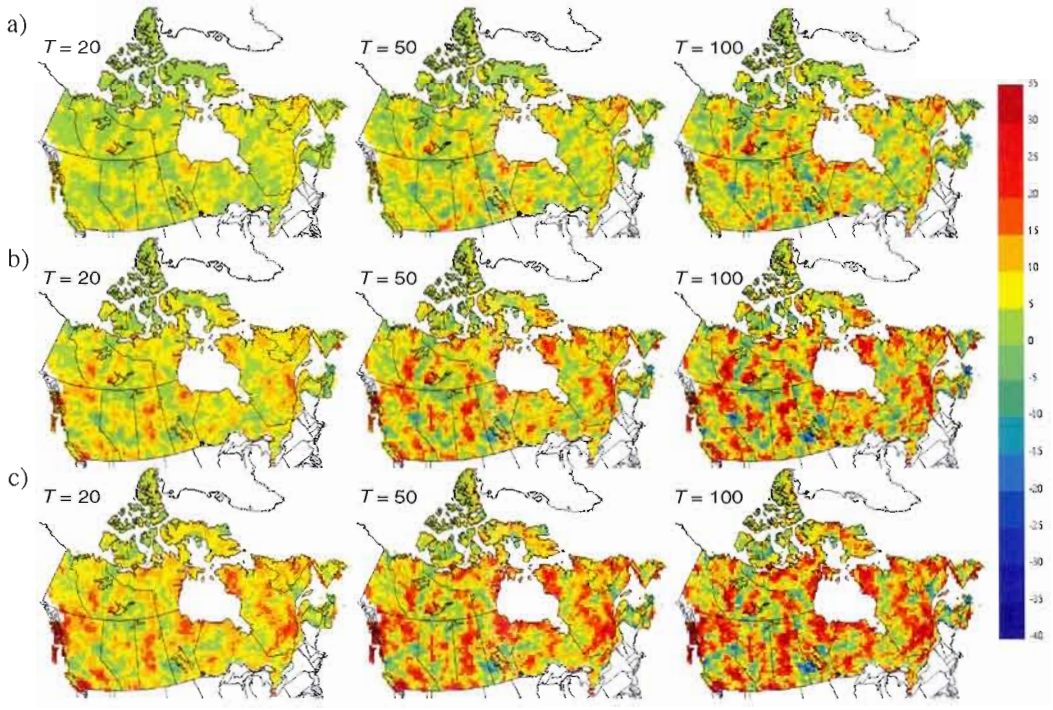

Figure A. 20 Difference (in mm) between future and reference period 20-year (left column), 50-year (middle column) and 100-year (right column) return levels (obtained using the GBA approach) of (a) 1-day, (b) 3-day and (c) 7-day precipitation extremes at the CRCM grid-cell level.

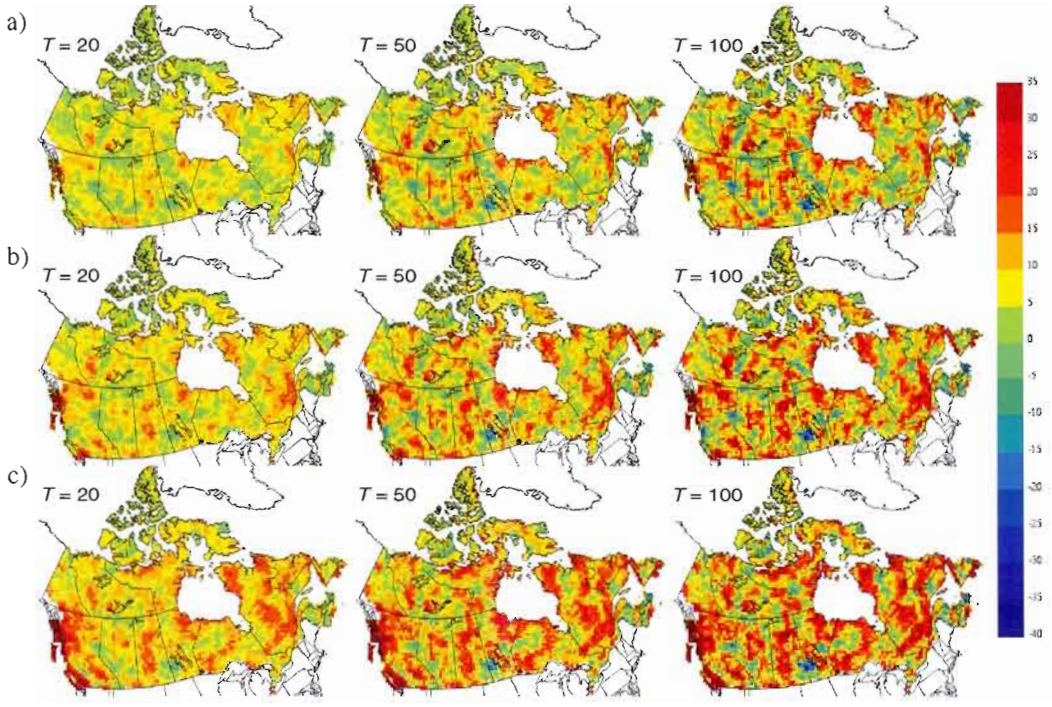

Figure A. 21 Difference (in mm) between future and reference period 20-year (left column), 50-year (middle column) and 100-year (right column) return levels (obtained using the GBA approach) of (a) 2-day, (b) 5-day and (c) 10-day precipitation extremes at the CRCM grid-cell level.

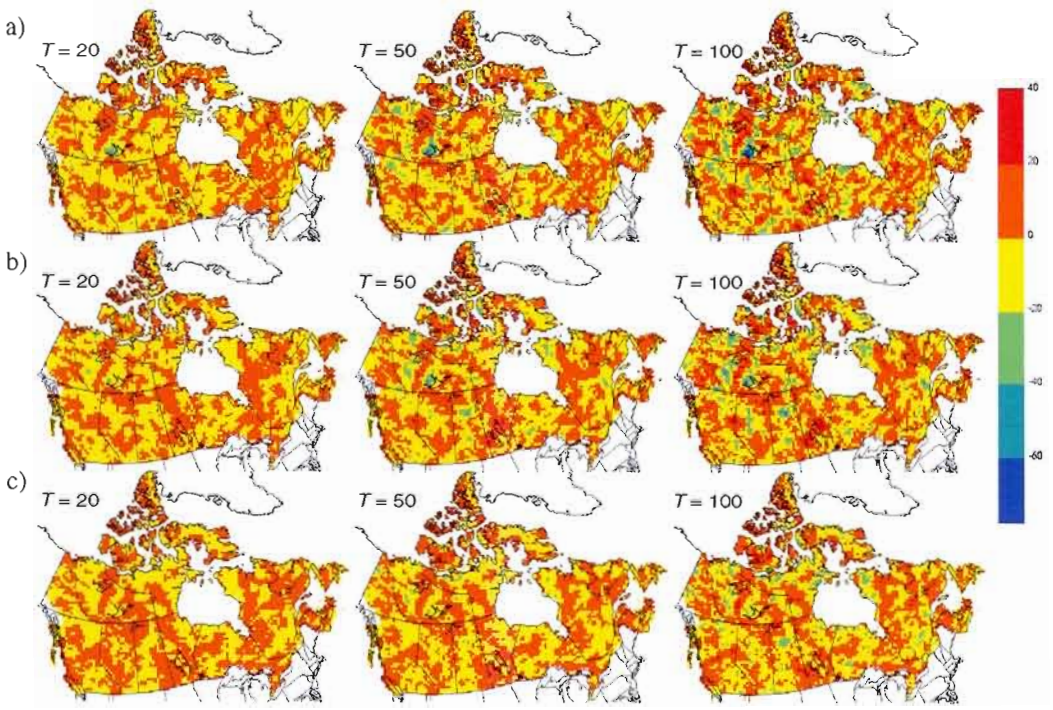

Figure A. 22 Difference (in %) between delta percentages between the RFA at grid-cell level and the GBA approaches for (a) 1-day, (b) 3-day and (c) 7-day precipitation extremes of 20-year (left column), 50-year (middle column) and 100-year (right column) return levels.

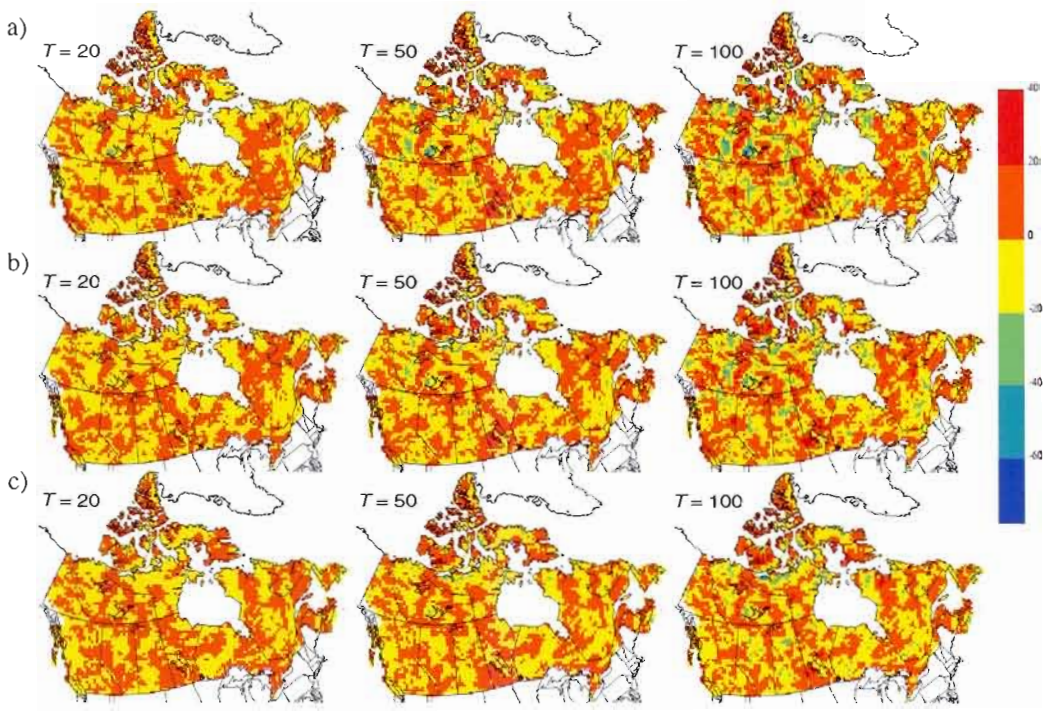

Figure A. 23 Difference (in %) between delta percentages between the RFA at grid-cell level and the GBA approach for (a) 2-day, (b) 5-day and (c) 10-day precipitation extremes of 20-year (left column), 50-year (middle column) and 100-year (right column) return levels.

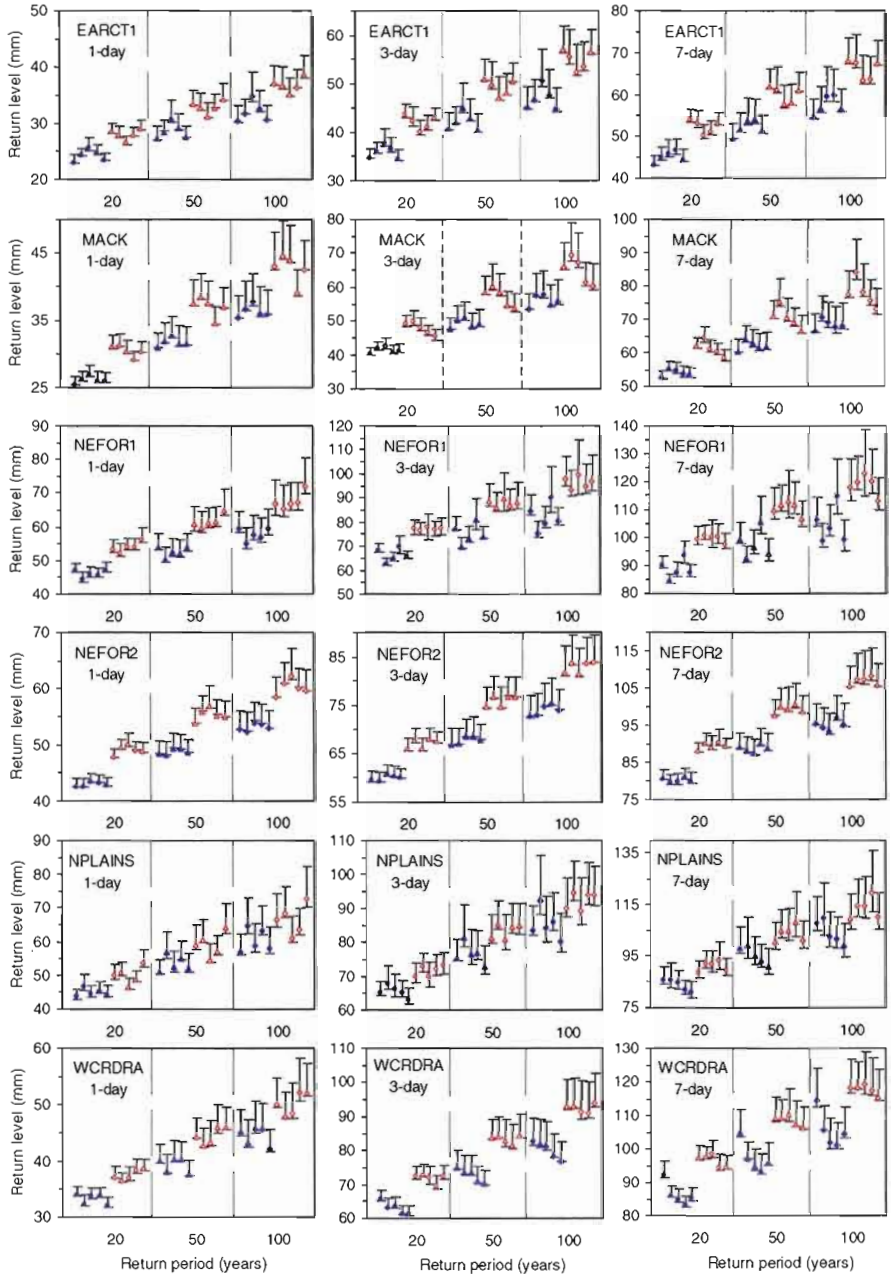

Figure A. 24 Regional scale 20-, 50- and 100-year return levels of 1-, 3- and 7-day precipitation extremes for the C1–C5 (filled blue symbols) and F1–F5 (unfilled red symbols) simulations. Vertical bars are the 95% confidence intervals obtained using the vector block bootstrap resampling approach and the test-inversion method. In each pentad, plots from left to right respectively correspond to C1–C5 simulations and the same description is applicable for F1–F5 simulations.

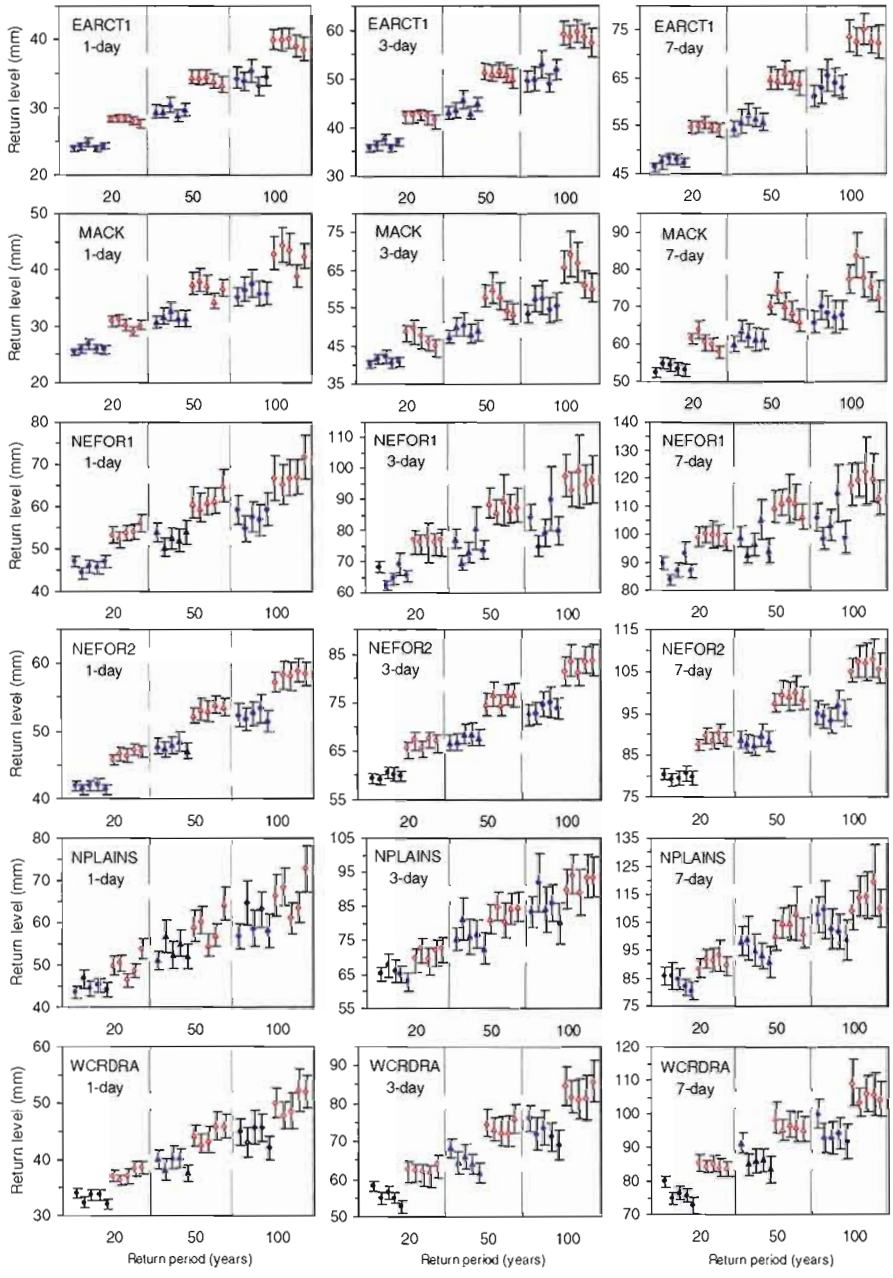

Figure A. 25 Regional scale 20-, 50- and 100-year return levels of 1-, 3- and 7-day precipitation extremes for the C1–C5 (filled blue symbols) and F1–F5 (unfilled red symbols) simulations. Vertical bars are the 95% confidence intervals obtained using the vector block bootstrap resampling approach and the standard error based method. In each pentad, plots from left to right respectively correspond to C1–C5 simulations and the same description is applicable for F1–F5 simulations.

ANNEXE B

RELEVANT SECTION OF THE PAPER WHERE IN THE RESULTS PRESENTED IN THE INDICATED TABLE ARE DIRECTLY OR INDIRECTLY USED

B.1	Section 2.2 Model and simulations
B.2	Subsection 2.4.1 Section 6
B.3	Subsection 2.4.1 Section 6
B.4	Subsection 2.5.2 Validation of the CRCM simulations
B.5	Subsection 2.5.2 Validation of the CRCM simulations

Table B. 1 Description of the CRCM simulations used in the study

Current	Future	Driving data
C1 (*aey)	F1 (*afb)	CGCM3.1#1
C2 (*aez)	F2 (*afc)	CGCM3.1#2
C3 (*afa)	F3 (*afd)	CGCM3.1#3
C4 (*aet)	F4 (*aeu)	CGCM3.1#4
C5 (*aev)	F5 (*aew)	CGCM3.1#5

* These abbreviations correspond to the naming convention used by Climate Simulation Team of Ouranos Consortium for various CRCM simulations.

Table B. 2 Best fitting rank of the five candidate distributions and values of the regional homogeneity measures H_1, H_2 and H_3-test

Region	Duration	Overall best fitting rank			H-test		
		1	2	3	H_1	H_2	H_3
YUKON	1-day	GLO	GEV	GNO	1.69	0.64	0.88
	2-day	GEV	GNO	PE3	2.68	-0.26	-0.59
	3-day	GLO	GEV	GNO	1.71	-0.43	-0.96
	5-day	GEV	GNO	PE3	1.44	-0.18	-0.73
	7-day	PE3	GEV	GNO	1.28	-0.34	-0.16
	10-day	PE3	GEV	GNO	1.68	-1.1	-1.31
WCOAST	1-day	GEV	GNO	PE3	0.38	-2.27	-1.73
	2-day	GNO	GEV	PE3	0.65	1.24	1.31
	3-day	GNO	GEV	PE3	0.53	0.97	1.58
	5-day	GNO	GEV	PE3	2.3	0.27	1.16
	7-day	PE3	GNO	GEV	1.87	-0.82	0.25
	10-day	PE3	GNO	GEV	2.27	-1.11	-1.06
MRTMS	1-day	GEV	GNO	GLO	0.49	0.01	-0.21
	2-day	GEV	GLO	GNO	-0.12	-0.64	-0.18
	3-day	GEV	GNO	PE3	-0.31	0.37	1.08
	5-day	GEV	GNO	PE3	-1.13	-0.1	0.76
	7-day	GEV	GNO	PE3	-0.67	0.53	2.3
	10-day	GEV	GNO	PE3	-2.02	0.82	1.59
GRTLKS	1-day	GNO	GEV	PE3	-1.89	-0.75	-0.89
	2-day	GEV	GLO	GNO	-0.25	-1.51	-1.19
	3-day	GEV	GNO	PE3	1.09	-0.63	0.04
	5-day	GEV	GNO	GLO	1.25	-1.32	-0.92
	7-day	GEV	GNO	PE3	2.4	-0.51	-1.35
	10-day	GNO	GEV	PE3	2.79	0.17	-0.32
NWFOR	1-day	GEV	GNO	PE3	2.46	1.52	1.62
	2-day	GNO	GEV	PE3	0.9	0.01	-0.39
	3-day	GEV	GNO	PE3	0.15	1.06	0.62
	5-day	GEV	GNO	PE3	-0.19	0.57	0.95
	7-day	GNO	GEV	PE3	-0.6	0.44	0.91
	10-day	GEV	GNO	PE3	-2.03	0.61	0.9
EARCT2	1-day	PE3	GNO	GEV	1.33	-0.26	0.00
	2-day	PE3	GNO	GPA	-0.16	0.69	0.64
	3-day	PE3	GNO	GEV	-0.62	0.79	0.62
	5-day	GNO	PE3	GEV	0.53	0.65	0.33
	7-day	PE3	GNO	GEV	0.9	-0.39	0.15
	10-day	GNO	GEV	PE3	0.93	0.13	0.23

Table B. 3 Best fitting rank of the five candidate distributions and values of the regional homogeneity measures H_1, H_2 and H_3-test

Region	Duration	Overall best fitting rank			H-test		
		1	2	3	H_1	H_2	H_3
EARCT1	1-day	GEV	GNO	GLO	1.64	0.53	-0.21
	2-day	GEV	GLO	GNO	0.15	1.49	1.16
	3-day	GLO	GEV	GNO	0.24	0.52	0.36
	5-day	GLO	GEV	GNO	0.77	1.23	1.12
	7-day	GLO	GEV	GNO	0.9	1.24	0.73
	10-day	GLO	GEV	GNO	2.35	1.16	1.1
MACK	1-day	GEV	GNO	PE3	0.32	-0.62	-0.02
	2-day	GNO	GEV	PE3	-0.06	-0.93	-1.08
	3-day	GNO	GEV	PE3	-0.81	-0.94	-1.02
	5-day	GLO	GEV	GNO	-0.92	-1.37	-0.66
	7-day	GLO	GEV	GNO	-0.73	-0.9	-0.82
	10-day	GLO	GEV	GNO	-0.61	-0.6	-0.77
NEFOR1	1-day	GNO	GEV	PE3	2.04	1.28	0.83
	2-day	GNO	PE3	GEV	1.64	0.73	0.35
	3-day	GEV	GNO	PE3	1.64	0.87	0.26
	5-day	GEV	GNO	PE3	1.48	-0.14	0.42
	7-day	GEV	GNO	PE3	2.04	0.4	-0.24
	10-day	GLO	GEV	GNO	0.47	0.07	-0.28
NEFOR2	1-day	GEV	GLO	GNO	1.26	-0.1	-0.38
	2-day	GNO	GEV	PE3	1.76	-0.98	-0.45
	3-day	GNO	GEV	PE3	1.38	-0.23	0.6
	5-day	GNO	GEV	PE3	1.16	-0.15	-0.31
	7-day	GNO	GEV	PE3	1.31	-0.5	0.05
	10-day	GNO	GEV	PE3	1.75	1.14	0.66
NPLAINS	1-day	GEV	GNO	GLO	1.1	1.08	0.47
	2-day	GNO	GEV	PE3	0.39	0.27	0.23
	3-day	GNO	PE3	GEV	0.82	0.94	0.86
	5-day	PE3	GNO	GEV	0.75	1.04	1.05
	7-day	GNO	GEV	PE3	0.99	-0.89	-0.4
	10-day	GEV	GNO	PE3	0.91	-0.34	-0.48
WCRDRA	1-day	GEV	GNO	GLO	2.6	0.38	-0.09
	2-day	GNO	PE3	GEV	3.07	2.13	1.6
	3-day	GNO	PE3	GEV	2.04	1.4	0.83
	5-day	GNO	GEV	PE3	0.96	0.66	0.49
	7-day	GEV	GNO	PE3	0.75	-0.59	-0.7
	10-day	GEV	GLO	GNO	1.21	-0.34	-0.5

Table B. 4 Average boundary forcing and performance errors in 20-, 50- and 100-year return levels for the Regional Frequency Analysis (RFA) method

Region	Duration	Average boundary forcing error (%)			Average performance error (%)		
		20-yr	50-yr	100-yr	20-yr	50-yr	100-yr
YUKON	1-day	-19.2	-18.8	-18.4	-15.7	-14.2	-12.9
	3-day	-20.5	-21.1	-21.3	-3.1	0.7	3.9
	7-day	-21.6	-23.1	-24.1	2.7	5.7	8.4
WCOAST	1-day	-5.0	-6.1	-7.0	-21.8	-24.0	-25.4
	3-day	-2.6	-3.4	-3.8	-6.2	-6.9	-7.6
	7-day	1.5	0.6	0.0	0.0	-1.5	-2.7
MRTMS	1-day	-2.0	-2.2	-2.4	-36.4	-36.9	-37.1
	3-day	-4.0	-4.0	-4.0	-29.0	-28.9	-28.6
	7-day	-2.3	-2.8	-3.2	-27.5	-28.4	-28.9
GRTLKS	1-day	-11.4	-12.2	-12.8	-30.4	-33.8	-36.3
	3-day	-11.3	-12.3	-12.8	-18.1	-19.3	-20.2
	7-day	-2.9	-4.0	-4.7	-20.1	-21.5	-22.4
NWFOR	1-day	-2.5	-2.4	-2.3	-39.7	-39.3	-38.8
	3-day	-4.7	-5.3	-5.7	-31.6	-30.6	-29.8
	7-day	-5.0	-6.6	-7.8	-29.0	-28.4	-27.7
EARCT2	1-day	-10.4	-10.2	-10.2	-29.1	-32.1	-34.5
	3-day	-10.1	-9.7	-9.5	-22.5	-26.0	-28.8
	7-day	-10.4	-9.5	-9.0	-19.8	-24.3	-27.6
EARCT1	1-day	-12.6	-11.3	-10.3	-30.5	-28.6	-35.7
	3-day	-14.2	-13.7	-13.4	-25.3	-23.1	-20.3
	7-day	-16.0	-14.7	-13.6	-24.9	-24.9	-24.1
MACK	1-day	-16.4	-17.6	-18.4	-34.9	-33.9	-33.0
	3-day	-12.2	-13.8	-14.9	-27.9	-26.7	-25.5
	7-day	-9.7	-11.7	-13.2	-25.4	-25.6	-25.5
NEFOR1	1-day	-9.6	-11.3	-12.7	-24.2	-23.6	-23.0
	3-day	-8.5	-10.0	-11.1	-17.4	-15.6	-13.9
	7-day	-13.1	-15.4	-17.2	-20.6	-20.8	-20.7
NEFOR2	1-day	-6.3	-6.4	-6.3	-33.9	-35.7	-37.3
	3-day	-9.8	-10.6	-10.6	-27.4	-28.3	-29.2
	7-day	-7.1	-7.9	-7.9	-25.5	-26.1	-26.5
NPLAINS	1-day	1.6	4.1	5.8	-34.0	-35.0	-35.8
	3-day	-3.3	-2.3	-1.4	-24.3	-24.5	-24.6
	7-day	-6.0	-7.2	-8.2	-17.2	-16.2	-15.2
WCRDRA	1-day	0.0	1.1	2.1	-25.0	-24.6	-24.3
	3-day	-1.1	-0.4	0.2	-13.7	-12.7	-11.7
	7-day	-3.6	-4.9	-5.9	-7.2	-5.9	-4.7

Table B. 5 Average boundary forcing and performance errors in 20-, 50- and 100-year return levels for the Regional Frequency Analysis (GBA) method

Region	Duration	Average boundary forcing error (%)			Average performance error (%)		
		20-yr	50-yr	100-yr	20-yr	50-yr	100-yr
YUKON	1-day	-20.1	-19.2	-18.3	-6.6	-6.5	-6.3
	3-day	-22.0	-22.0	-22.0	6.9	10.0	12.8
	7-day	-21.6	-22.3	-22.9	9.7	11.6	13.5
WCOAST	1-day	-8.6	-7.7	-6.9	17.5	10.1	5.0
	3-day	-11.2	-11.1	-11.0	46.0	42.3	40.0
	7-day	-10.0	-9.6	-9.2	57.4	51.6	48.1
MRTMS	1-day	-0.3	-0.5	-0.5	-31.3	-33.0	-34.0
	3-day	-2.0	-2.1	-2.0	-23.9	-24.4	-24.6
	7-day	-0.6	-0.5	-0.2	-24.2	-26.0	-27.2
GRTLKS	1-day	-8.9	-10.5	-11.6	-21.5	-24.3	-37.6
	3-day	-7.0	-7.7	-8.1	-17.1	-19.2	-20.7
	7-day	-2.4	-3.3	-3.9	-18.9	-21.0	-22.3
NWFOR	1-day	-2.8	-2.7	-2.6	-39.6	-39.1	-38.7
	3-day	-4.9	-5.5	-5.9	-31.5	-30.5	-29.6
	7-day	-5.0	-6.6	-7.8	-29.1	-28.3	-27.6
EARCT2	1-day	-10.2	-10.0	-9.8	-28.7	-31.8	-34.3
	3-day	-10.0	-9.4	-9.0	-22.0	-25.7	-28.6
	7-day	-10.0	-9.2	-8.6	-19.5	-24.0	-27.4
EARCT1	1-day	-13.1	-12.3	-11.7	-28.9	-27.0	-34.3
	3-day	-14.0	-13.8	-13.7	-24.3	-22.2	-19.4
	7-day	-16.0	-15.0	-14.2	-24.1	-24.1	-23.2
MACK	1-day	-16.5	-17.5	-18.3	-34.8	-34.1	-33.2
	3-day	-12.7	-14.3	-15.5	-27.5	-26.3	-25.1
	7-day	-9.9	-11.8	-13.4	-25.1	-25.3	-25.1
NEFOR1	1-day	2.9	3.5	3.9	-25.7	-27.5	-28.6
	3-day	-3.8	-5.3	-6.6	-20.2	-20.5	-20.4
	7-day	-0.4	-1.3	-2.0	-19.5	-20.3	-20.6
NEFOR2	1-day	-4.6	-4.8	-5.0	-33.0	-35.1	-36.9
	3-day	-7.4	-8.1	-8.1	-26.7	-28.0	-29.0
	7-day	-6.2	-7.0	-7.0	-25.0	-25.8	-26.3
NPLAINS	1-day	1.4	4.0	5.9	-33.8	-34.9	-35.7
	3-day	-3.6	-2.7	-2.0	-24.1	-24.1	-24.1
	7-day	-6.1	-7.4	-8.4	-17.1	-16.0	-15.0
WCRDRA	1-day	-5.3	-4.0	-3.0	-1.5	-3.3	-4.4
	3-day	-8.8	-7.9	-7.2	18.4	17.8	17.6
	7-day	-14.0	-14.4	-14.7	31.8	31.1	30.9

RÉFÉRENCES

Beniston, M., D. B. Stephenson, O. B. Christenson, C. A. T. Ferro, C. Frei, S. Goyette, K. Halsnaes, T. Holt, K. Jylhä, B. Koffi, J. Palutikof, R. Schöll, T. Semmler et K. Woth. 2007. «Future extreme events in European climate: an exploration of regional climate model projections». *Climatic Change*, 81, 71–95.

Burn, D. H. 2003. «The use of resampling for estimating confidence intervals for single site and pooled frequency analysis». *Hydrol. Sci. J.*, 48, 25–38.

Carpenter, J. 1999. «Test inversion bootstrap confidence intervals». *J. Roy. Statis. Soc.*, B61, 159–172.

Caya, D. et R. Laprise. 1999. «A semi-implicit semi-Lagrangian regional climate model: the Canadian RCM». *Mon. Wea. Rev.*, 127, 341–362.

Davison, A. C. et D. V. Hinkley. 1997. *Bootstrap methods and their application*. Cambridge University Press, Cambridge, UK. 582 pp.

Dalrymple, T. 1960. «Flood frequency analyses». *US Geol. Survey Wat. Supply Paper* 1543-A, Reston, VA.

Déqué, M., D. P. Rowell, D. Lüthi, F. Giorgi, J. H. Christensen, B. Rockel, D. Jacob, E. Kjellstrom, de M. Castro et B. van der Hurk. 2007. «An intercomparison of regional climate simulations of Europe: assessing uncertainties in model projections». Climatic Change 81, 53-70.

Efron, B. et R. J. Tibshirani. 1993. *An introduction to the bootstrap*. Chapman and Hall, London, UK. 436 pp.

Ekström, M., H. J. Fowler, C. G. Kilsby et P. D. Jones. 2005. «New estimates of future changes in extreme rainfall across the UK using regional climate model integrations. 2. Future estimates and use in impact studies». *J. Hydrol.*, 300(1–4), 234–251.

Emori, S., A. Hasegawa, T. Suzuki, et K. Dairaku. 2005. «Validation, parameterization dependence and future projection of daily precipitation simulated with a high-resolution atmospheric GCM». *Geophys. Res. Let.*, 32, L06708, doi: 10.1029/2004GL022306.

Faulkner, D. S. et D. A. Jones.1999. «The FORGEX method of rainfall growth estimation, III. Examples and confidence intervals». *Hydrol. Earth Sys. Sci.*, 3(2), 205–212.

Fowler, A. M. et K. J. Hennessy. 1995. «Potential impacts of global warming on the frequency and magnitude of heavy precipitation». *Nat. Hazard.*, 11, 283–303.

Fowler, H. J. et C. G. Kilsby. 2003. «A regional frequency analysis of United Kingdom extreme rainfall from 1961 to 2000». *Int. J. Climatol.*, 23(11), 1313–1334.

Fowler, H. J., M. Ekström, C. G. Kilsby et P. D. Jones. 2005. «New estimates of future changes in extreme rainfall across the UK using regional climate model integrations. 1: Assessment of control climate». *J. Hydrol.*, 300(1–4), 212–233.

GREHYS. 1996. «Presentation and review of some methods for regional flood frequency analysis». *J. Hydrol.*, 186 (1–4), 63–84.

Groisman, P. Y., T. R. Karl, D. R. Easterling, R. W. Knight, P. F. Jamason, K. J. Hennessy, R. Suppiah, C. M. Page, J. Wibig, K. Fortuniak, V. N. Razuvaev, A. Douglas, E. Forland et P. M. Zhai. 1999. «Changes in the probability of heavy precipitation: important indicators of climatic change». *Climatic Change*, 42, 243–283.

Groisman, P. Y., R. W. Knight, D. R. Easterling, T. R. Karl, G. C. Hegerl, V. N. Razuvaev et N. Vyacheslav. 2005. «Trends in intense precipitation in the climate record». *J. Climate*, 18, 1326–1350.

Hosking, J. R. M. 1986. «The theory of probability weighted moments». *Research Report* RC 12210. IBM Research Division, Yorktown Heights, NY, 160 pp.

Hosking, J. R. M. et J. R. Wallis. 1997. *Regional Frequency Analysis*. Cambridge University Press, 224 pp.

IPCC. Cimate Change 2007. The Physical Science Basis – Summary for Policy Makers. Contribution of Working Group I to the Fourth Assessment Report of the Intergovernmental Panel on Climate Change. IPCC, Geneva, Switzerland, 18 pp.

Khaliq, M. N., T. B. M. J. Ouarda, J.-C. Ondo, P. Gachon et B. Bobée. 2006. «Frequency analysis of a sequence of dependent and/or non-stationary hydro-meteorological observations: A review». *J. Hydrol.*, 329, 534–552.

Khaliq, M. N., T. B. M. J. Ouarda, L. Sushama et P. Gachon. 2009. «Identification of hydrological trends in the presence of serial and cross correlations: A review of selected methods and their application to annual flow regimes of Canadian rivers». *J. Hydrol.*, 368, 117–130.

Kharin, V. V. et F. W. Zwiers. 2000. «Changes in the extremes in an ensemble of transient climate simulations with a coupled atmosphere–ocean GCM». *J. Climate*, 13, 3760–3788.

Mailhot, A., S. Duchesne, D. Caya et G. Talbot, 2007. «Assessment of future change in Intensity–duration–frequency (IDF) curves for southern Quebec using the Canadian Regional Climate Model (CRCM)». *J. Hydrol.*, 347, 197–210

May, W. 2008. «Potential future changes in the characteristics of daily precipitation in Europe simulated by the HIRHAM regional climate model». *Climate Dyn.*, 30, 581–603.

McFarlane, N. A., J. F. Scinocca, M. Lazare, R. Harvey, D. Verseghy et J. Li. 2005. «The CCCma third generation atmospheric general circulation model». *Rapport interne du Centre Canadien de la Mod´elisation et de l'Analyse Climatique*, 25 pp.

McGuffie, K., A. Henderson-Sellers, N. Holbrook, Z. Kothavala, O. Balachova et J. Hoekstra. 1999. «Assessing simulations of daily temperature and precipitation variability with global climate models for present and enhanced greenhouse climates». *Int. J. Climatol.*, 19(1), 1–26.

Mekis, É. et W. D. Hogg. 1999. «Rehabilitation and analysis of Canadian daily precipitation time series». *Atmos.-Ocean*, 37(1), 53–85.

Nakićenović, N. and Coeditors. 2000. *IPCC Special Report on Emission Scenarios*. Cambridge University Press, 599 pp.

Vincent, L. A. et É. Mekis. 2009. «Discontinuities due to joining precipitation station observations in Canada». *J.Appl.Meteor. Climatol.*, 48(1), 156-166

Osborn, T. J. et M. Hulme. 1997. «Development of a relationship between station and grid-box rainday frequencies for climate model evaluation». *J. Climate*, 10, 1885–1908.

Palmer, T. N. et J. Räisänen. 2002. «Quantifying the risk of extreme seasonal precipitation events in a changing climate». *Nature*, 415, 512–514.

Parmesan C., T. L. Root et M. R. Willig. 2000. «Impacts of extreme weather and climate on terrestrial biota». *Bull. Amer. Meteor. Soc.*, 81: 443–450.

Plummer, D. A., D. Caya, A. Frigon, H. Côté, M. Giguère, D. Paquin, S. Biner, R. Harvey et R. de Elia. 2006. «Climate and climate change over North America as simulated by the Canadian RCM». *J. Climate*, 19, 3112–3132.

Scinocca, J. F. et N. A. McFarlane. 2004. «The variability of modelled tropical precipitation». *J. Atmos. Sci.*, 61, 1993–2015.

Sushama, L., R. Laprise, D. Caya, A. Frigon et M. Slivitzky. 2006. «Canadian RCM projected climate-change signal and its sensitivity to model errors». *Int. J. Climatol.*, 26, 2141–2159.

Tebaldi, C., K. Hayhoe, J. M. Arblaster et G. A. Meehl. 2006. «An intercomparison of model-simulated historical and future changes in extreme events». *Climatic Change*, 79, 185–211.

Trenberth, K. E. 1999. «Atmospheric moisture recycling: role of advection and local evaporation». *J. Climate*, 12, 1368–1381

Trenberth, K. E., A. Dai, R. M. Rasmussen et D. B. Parsons. 2003: «The changing character of precipitation». *Bull. Amer. Meteor.Soc.*, 84, 1205–1217.

Uppala, S.M. and 45 other authors. 2005. «The ERA-40 re-analysis». *Quart. J. Roy. Meteor. Soc.*, 131, 2961–3012.

Vincent, L.A. et E. Mekis. 2009. «Discontinuities due to joining precipitation station observations in Canada». *J. Appl. Meteor. Climatol.*, 48, 156–166.

Zwiers, F. W. et V. V. Kharin. 1998. «Changes in the extremes of the climate simulated by CCC GCM2 under CO2 doubling». *J. Climate*, 11, 2200–2222.